Interreg Co-funded by the European Union

Italy – Croatia

CRESCO Adria

University of Rijeka Faculty of Civil Engineering

D.1.4.4. Distribution of flooding areas

Rijeka, Croatia, 2025.

Project id	ITHR0200245
Name of the lead partner organisation	University of Rijeka, Faculty of Economics and Business
Project title	Climate RESiliEnt COastal planning in Adriatic
Project acronym	CRESCO Adria
Programme priority	Green and resilient shared environment
Specific objective	2.1: Promoting climate change adaptation and disaster risk prevention, resilience, taking into account eco-system based approaches

Activity: **1.4 Pilot are climate change sensitivity survey**

Deliverable: **D1.4.4. Distribution of flooding areas**

Name of the partner organization: University of Rijeka, Faculty of Civil Engineering (GRADRI)

Dean: Assoc. Prof. Mladen Bulić

Project Manager: Assoc. Prof. Iva Mrak

Research team: Assoc. Prof. Nino Krvavica
Marta Marija Gržić, MEng
Ivona Petković, MEng

Date: March 2025

Content

1. INTRODUCTION 1
1.1. Study area 2
1.1.1. Geographical location 2
1.1.2. Climate 4
1.1.3. Catchment characteristics 6
1.2. Rainfall regime 12
1.2.1. Statistical Analysis of Annual and Monthly Rainfall at the Crikvenica station 13
1.2.2. Statistical Analysis of Annual and Monthly Rainfall at the Novi Vinodolski station 22
1.3. Climate projections for rainfall 32
2. FLOOD HAZARD ASSESSMENT DUE TO HEAVY RAINFALL 35
2.1. Introduction to flood hazard assessment 35
2.1.1. Definitions 38
2.1.2. Conceptual model for assessment of flood from heavy rainfall 40
2.1.3. Levels of complexity and flood mapping 40
2.2. Methodology for assessment of flood hazards 45
2.2.1. Flood hazard analysis 46
2.3. Results of the pluvial flood hazard assessment 54
2.3.1. Hydrologic–hydraulic model for rainfall-runoff processes 54
2.3.2. Pluvial flood hazard assessment for the Municipality of Vinodolska općina 55
2.3.3. Pluvial flood hazard assessment for the City of Novi Vinodolski 74
3. CONCLUSIONS 93
3.1. Rainfall regime 93
3.2. Flood hazard assessment 94
REFERENCES 96
APPENDIX 98
A. MAPS 98
B. GIS DATABASE 99

1. INTRODUCTION

This document presents a report on Deliverable D1.4.4, *Distribution of Flooding Area*, from Activity 1.4, *Pilot Area Climate Change Sensitivity Survey*, developed within the international project CRESCO Adria, funded by the Interreg Italy-Croatia program.

This study focuses on flood hazard analysis for the Municipality of Vinodolska općina and the City of Novi Vinodolski, with the primary objective of determining the flood extent – distribution of flooding area - in these two pilot areas.

The Faculty of Civil Engineering in Rijeka will conduct an analysis of the annual, monthly and daily rainfall regime, as well as an analysis of short-term heavy rainfall over a 30-year period, using data from the nearest rain gauge station. The analysis of short-term heavy rainfall will include:

- Trend assessments, anomaly detection, and inter-annual variability of annual, monthly and daily rainfall.
- Definition of DDF and IDF curves for rainfall durations up to 24 hours.
- Analysis of design storms for different duration classes within the range of up to 24 hours.
- Assessment of future climate change impacts on annual, monthly, and short-term heavy rainfall patterns.

Additionally, the Faculty of Civil Engineering in Rijeka will carry out flood hazard analyses due to heavy rainfall for three different probabilities of occurrence in the study area. These analyses will include:

- Compilation and processing of datasets required for hydrological-hydraulic modeling, including topographic, hydrological, geological, and land cover data.
- Development of a hydrological-hydraulic rainfall-runoff model using an appropriate numerical model.
- Simulation of flood events for all rainfall durations from 1 to 24 hours across three different probabilities of occurrence.
- Development of flood hazard maps corresponding to three different probabilities of heavy rainfall events.

The flood hazard maps will show water depth, water velocity, severity, and the spatial extent of flooding for the selected rainfall probabilities. The maps will be developed at a 1:25,000 scale within a Geographic Information System (GIS).

1.1. Study area

1.1.1. Geographical location

The Municipality of Vinodolska općina and the City of Novi Vinodolski are located in the Primorje-Gorski Kotar County in western Croatia, along the northern Adriatic coast.

The Municipality of Vinodolska općina (shown in Figure 1.1) is situated inland, bordering the City of Novi Vinodolski to the southeast, the City of Crikvenica to the southwest, the City of Kraljevica and the City of Bakar to the west, the Municipality of Fužine to the north, and the Municipality of Mrkopalj to the northeast. It encompasses a diverse landscape characterized by coastal hills, valleys, and the Vinodol Valley, which extends from the interior towards the sea. The municipality covers an area of approximately 152.9 km² and includes several settlements, with Bribir as the administrative center.

The City of Novi Vinodolski (shown in Figure 1.2) lies directly on the Adriatic coast and serves as an important historical, cultural, and tourism hub in the region. It shares borders with the Municipality of Vinodolska općina and the City of Crikvenica to the west, the Municipality of Mrkopalj to the north, the City of Ogulin to the northeast, the Municipality of Brinje to the east, and the City of Senj to the south. The city has a well-developed coastline with beaches and marinas, making it a popular tourist destination. It covers an area of approximately 261.3 km² and includes several smaller settlements, with Novi Vinodolski as its administrative center.

Both areas are influenced by their proximity to the sea and the surrounding mountainous terrain, which significantly affects their climate, hydrology, and flood hazard. The combination of coastal and inland topography makes these areas relevant for flood hazard and climate change sensitivity studies.

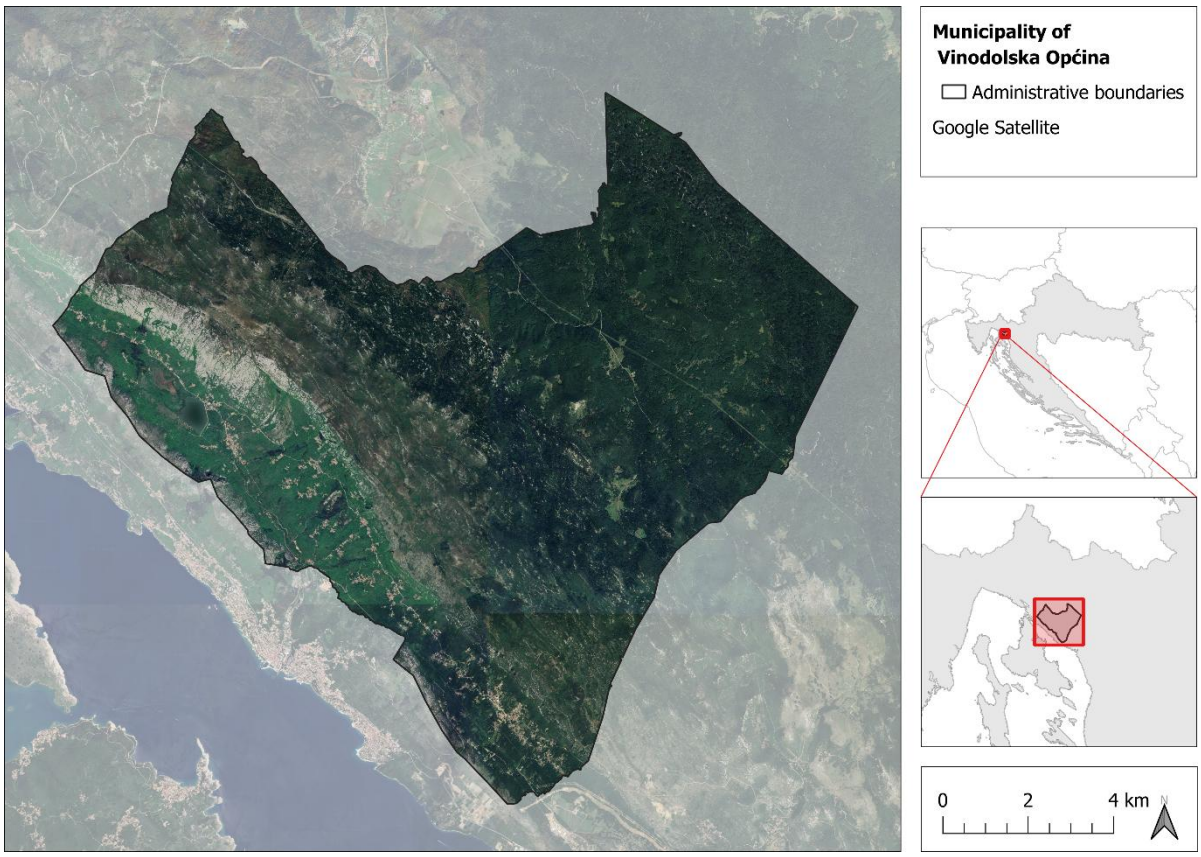

Figure 1.1. Location and administrative boundaries of the Municipality of Vinodolska općina.

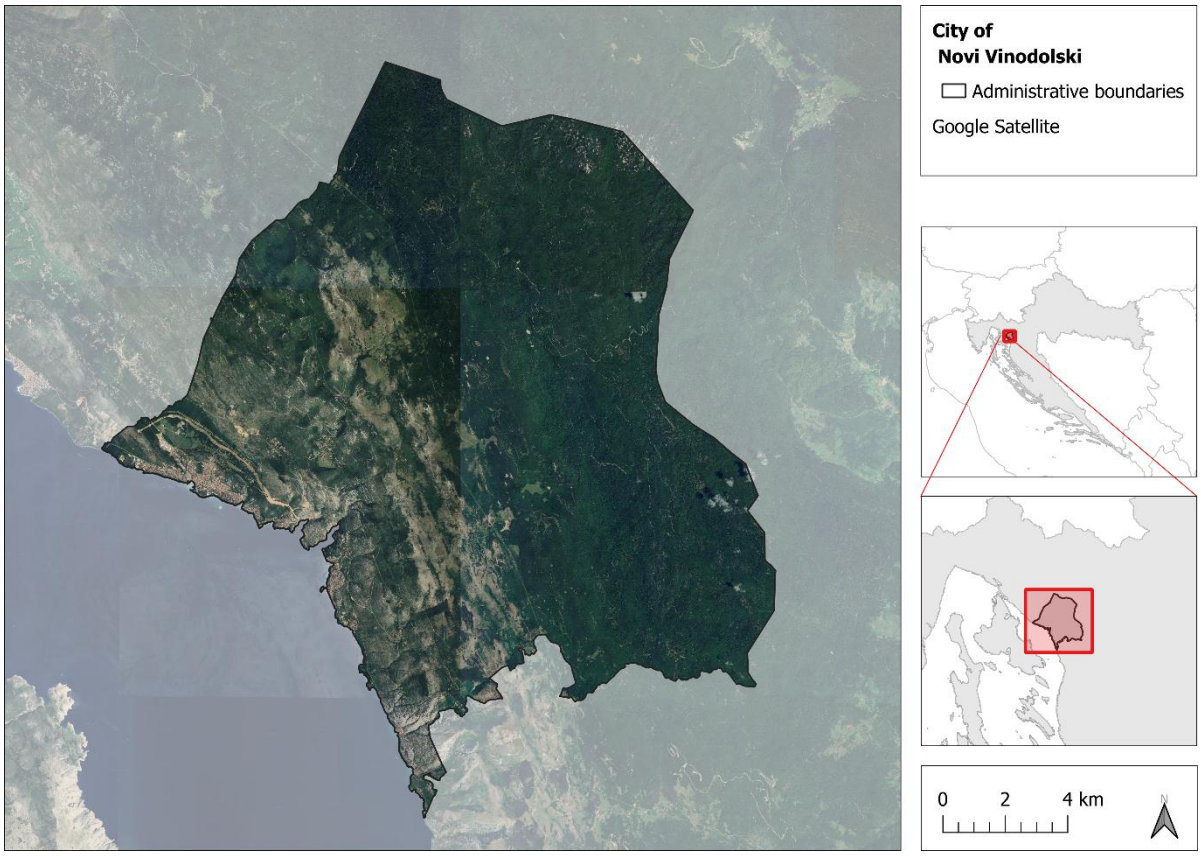

Figure 1.2. Location and administrative boundaries of the City of Novi Vinodolski.

1.1.2. Climate

According to the Köppen-Geiger climate classification, the climate of the Municipality of Vinodolska općina is classified as Cfb (*Temperate oceanic climate with warm summers*), while the and the City of Novi Vinodolski is predominantly classified as Cfb, with a narrow coastal strip exhibiting Cfa (*Humid subtropical climate with hot summers*) characteristics (Figure 1.3). Additionally, the eastern mountainous part of the City of Novi Vinodolski transitions into a Df climate (*humid continental climate*), characterized by colder winters and increased snowfall due to higher elevations.

Inland Climate (Cfb – Temperate oceanic climate with warm summers)

The Vinodol Valley and the surrounding inland areas of Vinodolska općina experience a Cfb climate, characterized by:

- Moderate temperatures throughout the year, with warm summers and cool, but not severe, winters.
- Higher precipitation levels, particularly during autumn and winter, due to the influence of moist air masses from the Adriatic Sea.
- Frequent orographic effects, as the surrounding mountains, particularly the Velika Kapela range, contribute to increased rainfall and cloud cover.
- Occasional snowfall in winter, especially in elevated areas, though it is generally not persistent due to moderate temperatures.

Mountain Climate (Df – Humid Continental Climate)

The eastern mountainous part of the City of Novi Vinodolski, at higher elevations, experiences a Df climate, characterized by:

- Colder winters, with temperatures often falling below freezing.
- Higher snowfall, which can accumulate over extended periods.
- More pronounced seasonality, with cooler summers compared to the lower-lying areas.

Coastal Climate (Cfa – Humid subtropical climate with hot summers)

The City of Novi Vinodolski and the immediate coastal strip exhibit a Cfa climate, which is distinguished by:

- Hot summers, with average daily temperatures frequently exceeding 25°C during July and August.
- Mild winters, with temperatures rarely dropping below freezing, due to the moderating influence of the Adriatic Sea.
- More evenly distributed precipitation throughout the year, although late summer and autumn can bring intense rainfall events, sometimes associated with Mediterranean cyclones.

- Occasional strong Bora (Bura) winds, particularly in winter, which can lead to sudden drops in temperature and dry conditions despite proximity to the sea.
- Mountainous Df areas contribute to seasonal snowmelt, which can impact river discharge and potential flooding during transitional seasons.

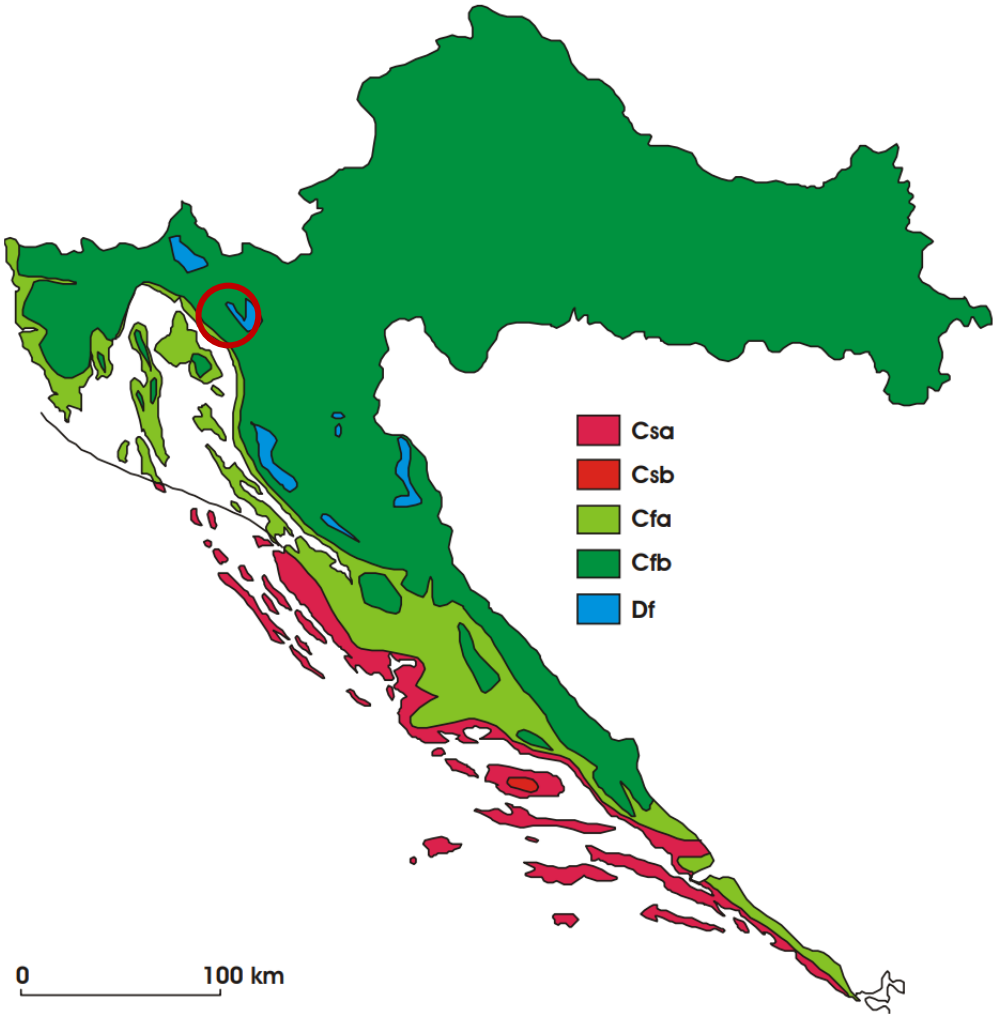

Figure 1.3. Geographical distribution of climate types according to W. Köppen in Croatia for the standard period 1961–1990 (Šegota & Filipčić, 2003.), with the location of the two pilot areas (red circle).

Climate Implications for Hydrology and Flood Risk

The combination of these two climate types has important implications for hydrology and flood risk in the area:

- Heavy rainfall events, particularly in autumn and winter, can lead to rapid runoff and flash flooding in low-lying and urbanized coastal areas.
- Orographic effects in the inland Cfb zone contribute to higher precipitation totals, increasing the risk of prolonged saturation and localized flooding.

- Summer convective storms, particularly in the Cfa zone, can produce short-duration, high-intensity rainfall, leading to pluvial flooding in urbanized areas.

The interaction between the coastal and inland climates, combined with the complex topography of the Vinodol Valley and the Adriatic coastline, makes these areas particularly relevant for climate change impact assessments, flood risk modeling, and hydrological studies.

1.1.3. Catchment characteristics

The area of the Municipality of Vinodolska općina was analyzed from the perspective of morphometric terrain features. The analysis included elevation, terrain slope, and aspect (orientation) of slopes. These analyses were carried out based on a digital elevation model (DEM) with a 10-meter resolution.

Figure 1.4 shows the elevation map with contour lines on a shaded relief. Elevations within the administrative area of the Municipality range from 16 to 1392 meters above sea level. The Vinodol Valley near the coastline is characterized by lower elevations, which increase towards inland in the northeast.

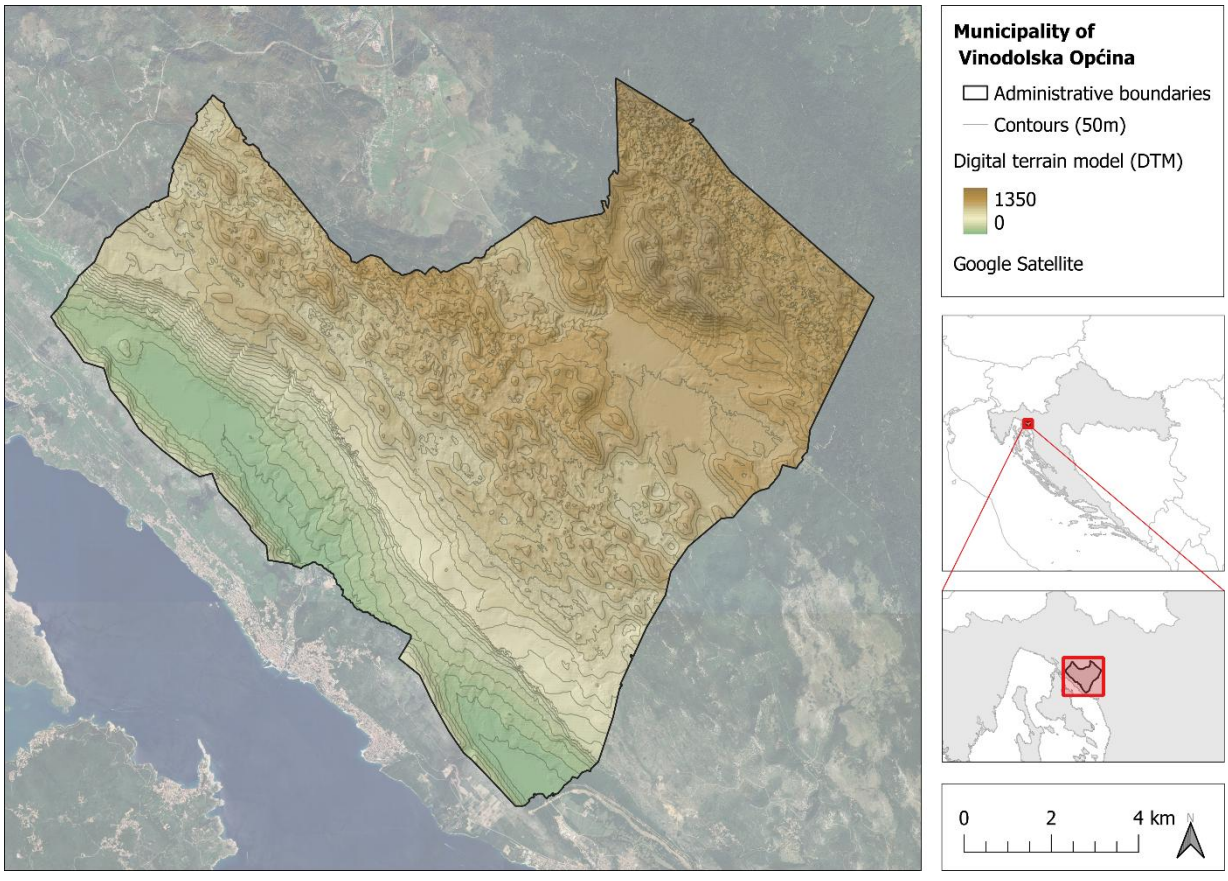

Figure 1.4. Elevation map with contour lines on a shaded relief for the Municipality of Vinodolska općina.

Figure 1.5 shows the terrain slope map derived from a 10-m digital terrain model. The map of the Municipality of Vinodolska općina reveals a varied slope distribution across the catchment. Steeper slopes, shown in red and orange, are primarily concentrated along the western edges and along distinct ridgelines and escarpments, indicating rugged terrain and elevated topography. In contrast, flatter areas, represented in green, are located mainly in the Vinodol Valley and northeastern parts of the catchment, corresponding to valleys and lower-lying terrain.

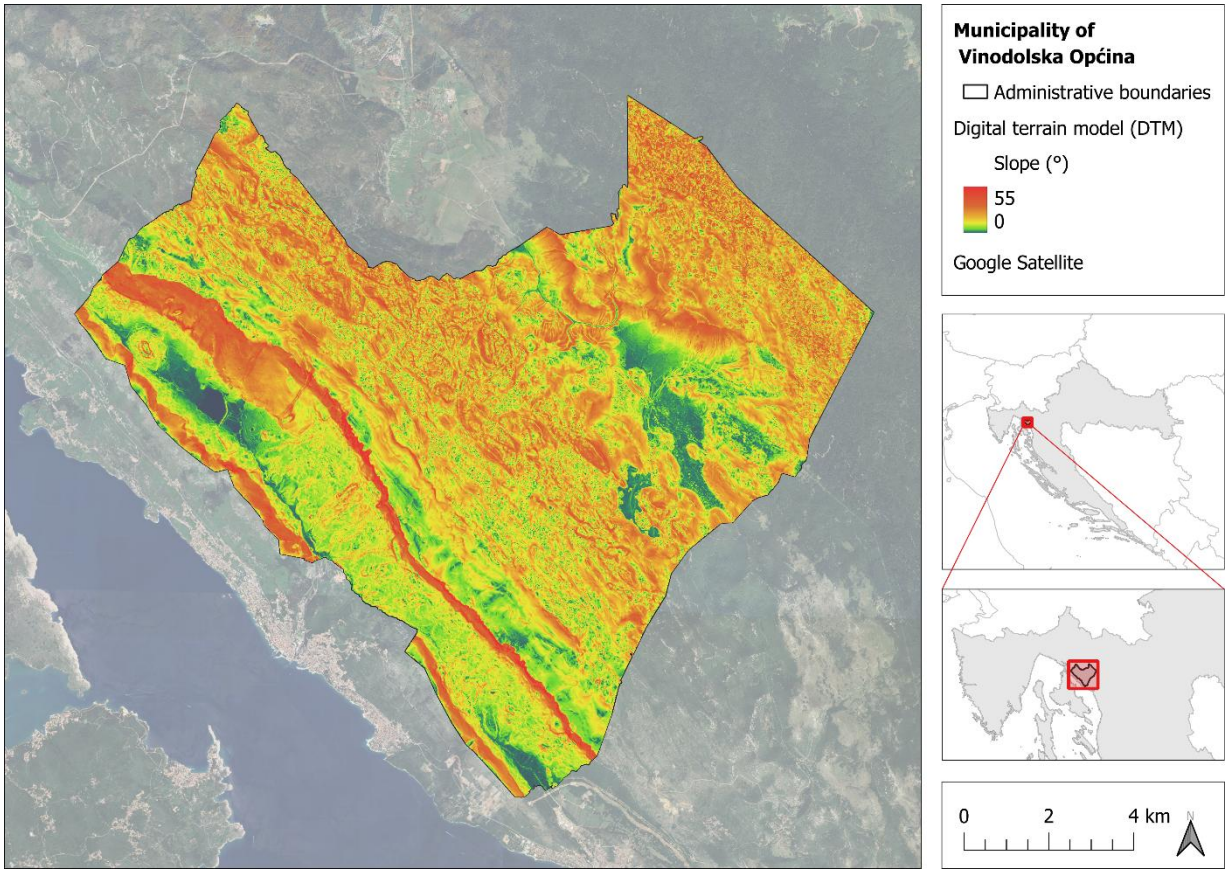

Figure 1.5. Terrain slope map for the Municipality of Vinodolska općina.

Figure 1.6 shows the terrain aspect map, indicating the orientation of slopes. The aspect map of the Municipality of Vinodolska općina, derived from a 10-m DTM, shows a heterogeneous distribution of slope orientations. The terrain faces all cardinal and intercardinal directions, with notable spatial patterns. South-facing slopes (purple) and southwest-facing slopes (red) dominate the central and western parts of the catchment, indicating areas with higher solar exposure. North-facing slopes (yellow-green) are also widely distributed, particularly along the steeper valley sides, suggesting cooler and moister microclimates. Eastern and southeastern slopes (turquoise to blue) appear mainly in the northeastern sections, while west and northwest aspects (orange to yellow) are common in elevated ridgelines. This diverse orientation reflects the complex terrain and influences factors such as vegetation, microclimate, and runoff patterns.

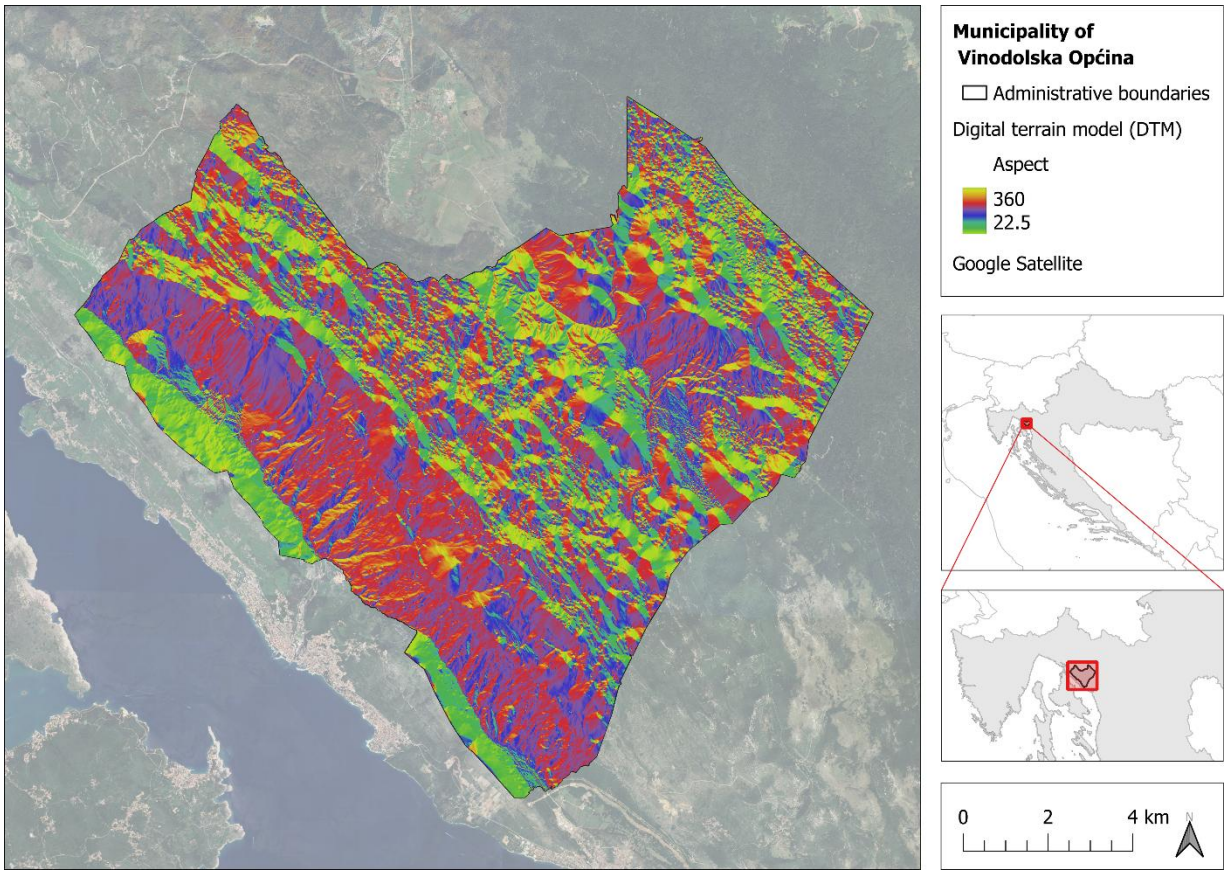

Figure 1.6. Terrain aspect map (orientation of slopes) for the City of Novi Vinodolski.

The area of the City of Novi Vinodolski was also analyzed from the perspective of morphometric terrain features. The analysis included elevation, terrain slope, and aspect (orientation) of slopes. These analyses were carried out based on a digital elevation model (DEM) with a 10-meter resolution.

Figure 1.7 shows the elevation map with contour lines on a shaded relief. Elevations within the administrative area of the City range from 0 to 1357 meters above sea level. The coastal area is characterized by lower elevations, which increase towards the east-northeast.

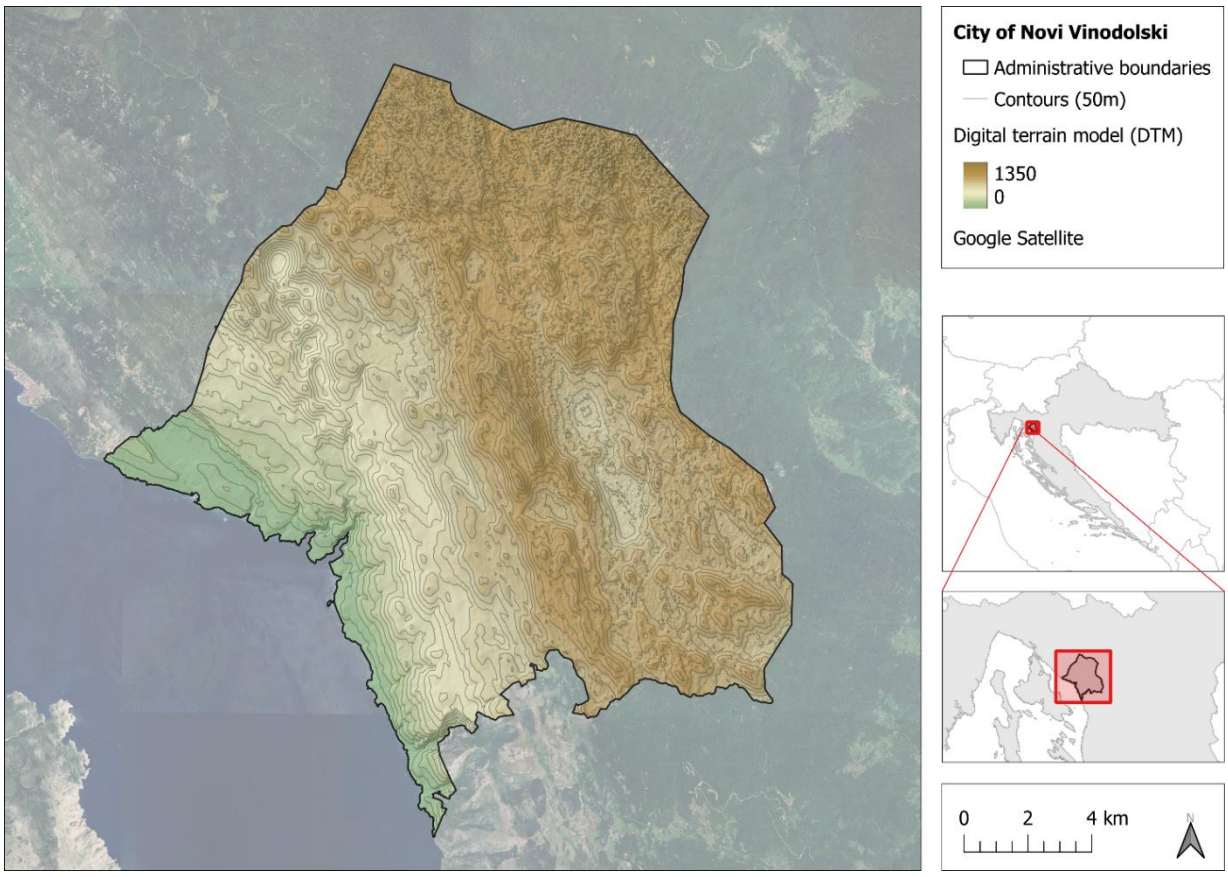

Figure 1.7. Elevation map with contour lines on a shaded relief for the City of Novi Vinodolski.

Figure 1.8 shows the terrain slope map. The slope map of the City of Novi Vinodolski, derived from the 10-m DTM, displays a terrain with generally steep characteristics, especially in the western and central parts of the catchment. These areas, marked in red and orange, indicate slopes exceeding 30° and in some cases reaching over 50°, suggesting rugged and elevated topography. In contrast, the flatter areas, shown in green, are mostly located along the coastal zones and some interior valleys, representing low-lying or gently sloped terrain. The slope variability across the catchment reflects its complex geomorphology, influencing surface runoff, erosion potential, and suitability for development or land use planning.

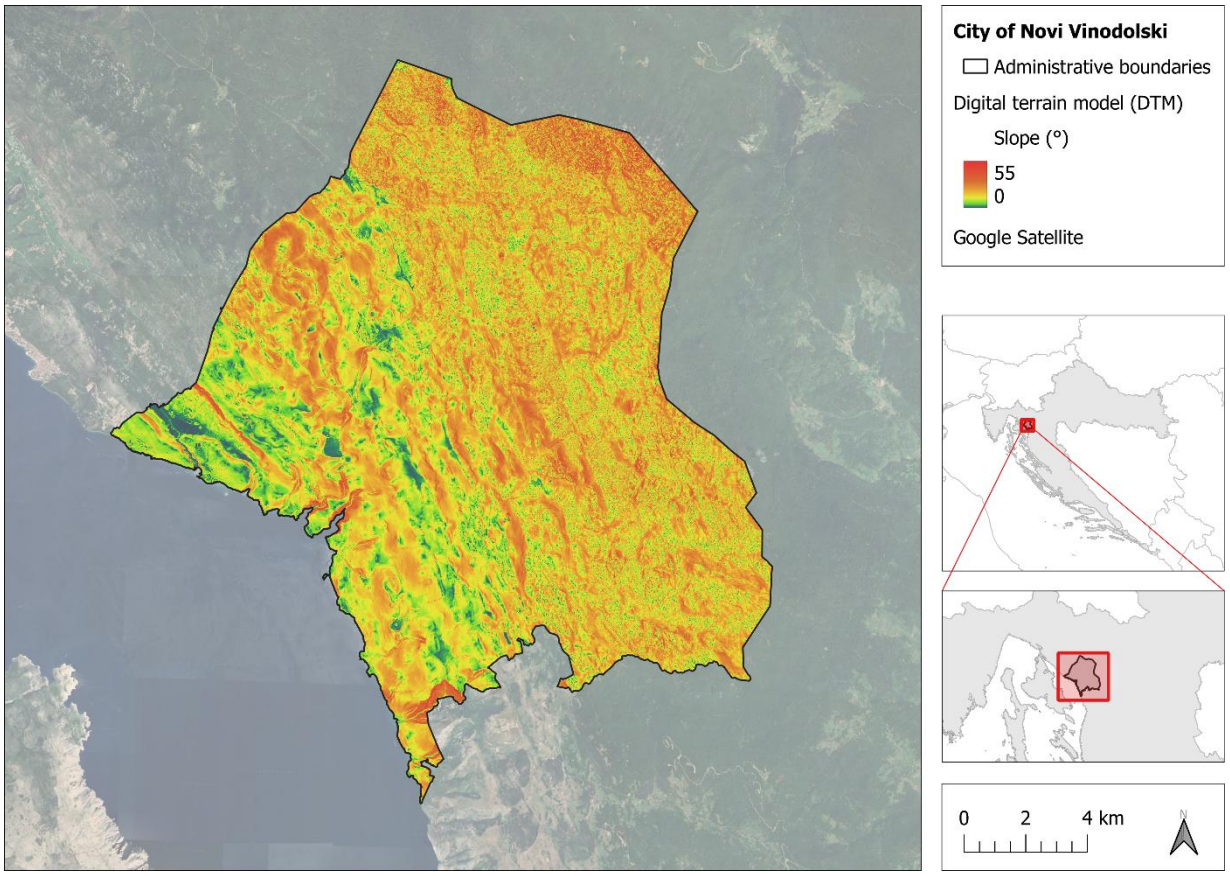

Figure 1.8. Terrain slope map for the City of Novi Vinodolski.

Figure 1.9 shows the terrain aspect map, indicating the orientation of slopes. The aspect map of the City of Novi Vinodolski derived from the 10-m DTM reveals a highly diverse terrain orientation pattern. The slopes face in all cardinal and intercardinal directions, as indicated by the multicolored distribution. South-facing slopes (purple) and southwest-facing slopes (red) dominate the coastal and southwestern parts of the catchment, where steeper terrain is prevalent. Northeast-facing (green) and east-facing slopes (turquoise) are more common in the central and northeastern regions, while north-facing slopes (yellow-green) appear sporadically throughout the catchment. This varied aspect distribution is characteristic of rugged karst terrain and has significant implications for local microclimates, vegetation cover, solar radiation exposure, and hydrological response.

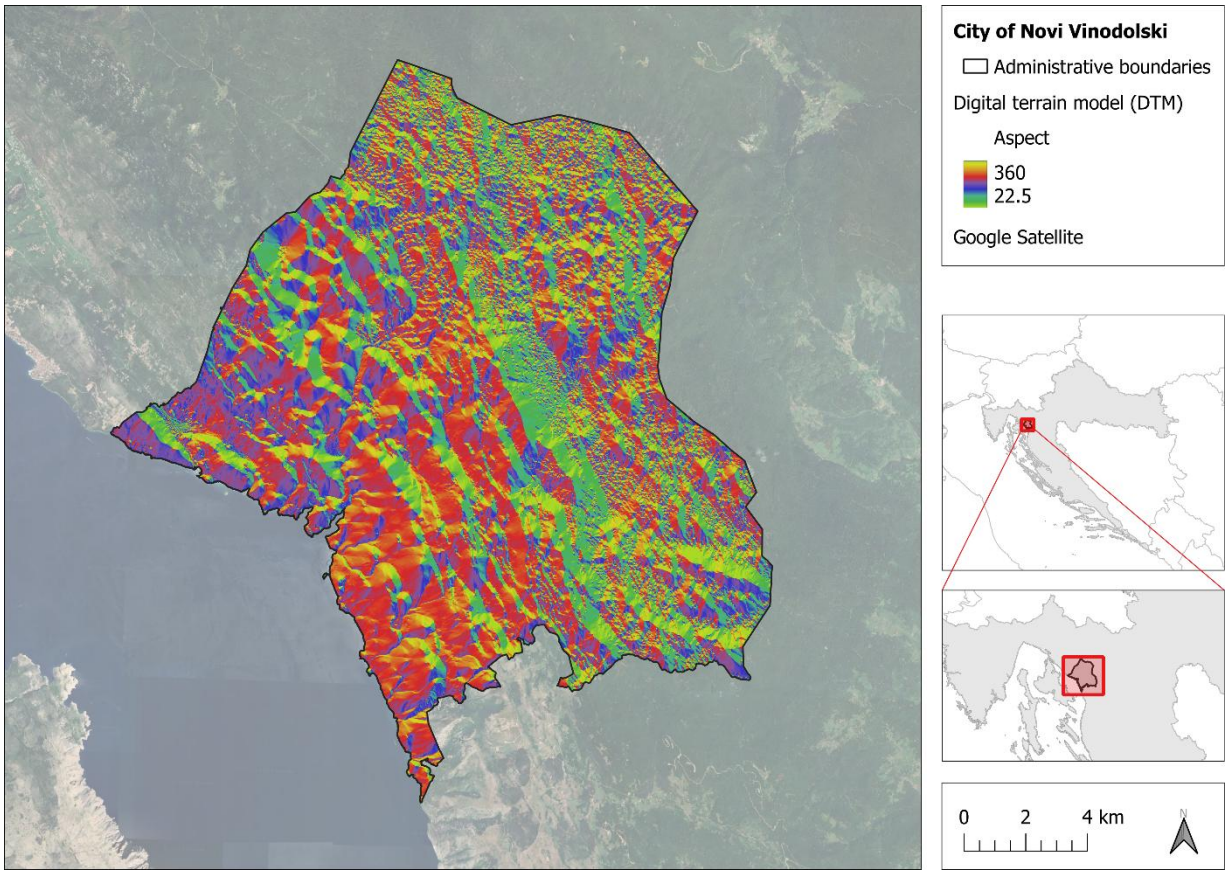

Figure 1.9. Terrain aspect map (orientation of slopes) for the City of Novi Vinodolski.

1.2. Rainfall regime

To better understand the full scope of the rainfall regime at the pilot sites it is crucial to analyse various rainfall characteristics, such as total rainfall, number of rainy days, number of heavy rainfall days, and maximum daily rainfall. These characteristic values are determined from a time series of observed daily rainfall at the station Crikvenica from the period 1990-2023 for the Municipality of Vinodolska općina and station Novi Vinodolski from the period 1991-2023 for the City of Novi Vinodolski. Each of these series provides different insights into the nature of rainfall patterns and their potential impacts. In particular, for the purpose of this study the following rainfall indicators are investigated:

- **Total rainfall** refers to the cumulative daily rainfall over a specific period, such as year, season or month. This is one of the most fundamental indicators of a region's climate and hydrological regime. It provides a broad view of how much water is available from rainfall at a specific site.
- **Number of rainy days** (daily rainfall above 0.5 mm) provides insight into how often rainfall events occur in a given period (annually, seasonally or monthly). This indicator helps to assess the general distribution and frequency of rainfall. Like dry days, understanding rainy periods is essential for managing irrigation systems and planning water storage and distribution.
- **Number of heavy rainfall days** (daily rainfall exceeding 20 mm) is a key indicator of extreme weather events. These events are often associated with floods and erosion. Understanding the frequency of heavy rainfall days is critical for flood risk management, designing infrastructure, and preparing for natural disasters.
- **Maximum daily rainfall** represents the most intense rainfall event over a given period (annually, seasonally or monthly). This statistic highlights the extreme limits of rainfall. Tracking maximum daily rainfall helps to assess flood risk and plan mitigation measures. It also helps predict the likelihood of rare but catastrophic events, ensuring preparedness in the face of climate extremes.

Based on these series of different rainfall indicators, we perform several analyses, which include time series plots, anomaly detection, trend assessments, and inter-annual variability. By conducting these types of analyses, we can gain valuable insights for understanding the impacts of climate variability and long-term climate change.

First, we plot time series data and determine the long-term trend using a Mann-Kendall test. Analysing time series data helps detect trends that may indicate shifts in regional climate patterns. Although some fluctuations are part of natural variability, detecting significant long-term trends can provide early signs of changing rainfall regimes. Conducting statistical tests like the Mann-Kendall test ensures that observed trends are not merely random variations but reflect significant changes over time. This is done for both annual time series and seasonal time series (3-month segments).

Next, we compute the anomalies that provide insights into the extent to which particular years deviate from the long-term mean. These anomalies are important for evaluating the impact of climate extremes, such as floods or prolonged droughts. In addition, the five-year running mean helps identify underlying trends that might not be obvious from short-term fluctuations.

Finally, we perform statistical analysis of monthly rainfall data and present the results in both table and figure format. While table data gives precise information, the boxplot effectively shows how rainfall distribution changes throughout the year, both in terms of typical behaviour (median and mean) and the variation (range and outliers). We assess the following statistical metrics: mean, minimum, 25-th percentile, median (50-th percentile), 75-th percentile, maximum, standard deviation, skewness and kurtosis.

1.2.1. Statistical Analysis of Annual and Monthly Rainfall at the Crikvenica station

Figure 1.10 shows a time series plot and the trend of annual rainfall at the Crikvenica station for the period 1990-2023. There is some variability in the annual rainfall, with a mean value of 1270 mm. The highest recorded rainfall amount was 1803.9 mm, and the lowest recorded rainfall amount was 752.4 mm. Despite the increasing trend, the Mann-Kendall test indicates that the trend is not strong enough to be considered statistically significant at the 95% confidence level.

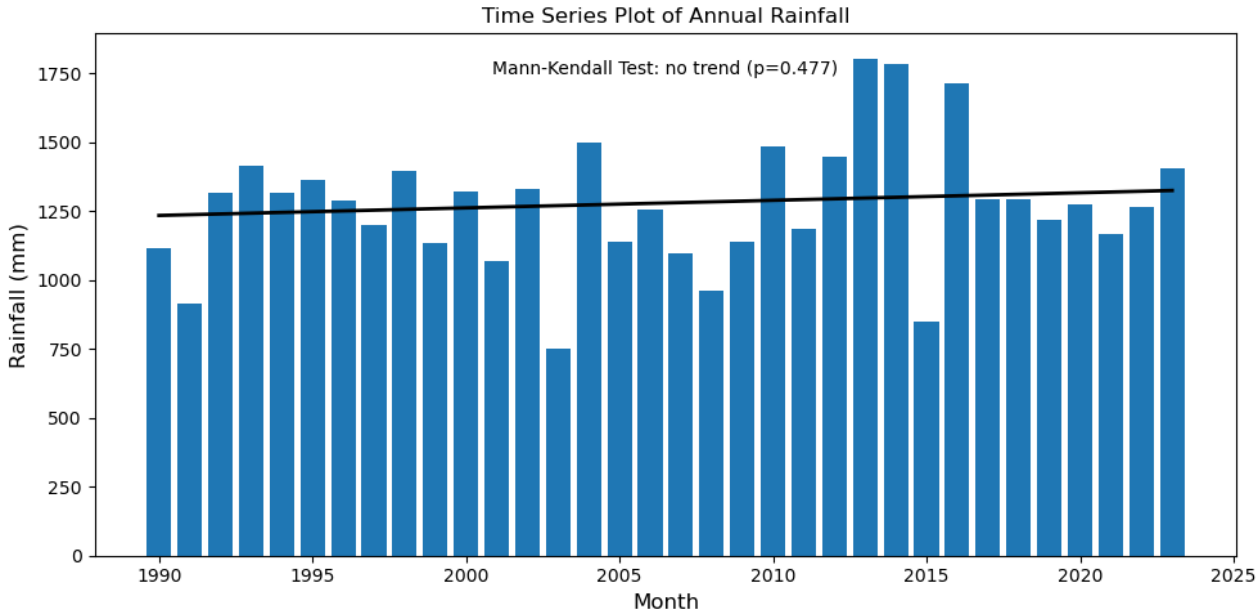

Figure 1.10. Time series of annual rainfall and trend line at the Crikvenica station (1990-2023).

Figure 1.11 shows a plot of the annual rainfall anomaly in combination with a five-year running mean. In the early 1990s and 2000s, the anomalies were mostly negative (below-average rainfall). A series of positive anomalies (above average) occurs from around 2010 to 2017, followed by more neutral anomalies in the recent period. The five-year running mean shows decadal variability.

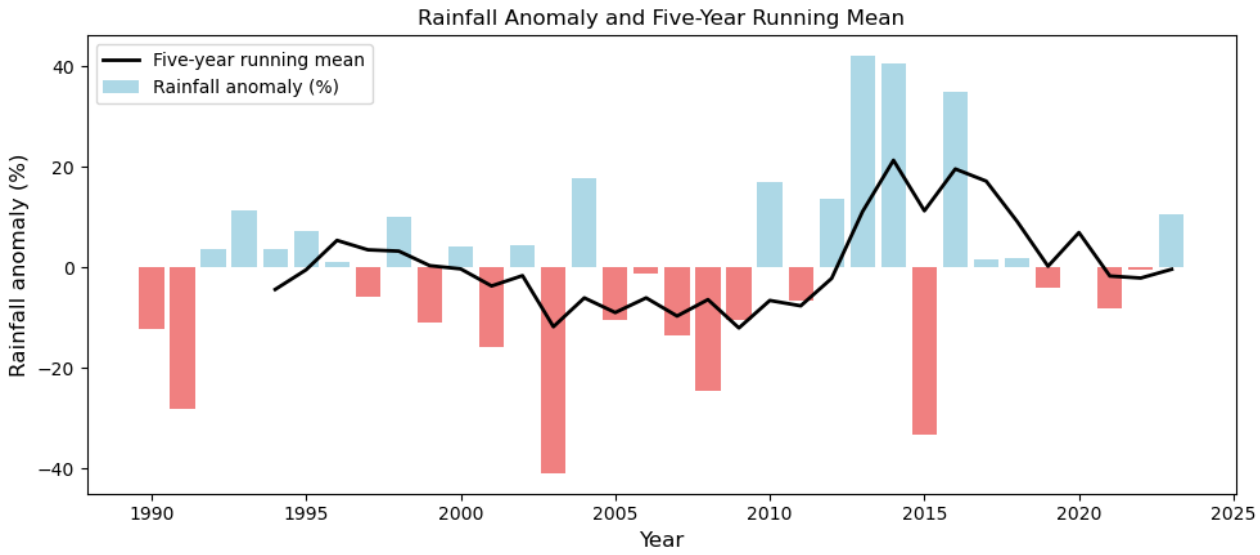

Figure 1.11. Time series of annual rainfall anomalies at the Crikvenica station (1990-2023).

Figure 1.12 shows a time series plot and the trend of seasonal rainfall (cumulative 3-month rainfall) at the Crikvenica station for the period 1990-2023. The highest seasonal rainfall is observed in autumn, followed by winter and spring. The lowest amount of rainfall occurs in summer. There is some variability in all seasons, but the Mann-Kendall test indicates that the trend is statistically significant only for the winter season (95% confidence level), where an increasing trend of 5 mm of total seasonal rainfall per year is observed.

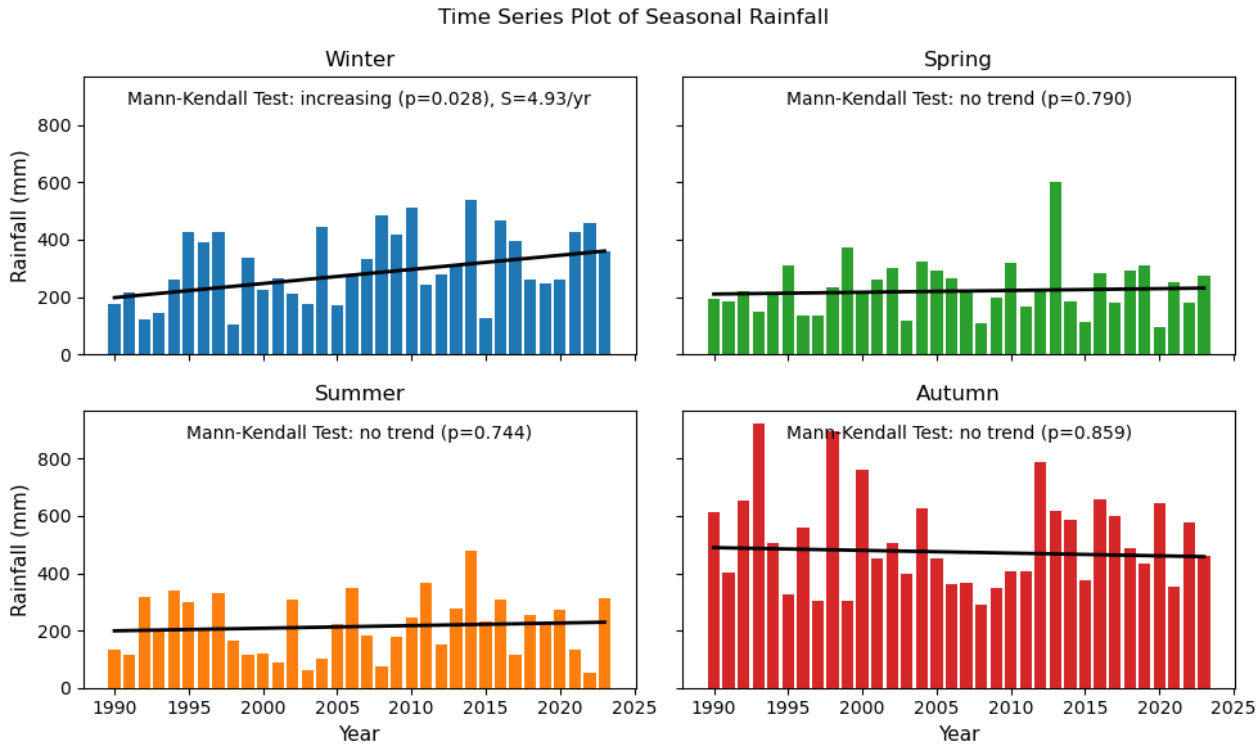

Figure 1.12. Time series of 3-month rainfall for different seasons and trend lines at the Crikvenica station (1990-2023).

The statistical analysis of annual and monthly rainfall is shown in Figure 1.13. Overall, the autumn months (especially October and November) have the highest amount of rainfall (evident from the mean and median values) and the greatest variability (evident from the spread of the boxes and whiskers), while the summer months (July and August) have the lowest amount of rainfall and the least variability.

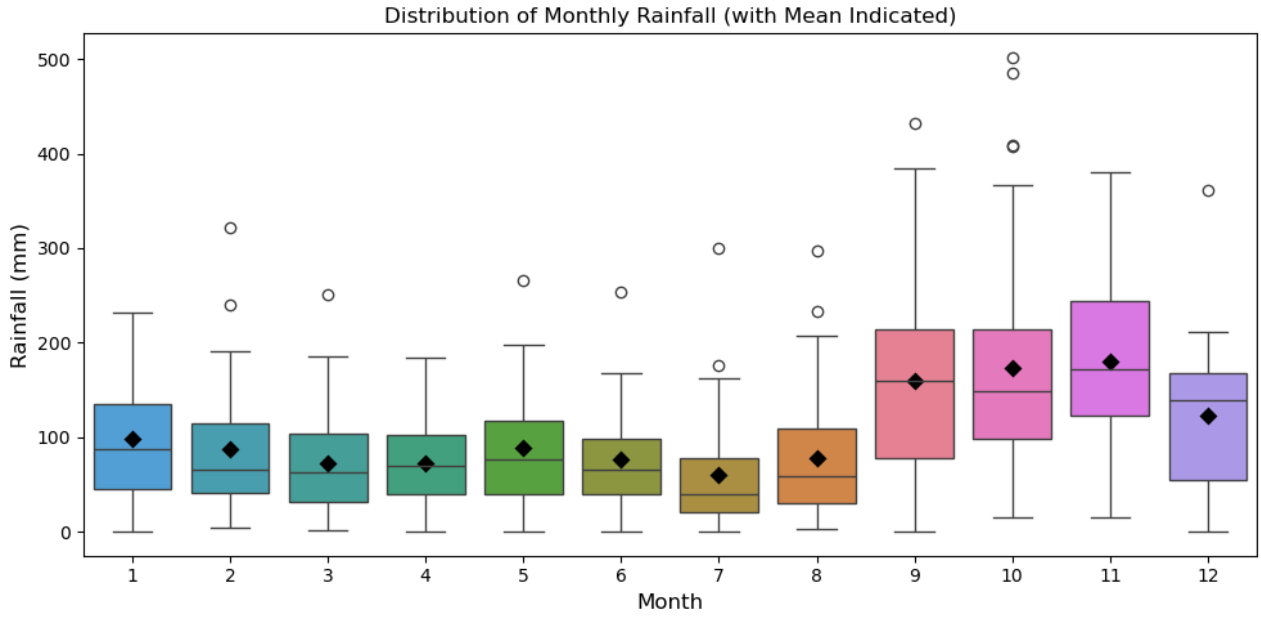

Figure 1.13. Inter-annual distribution of monthly rainfall at Crikvenica station (1990-2023).

Figure 1.14 shows a time series plot and the trend of rainy days at the Crikvenica station for the period 1990-2023. There is some variability in the number of rainy days, with a mean value of 26.9 % of rainy days per year. Despite the increasing trend, the Mann-Kendall test indicates that the trend is not strong enough to be considered statistically significant at the 95% confidence level.

Figure 1.15 shows a plot of the anomaly of rainy days in combination with a five-year running mean. In the early 1990s and 2000s, the anomalies were mostly negative (below-average rainfall). A series of positive anomalies (above average) occurs from around 2009 to the 2015, followed by more neutral anomalies in the recent period. The five-year running mean shows decadal variability.

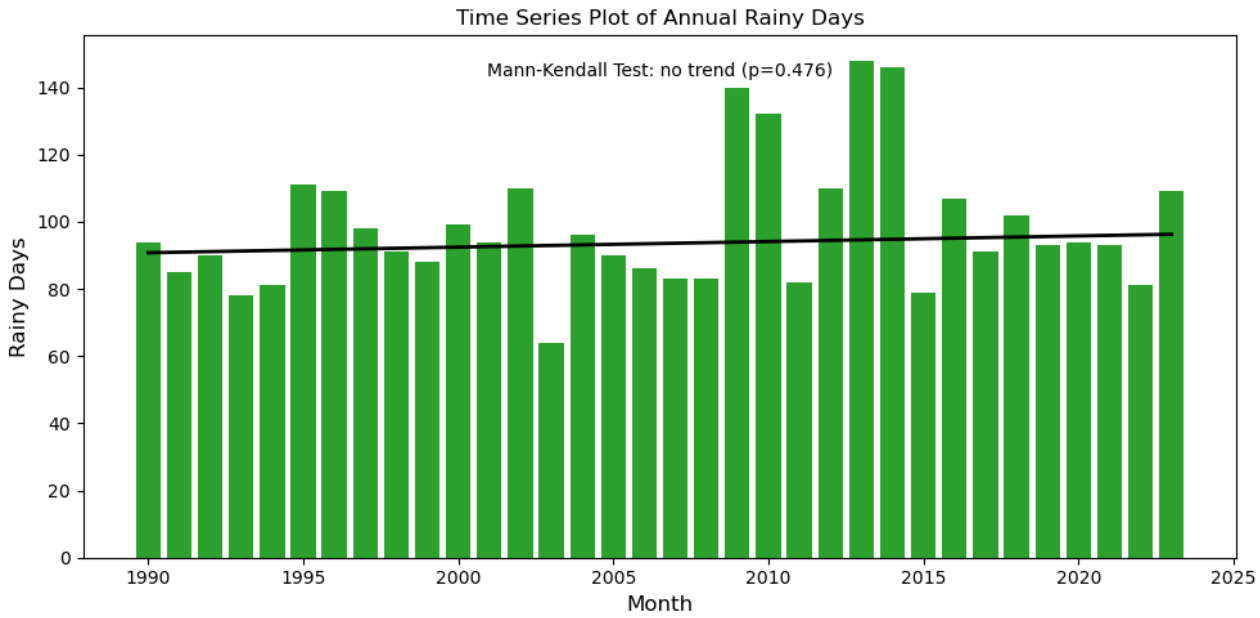

Figure 1.14. Time series of annual rainy days (H > 0.5 mm) and trend line at the Crikvenica station (1990-2023).

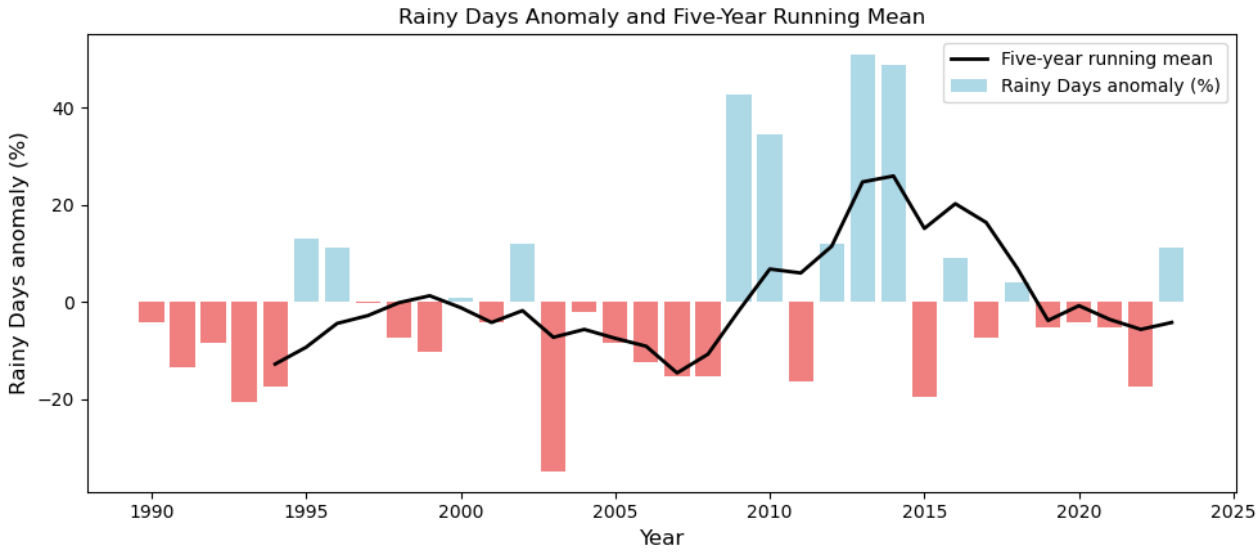

Figure 1.15. Time series of annual rainy days anomalies at the Crikvenica station (1990-2023).

Figure 1.16 shows a time series plot and the trend of seasonal number of rainy days (cumulative 3-month number) at the Crikvenica station for the period 1990-2023. The highest number of rainy days is observed in winter and autumn. The lowest number of rainy days is observed in summer. There is some variability in all seasons, but the Mann-Kendall test indicates that the trends are statistically significant (95% confidence level) only for Winter, where we a trend indicates an increase of 3.7 rainy days per decade.

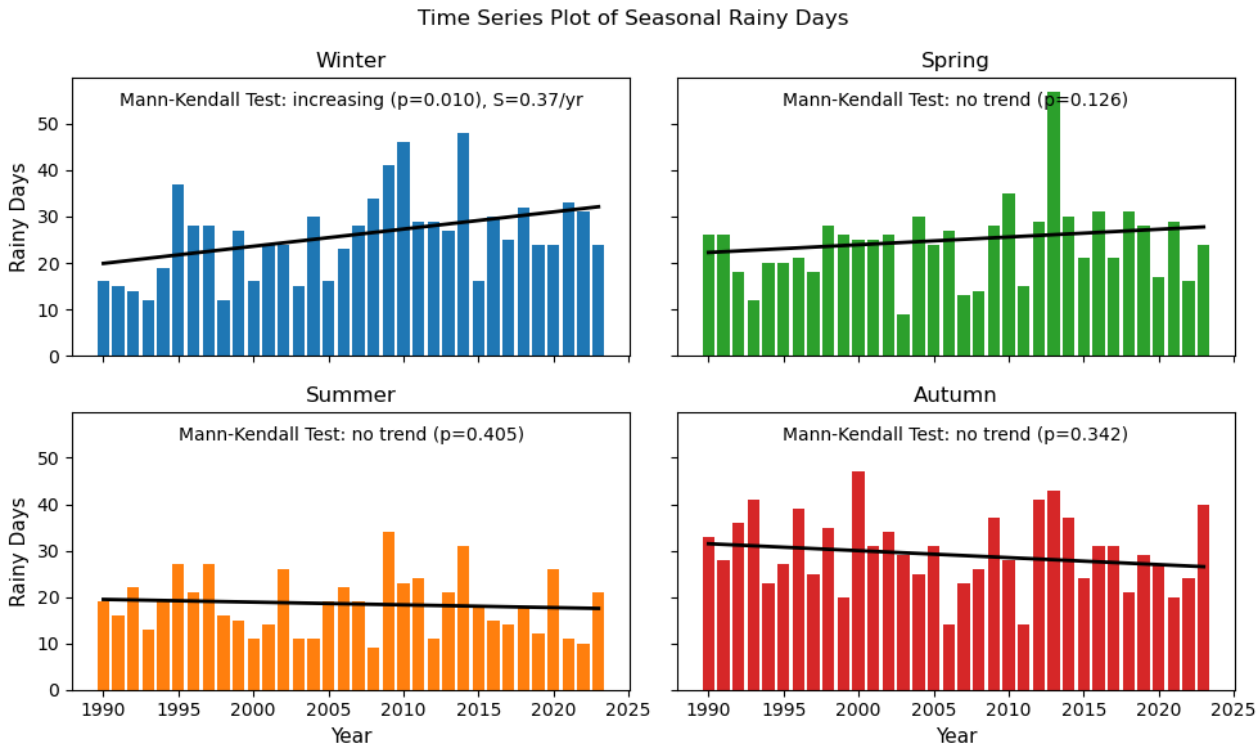

Figure 1.16. Time series of 3-month rainy days for different seasons and trend lines at the Crikvenica station (1990-2023).

The statistical analysis of annual and monthly number of rainy days is shown in Figure 1.17. Overall, the autumn and winter months (especially November) have the highest number of rainy days (evident from the mean and median values). The summer months (July and August) have the lowest number of rainy days and the least variability (July).

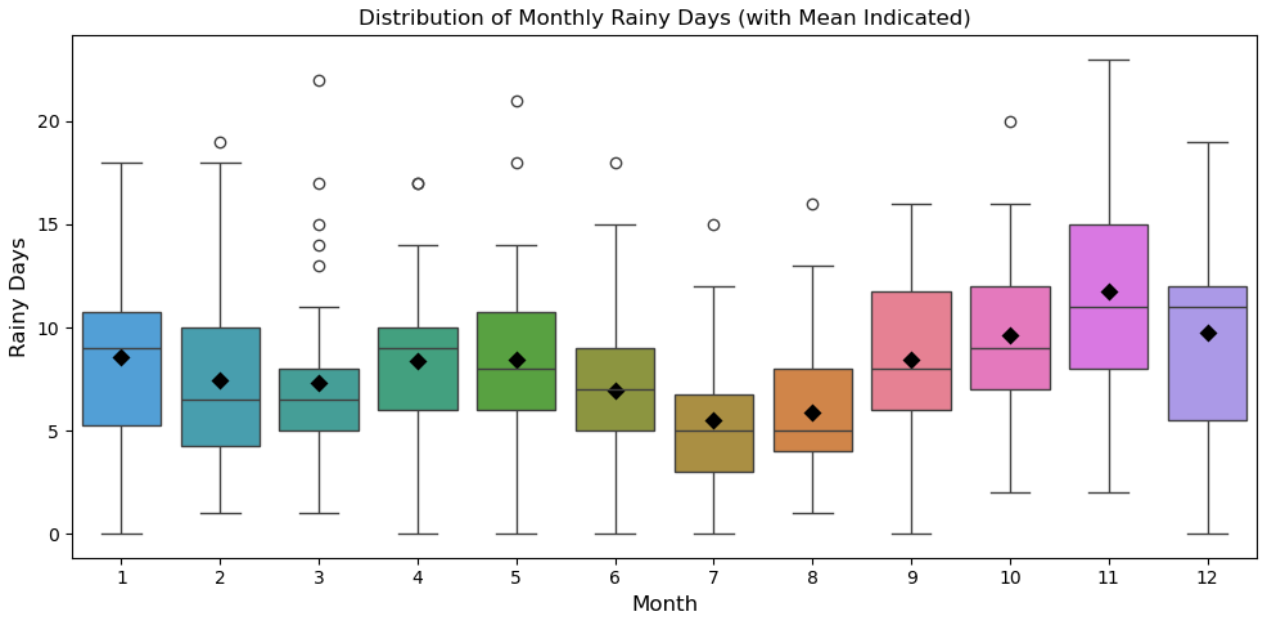

Figure 1.17. Inter-annual distribution of monthly rainy days at Crikvenica station (1990-2023).

Figure 1.18 shows a time series plot and the trend of heavy rainfall days (number of days where rainfall exceeds 20 mm) at the Crikvenica station for the period 1990-2023. There is some variability in the number of heavy rainfall days, with a mean value of 5.5 % of heavy rainfall days per year. The Mann-Kendall test indicates that the trend is not statistically significant at the 95% confidence level.

Figure 1.19 shows a plot of the anomaly of heavy rainfall days in combination with a five-year running mean. 2000s were characterised by alternating positive and negative anomalies, while in 2013, 2014 and 2016 we have some prominent peaks (significant above-average number of heavy rainfall days). The five-year running mean shows a decadal variability.

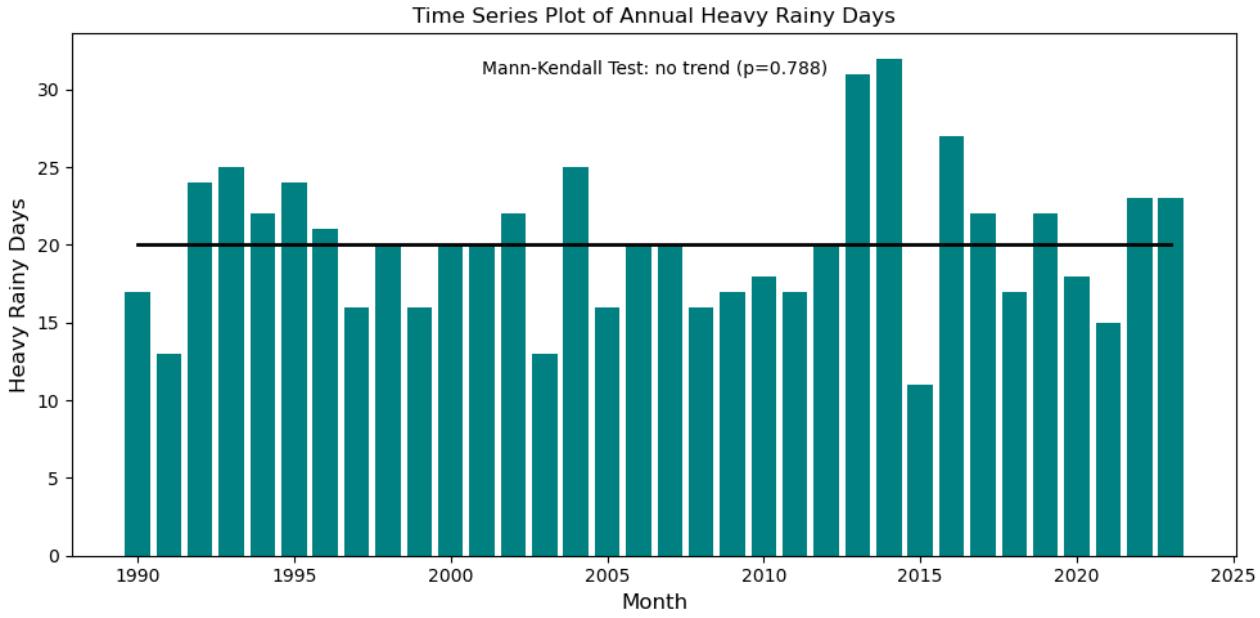

Figure 1.18. Time series of annual heavy rainfall days (H > 20 mm) and trend line at the Crikvenica station (1990-2023).

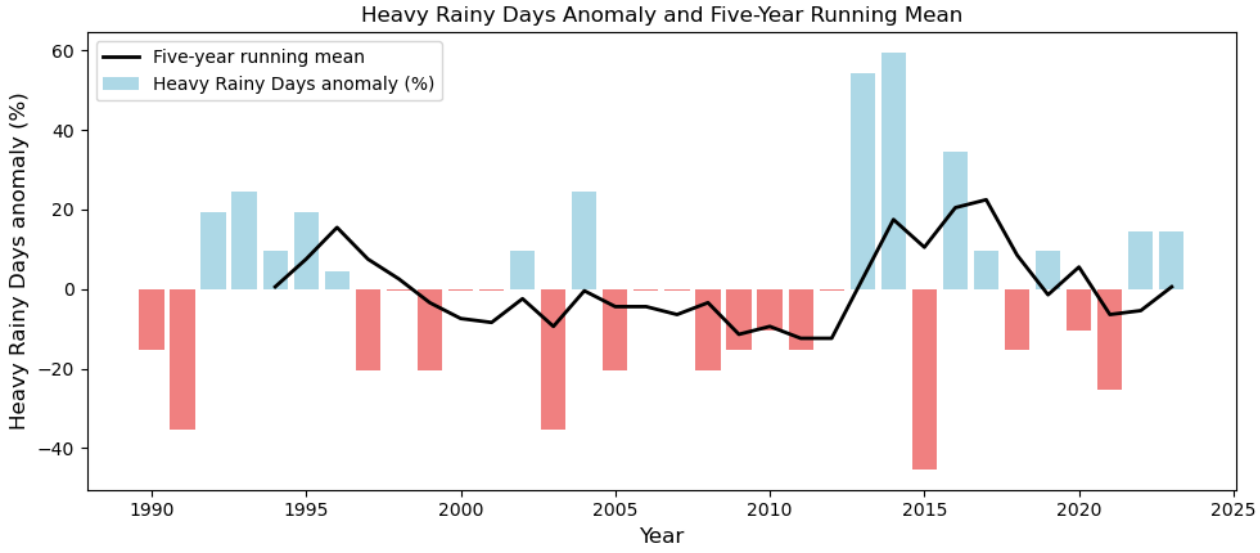

Figure 1.19. Time series of annual heavy rainfall days anomalies at the Crikvenica station (1990-2023).

Figure 1.20 shows a time series plot and the trend of seasonal number of heavy rainfall days (cumulative 3-month number) at the Crikvenica station for the period 1990-2023. The highest number of heavy rainfall days is observed in autumn. The lowest number of rainy days is observed in summer. There is some variability in all seasons, but the Mann-Kendall test indicates that the trend is statistically significant only for the winter season (95% confidence level), where an increasing trend of 1.3 heavy rainfall days per decade (10 years) is observed.

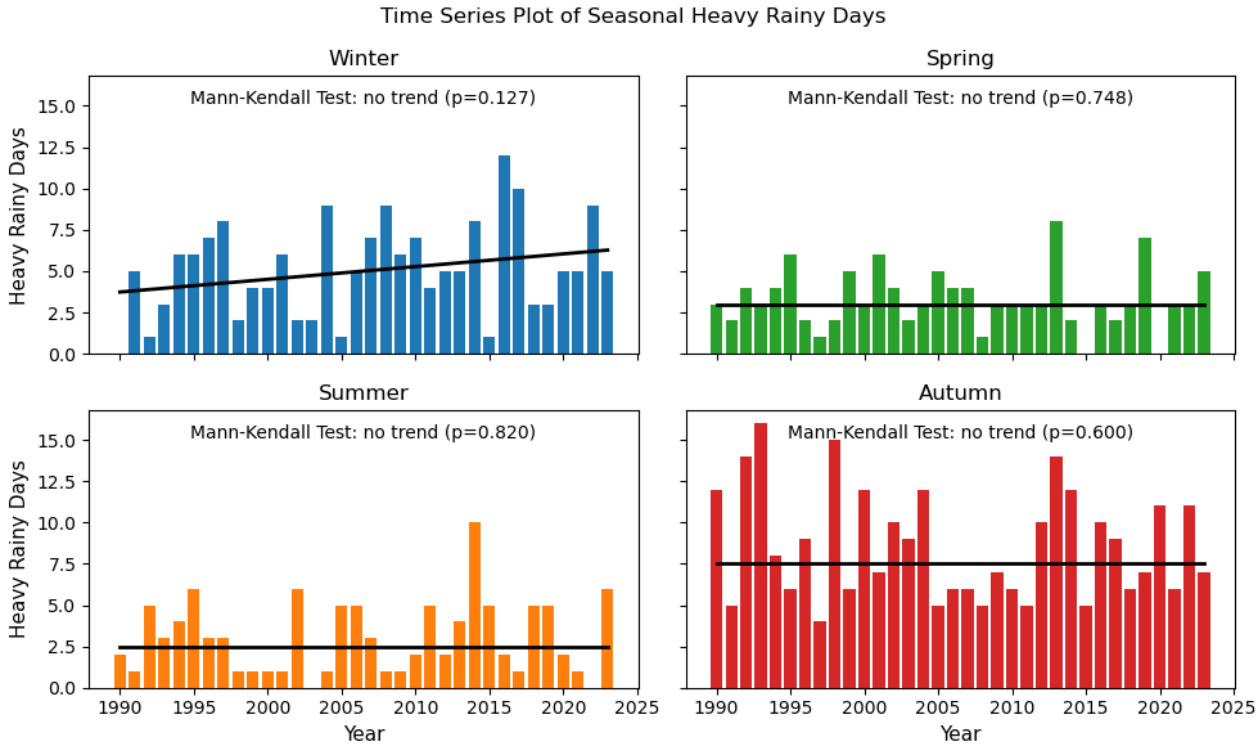

Figure 1.20. Time series of 3-month heavy rainfall days for different seasons and trend lines at the Crikvenica station (1990-2023).

The statistical analysis of annual and monthly number of heavy rainfall days is shown in Figure 1.21. Overall, only autumn months stand out (especially September and November) with the highest number of heavy rainfall days (evident from the mean and median values), and larger variability (evident from the spread of the boxes and whiskers). The summer months (July and August) have the lowest number of heavy rainfall days and the least variability.

Figure 1.22 shows a time series plot and the trend of annual maximum daily rainfall at the Crikvenica station for the period 1990-2023. There is a noticeable variability in the maximum daily rainfall amount, with a maximum 191.2 mm of daily rainfall. Despite the increasing trend, the Mann-Kendall test indicates that the trend is not strong enough to be considered statistically significant at the 95% confidence level.

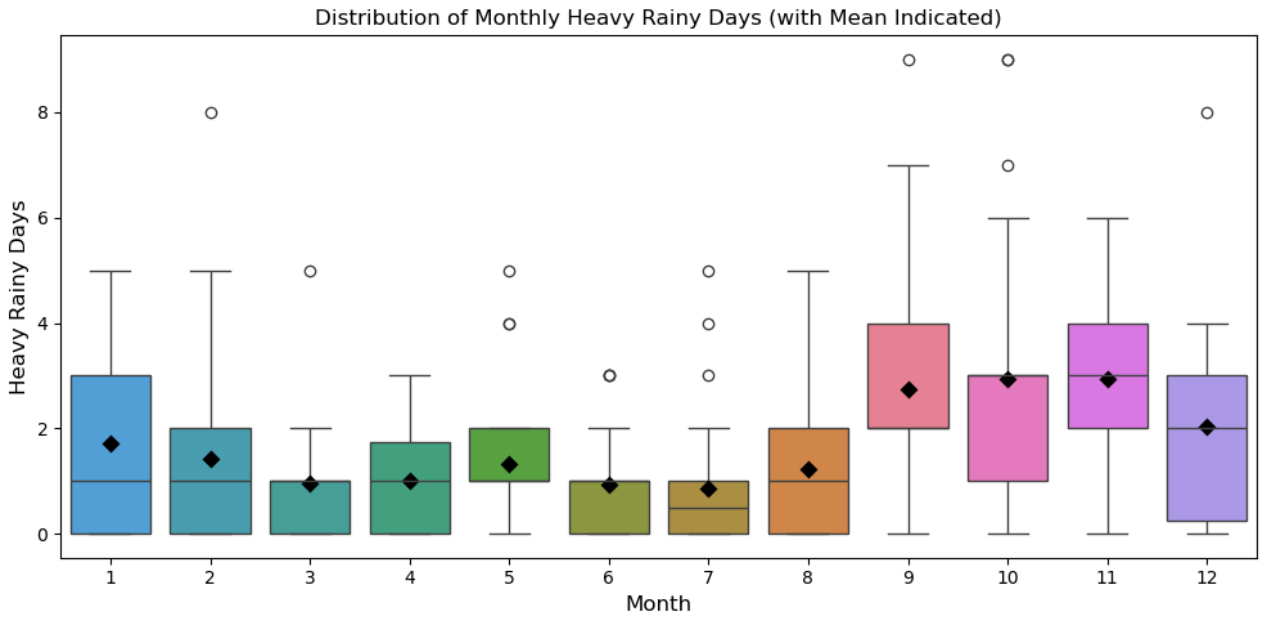

Figure 1.21. Inter-annual distribution of monthly heavy rainfall days at Crikvenica station (1990-2023).

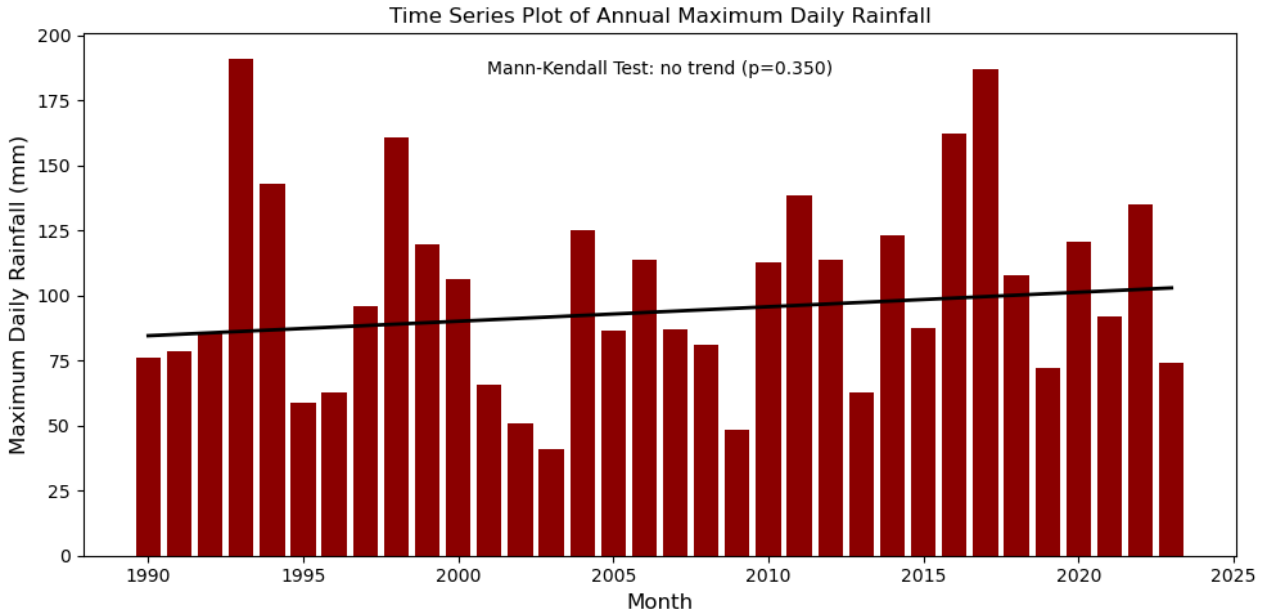

Figure 1.22. Time series of annual maximum daily rainfall and trend line at the Crikvenica station (1990-2023).

Figure 1.23 shows a plot of the anomaly of maximum daily rainfall in combination with a five-year running mean. In the entire period the anomalies were mostly highly variable, with interchanging 2-3 years of negative followed by positive anomalies. The five-year running mean shows a multidecadal variability.

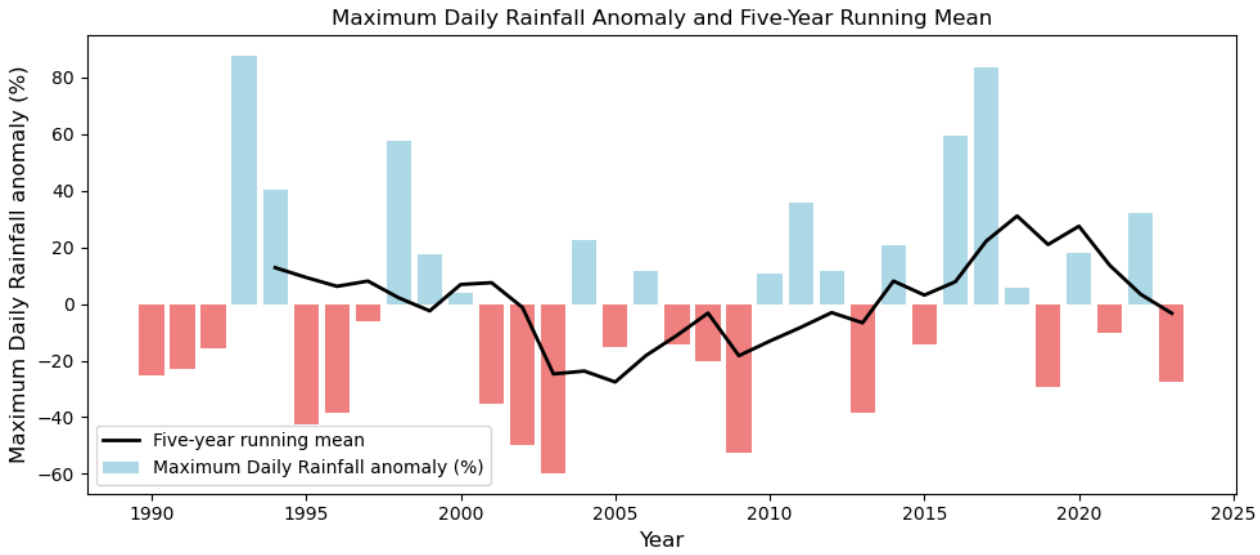

Figure 1.23. Time series of annual maximum daily rainfall anomalies at the Crikvenica station (1990-2023).

Figure 1.24 shows a time series plot and the trend of seasonal maximum daily rainfall (3-month maximum) at the Crikvenica station for the period 1990-2023. The highest maximum daily rainfall is observed in autumn. The lowest maximum daily rainfall is observed in spring (lower variability) and summer (higher variability). There is some variability in all seasons, but the Mann-Kendall test indicates that the trend is not statistically significant (95% confidence level).

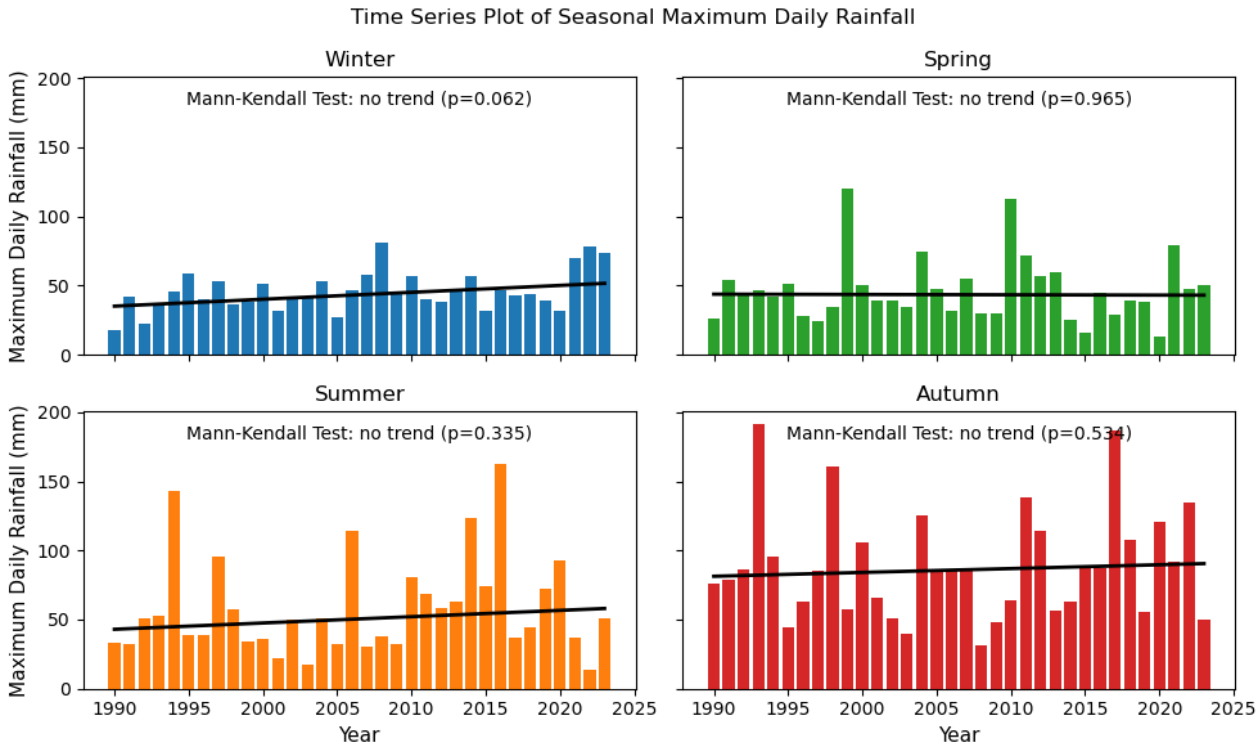

Figure 1.24. Time series of 3-month maximum daily rainfall for different seasons and trend lines at the Crikvenica station (1990-2023).

The statistical analysis of annual and monthly maximum daily rainfall is shown in Figure 1.25. Overall, autumn months have the highest maximum daily rainfall, with September and October having the highest average values (evident from the mean and median values), and having the highest extremes. Variability is similar for all months. The summer months (July) have the lowest maximum daily rainfall amounts and the least variability.

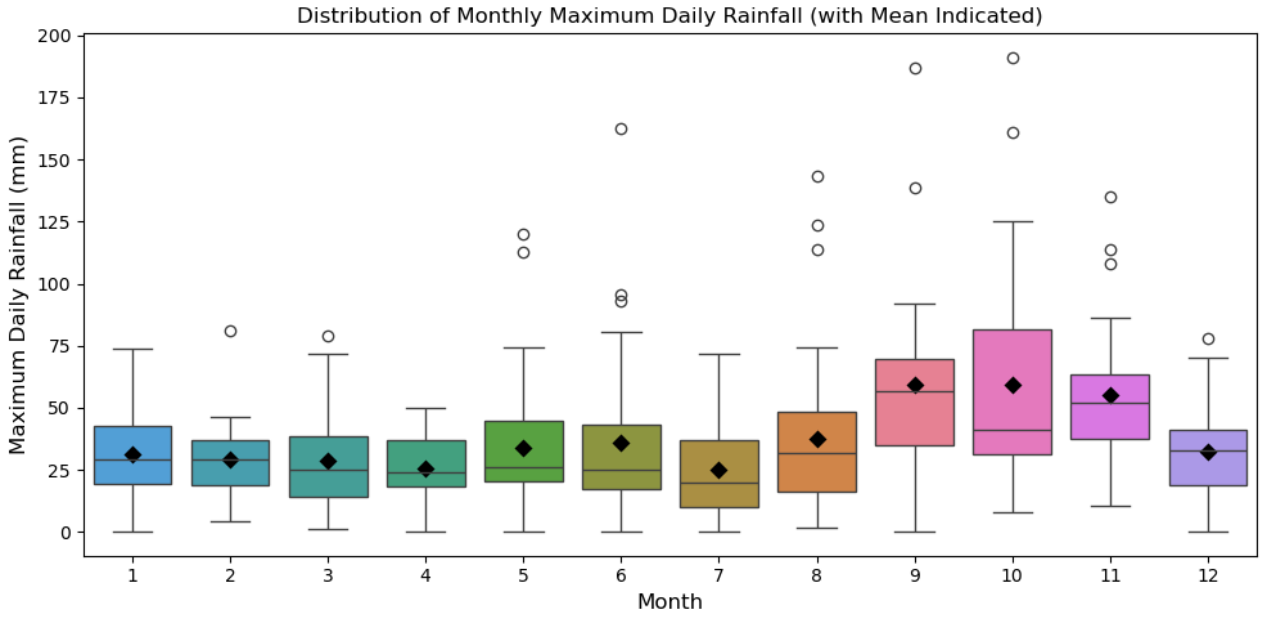

Figure 1.25. Inter-annual distribution of monthly maximum daily rainfall at Crikvenica station (1990-2023).

1.2.2. Statistical Analysis of Annual and Monthly Rainfall at the Novi Vinodolski station

Figure 1.26 shows a time series plot and the trend of annual rainfall at the Novi Vinodolski station for the period 1991-2023. There is some variability in the annual rainfall, with a mean value of 1250 mm. The highest recorded rainfall amount was 1703.0 mm, and the lowest recorded rainfall amount was 655.2 mm. Despite the increasing trend, the Mann-Kendall test indicates that the trend is not strong enough to be considered statistically significant at the 95% confidence level.

Figure 1.27 shows a plot of the annual rainfall anomaly in combination with a five-year running mean. In the early 1990s the anomalies where slightly positive, while during the 2000s, the anomalies were mostly negative (below-average rainfall). A series of positive anomalies (above average) occurs from 2013 to 2017, and then again in 2022 and 2023. The five-year running mean shows decadal variability.

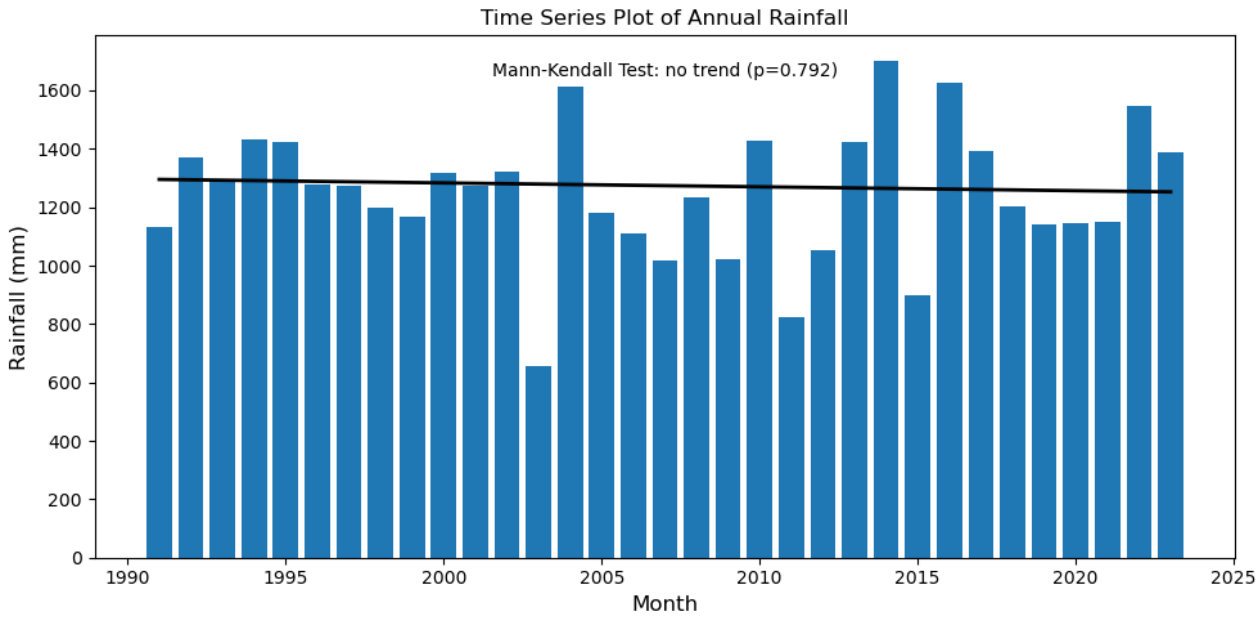

Figure 1.26. Time series of annual rainfall and trend line at the Novi Vinodolski station (1991-2023).

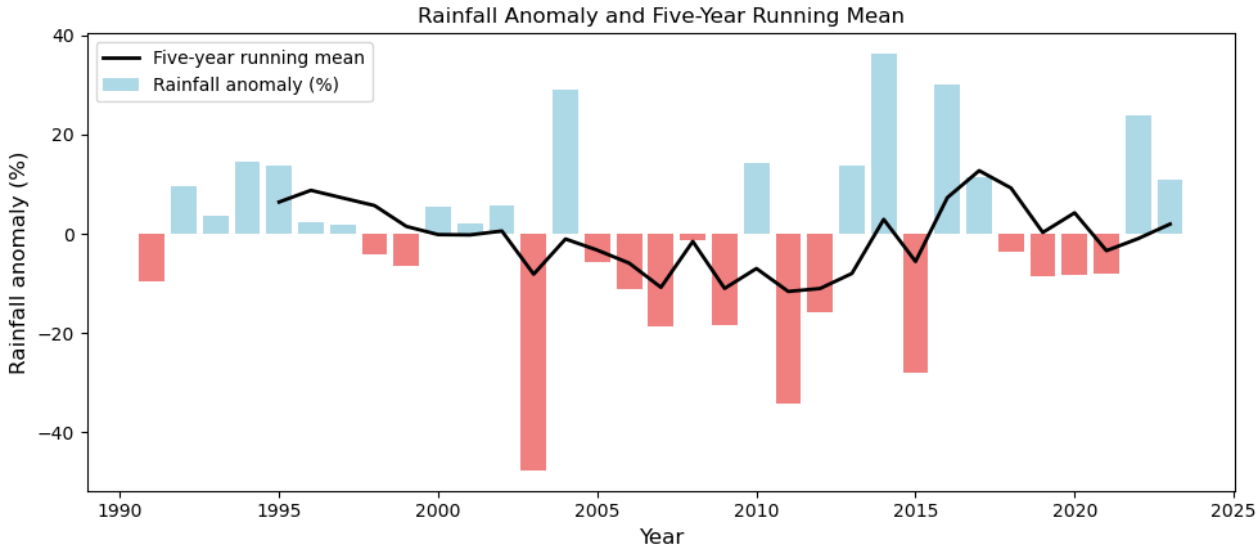

Figure 1.27. Time series of annual rainfall anomalies at the Novi Vinodolski station (1991-2023).

Figure 1.28 shows a time series plot and the trend of seasonal rainfall (cumulative 3-month rainfall) at the Novi Vinodolski station for the period 1991-2023. The highest seasonal rainfall is observed in autumn, followed by winter and spring. The lowest amount of rainfall occurs in summer. There is some variability in all seasons, but the Mann-Kendall test indicates that the trend is statistically significant only for the winter season (95% confidence level), where an increasing trend of 5 mm of total seasonal rainfall per year is observed.

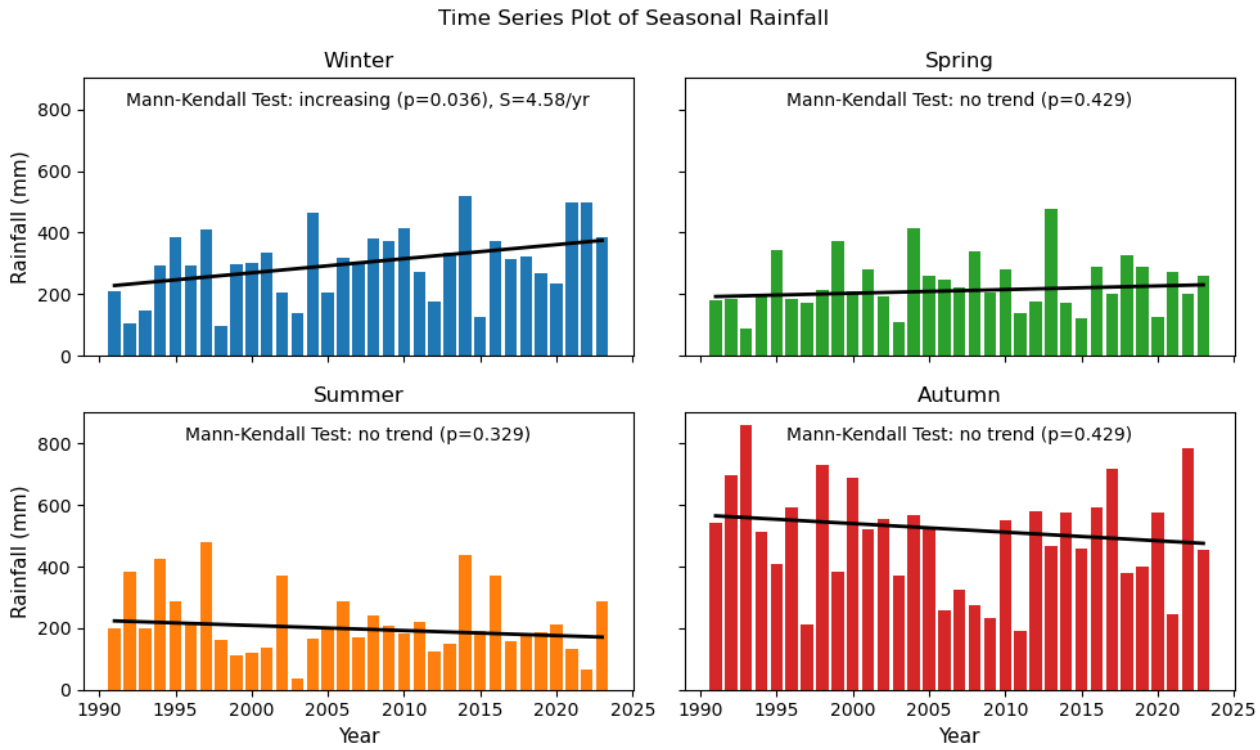

Figure 1.28. Time series of 3-month rainfall for different seasons and trend lines at the Novi Vinodolski station (1991-2023).

The statistical analysis of annual and monthly rainfall is shown in Figure 1.29. Overall, the autumn months (especially November) have the highest amount of rainfall (evident from the mean and median values) and the greatest variability (evident from the spread of the boxes and whiskers), while the summer months (July and August) have the lowest amount of rainfall and the least variability.

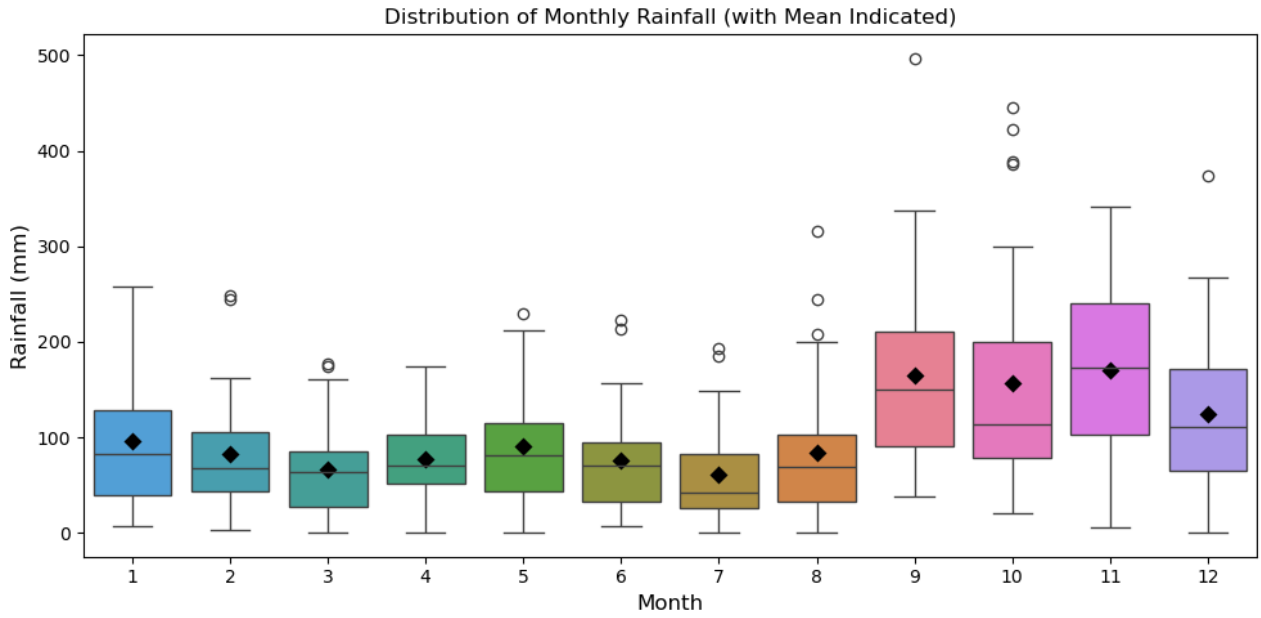

Figure 1.29. Inter-annual distribution of monthly rainfall at Novi Vinodolski station (1991-2023).

Figure 1.30 shows a time series plot and the trend of rainy days at the Novi Vinodolski station for the period 1991-2023. There is some variability in the number of rainy days, with a mean value of 25.9 % of rainy days per year. Despite the increasing trend, the Mann-Kendall test indicates that the trend is not strong enough to be considered statistically significant at the 95% confidence level.

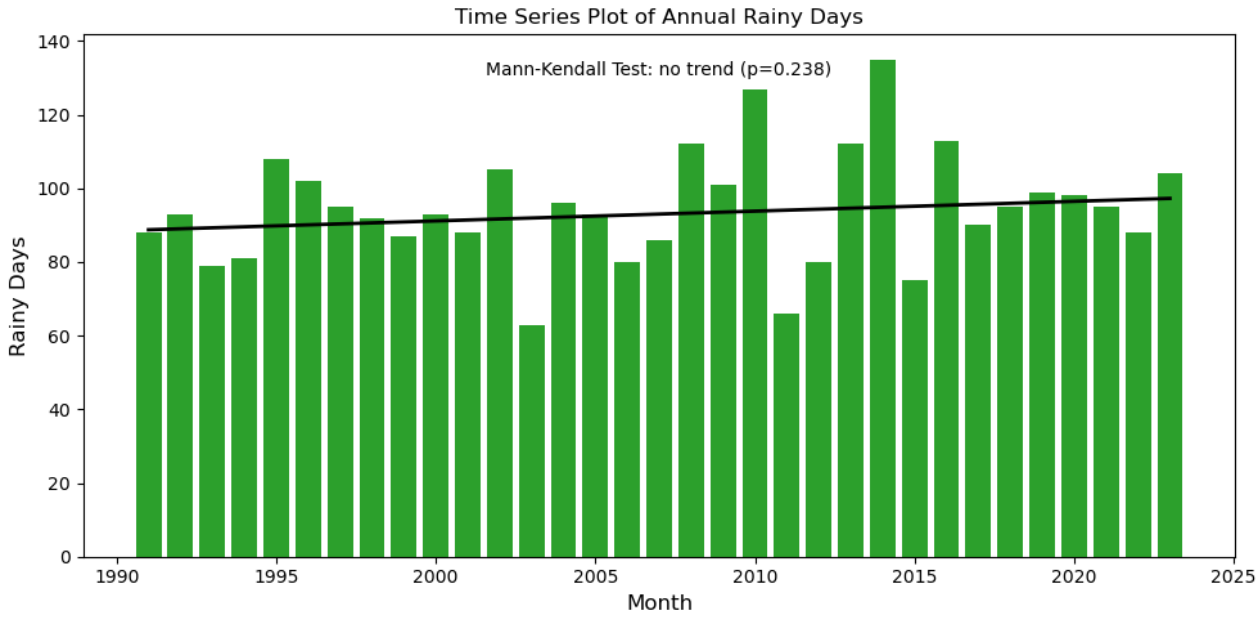

Figure 1.30. Time series of annual rainy days (H > 0.5 mm) and trend line at the Novi Vinodolski station (1991-2023).

Figure 1.31 shows a plot of the anomaly of rainy days in combination with a five-year running mean. In the early 1990s and 2000s, the anomalies were mostly neutral. A series of positive anomalies (above average) occurs from 2008 to the 2010 and then in 2013 and 2014, followed by more neutral anomalies in the recent period. The five-year running mean shows decadal variability.

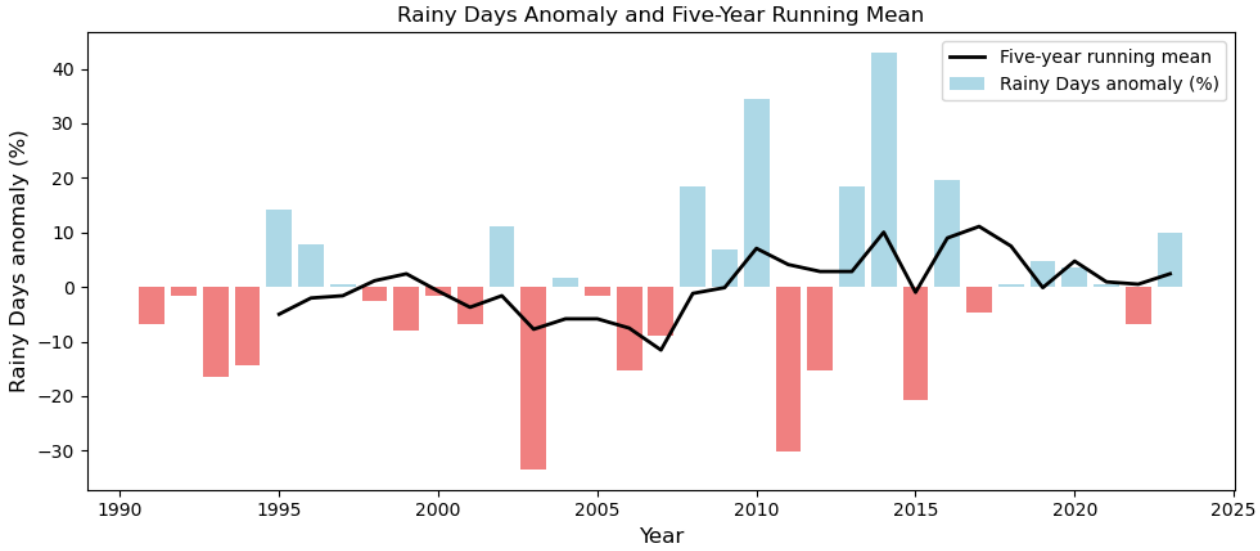

Figure 1.31. Time series of annual rainy days anomalies at the Novi Vinodolski station (1991-2023).

Figure 1.32 shows a time series plot and the trend of seasonal number of rainy days (cumulative 3-month number) at the Novi Vinodolski station for the period 1991-2023. The highest number of rainy days is observed in winter and autumn. The lowest number of rainy days is observed in summer. There is some variability in all seasons, but the Mann-Kendall test indicates that the trends are statistically significant (95% confidence level) only for Winter, where we a trend indicates an increase of 4 rainy days per decade.

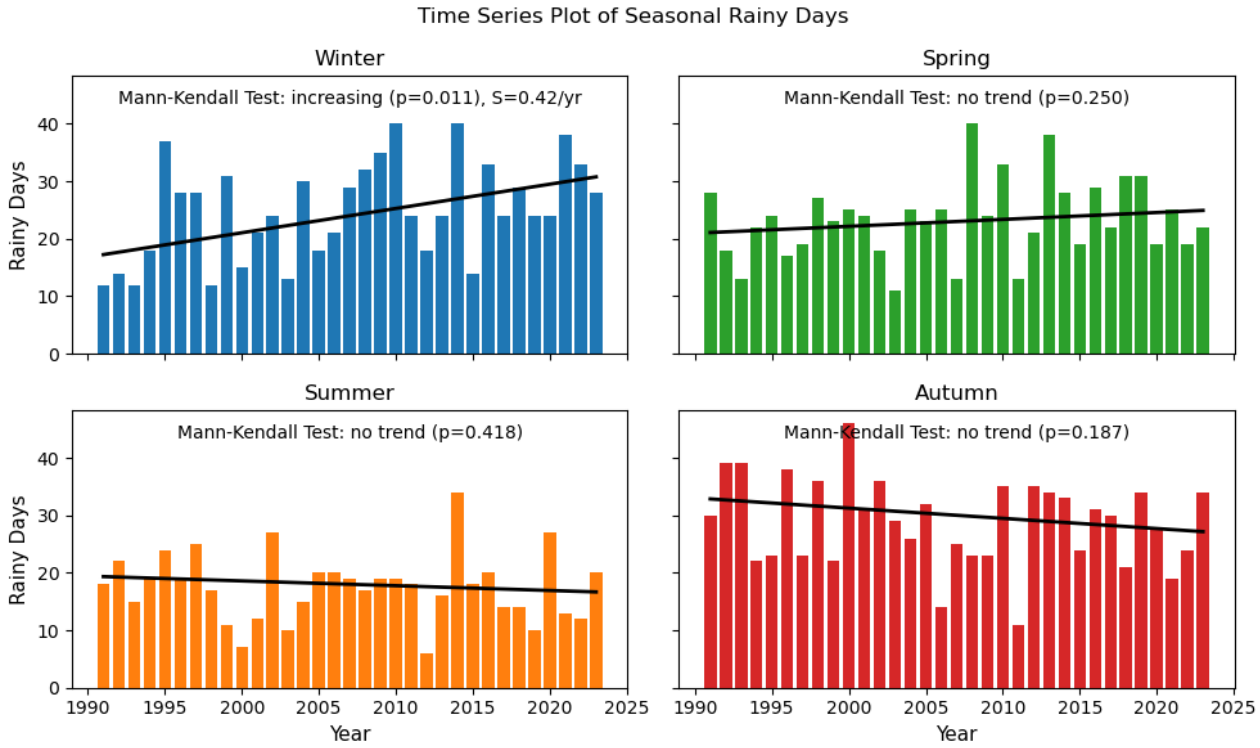

Figure 1.32. Time series of 3-month rainy days for different seasons and trend lines at the Novi Vinodolski station (1991-2023).

The statistical analysis of annual and monthly number of rainy days is shown in Figure 1.33. Overall, the autumn and winter months (especially November) have the highest number of rainy days (evident from the mean and median values). The summer months (July and August) have the lowest number of rainy days and the least variability (July).

Figure 1.34 shows a time series plot and the trend of heavy rainfall days (number of days where rainfall exceeds 20 mm) at the Novi Vinodolski station for the period 1991-2023. There is some variability in the number of heavy rainfall days, with a mean value of 5.6 % of heavy rainfall days per year. The Mann-Kendall test indicates that the trend is not statistically significant at the 95% confidence level.

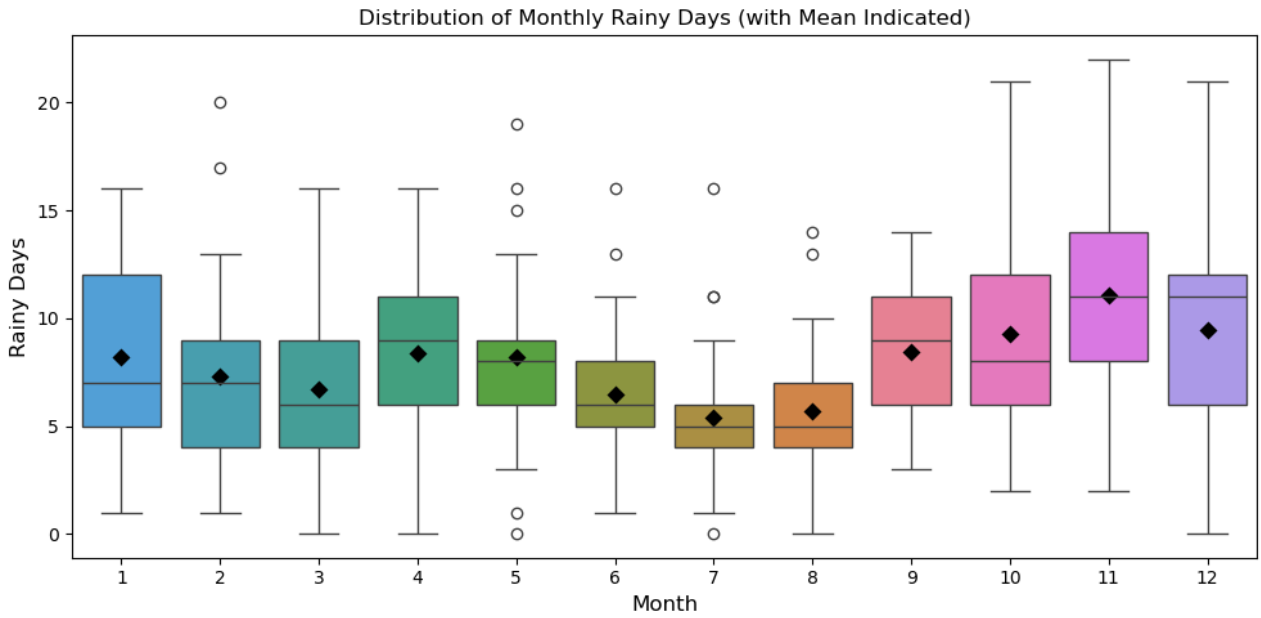

Figure 1.33. Inter-annual distribution of monthly rainy days at Novi Vinodolski station (1991-2023).

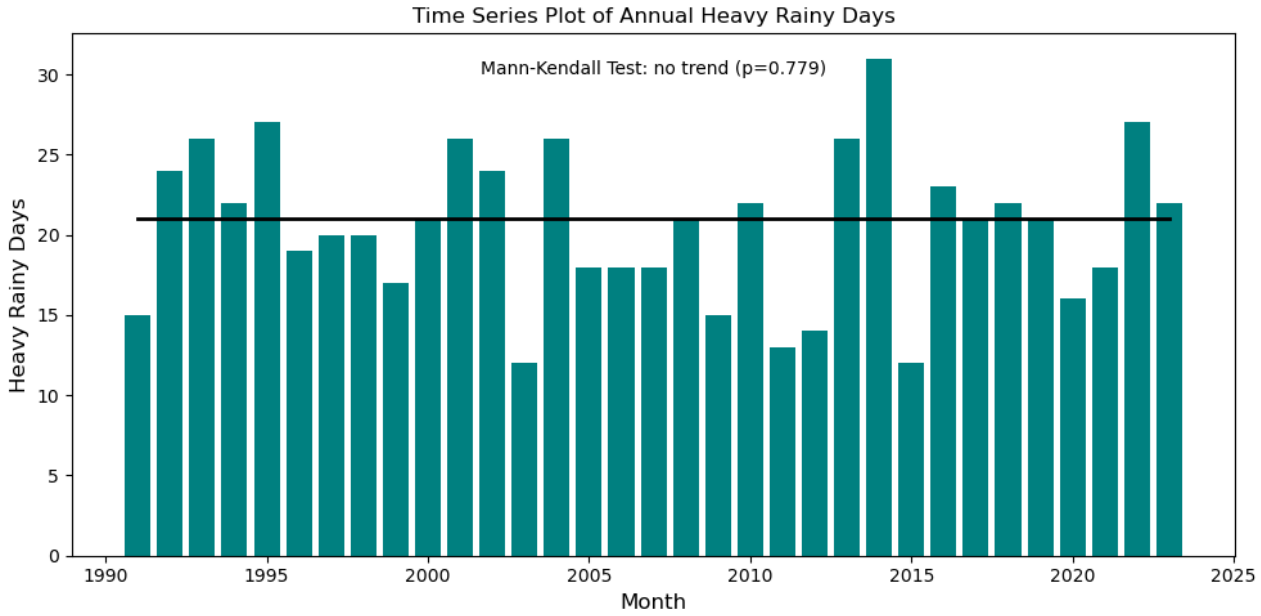

Figure 1.34. Time series of annual heavy rainfall days (H > 20 mm) and trend line at the Novi Vinodolski station (1991-2023).

Figure 1.35 shows a plot of the anomaly of heavy rainfall days in combination with a five-year running mean. 2000s were characterised by alternating positive and negative anomalies, while in 2013 and 2014 we have some prominent peaks (significant above-average number of heavy rainfall days). The five-year running mean shows a decadal variability.

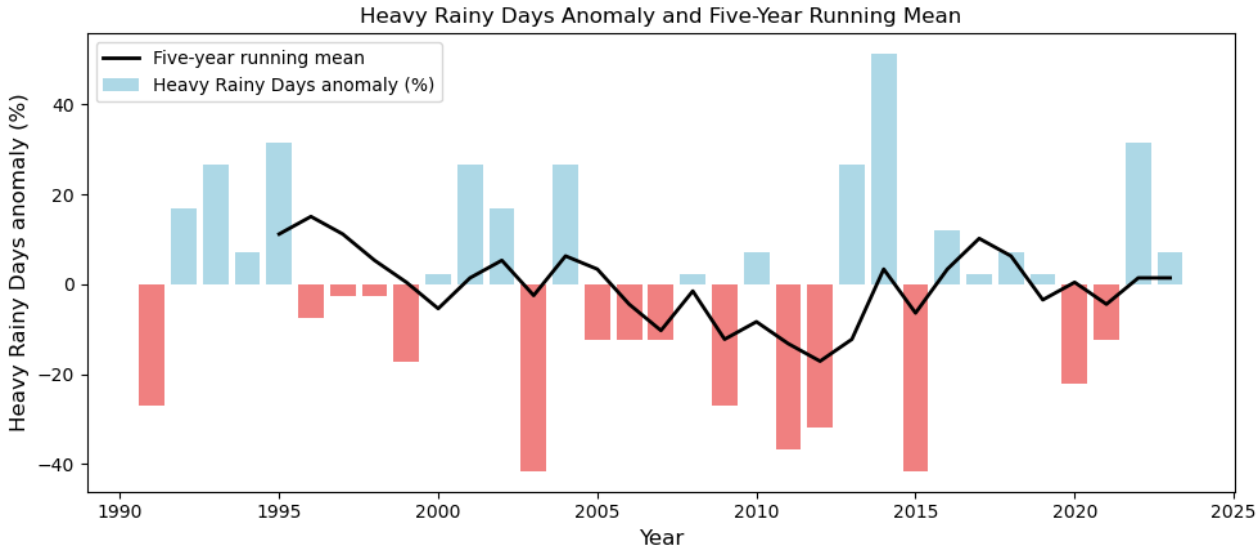

Figure 1.35. Time series of annual heavy rainfall days anomalies at the Novi Vinodolski station (1991-2023).

Figure 1.36 shows a time series plot and the trend of seasonal number of heavy rainfall days (cumulative 3-month number) at the Novi Vinodolski station for the period 1991-2023. The highest number of heavy rainfall days is observed in autumn. The lowest number of rainy days is observed in summer. There is some variability in all seasons, but the Mann-Kendall test indicates that the trend is not statistically significant (95% confidence level).

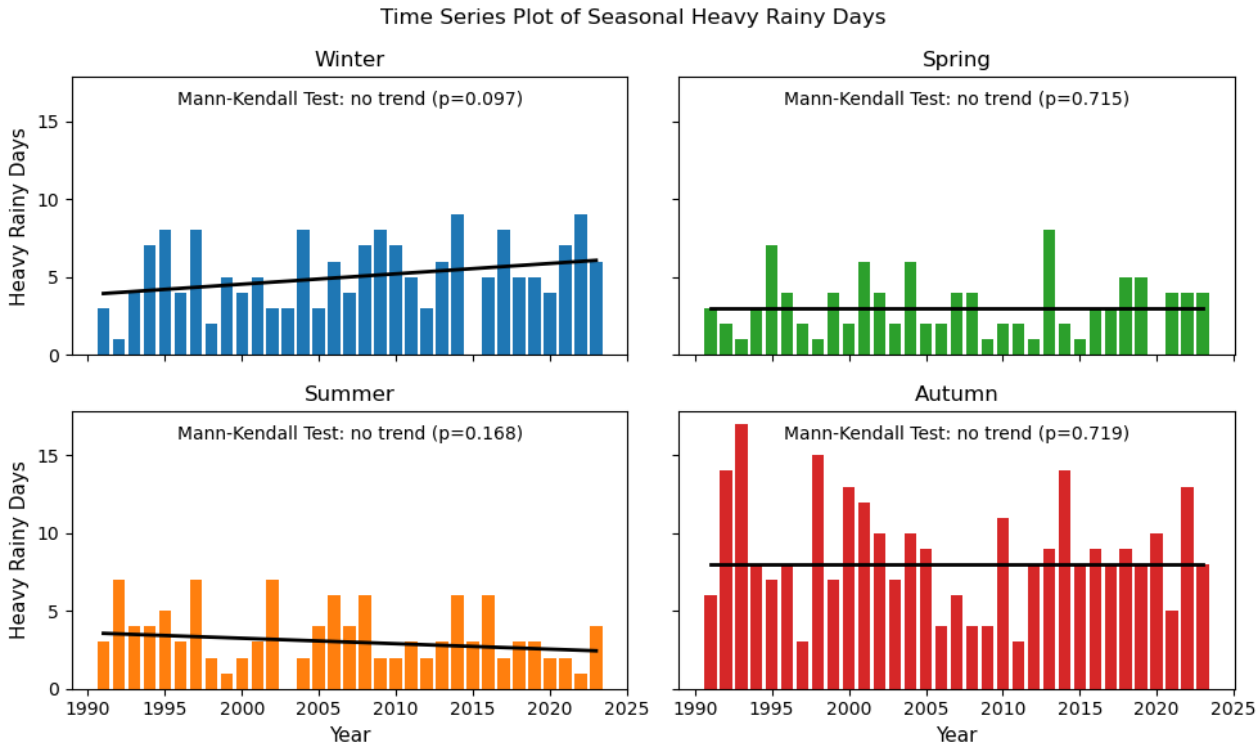

Figure 1.36. Time series of 3-month heavy rainfall days for different seasons and trend lines at the Novi Vinodolski station (1991-2023).

The statistical analysis of annual and monthly number of heavy rainfall days is shown in Figure 1.37. Overall, only autumn months stand out (September, October, and November) with the highest number of heavy rainfall days (evident from the mean and median values), and larger variability (evident from the spread of the boxes and whiskers). The summer months (July and August) have the lowest number of heavy rainfall days and the least variability.

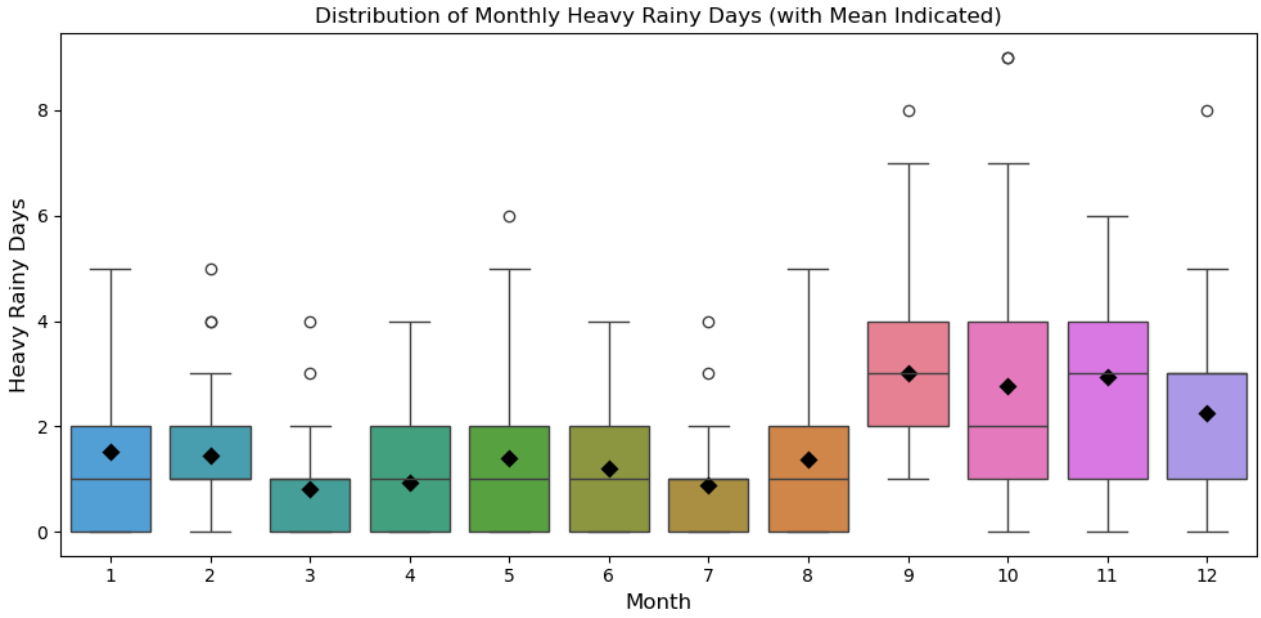

Figure 1.37. Inter-annual distribution of monthly heavy rainfall days at Novi Vinodolski station (1991-2023).

Figure 1.38 shows a time series plot and the trend of annual maximum daily rainfall at the Novi Vinodolski station for the period 1991-2023. There is a noticeable variability in the maximum daily rainfall mount, with a maximum 195.9 mm of daily rainfall. The Mann-Kendall test indicates that the trend is not strong enough to be considered statistically significant at the 95% confidence level.

Figure 1.39 shows a plot of the anomaly of maximum daily rainfall in combination with a five-year running mean. In the entire period the anomalies were mostly highly variable, with interchanging 2-3 years of negative followed by positive anomalies. Maximum positive anomalies occur in2016 and 2017. The five-year running mean shows a multidecadal variability.

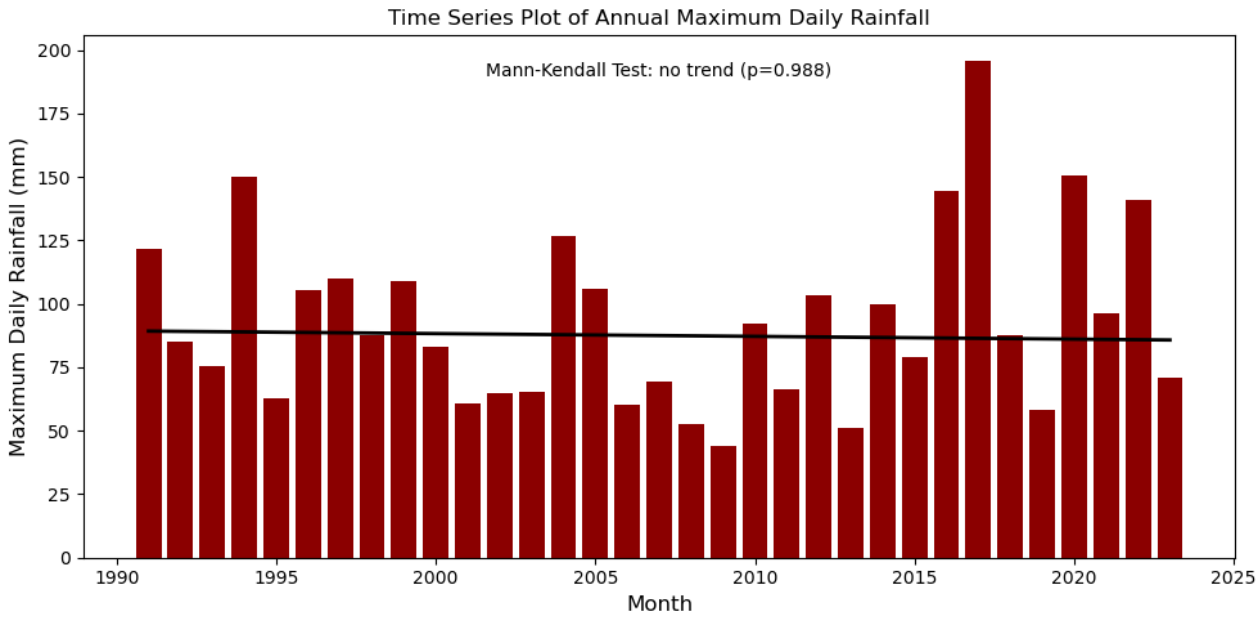

Figure 1.38. Time series of annual maximum daily rainfall and trend line at the Novi Vinodolski station (1991-2023).

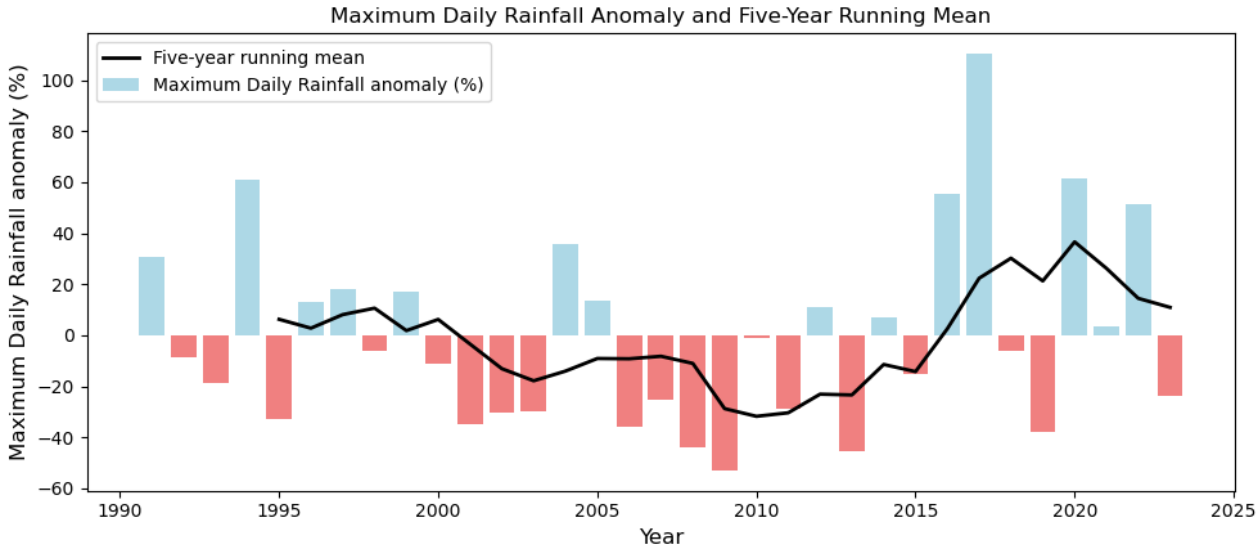

Figure 1.39. Time series of annual maximum daily rainfall anomalies at the Novi Vinodolski station (1991-2023).

Figure 1.40 shows a time series plot and the trend of seasonal maximum daily rainfall (3-month maximum) at the Novi Vinodolski station for the period 1991-2023. The highest maximum daily rainfall is observed in autumn. The lowest maximum daily rainfall is observed in spring (lower variability) and summer (higher variability). There is some variability in all seasons, but the Mann-Kendall test indicates that the trend is not statistically significant (95% confidence level).

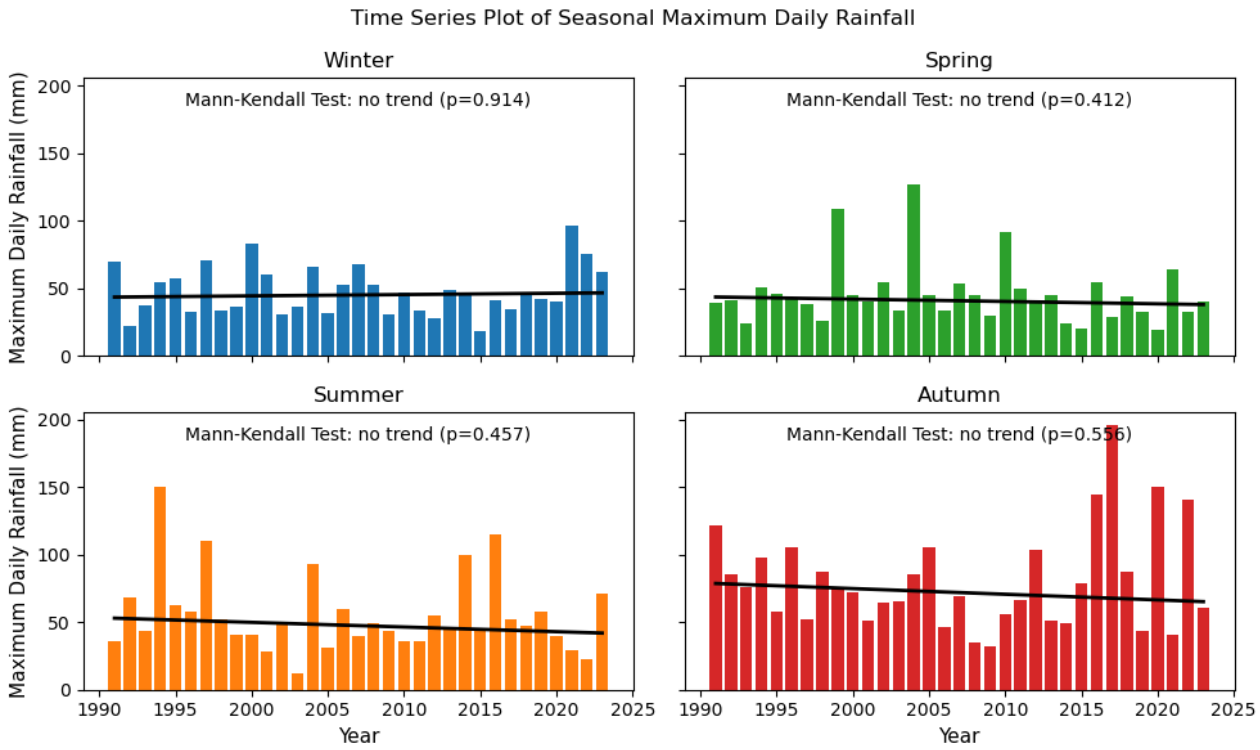

Figure 1.40. Time series of 3-month maximum daily rainfall for different seasons and trend lines at the Novi Vinodolski station (1991-2023).

The statistical analysis of annual and monthly maximum daily rainfall is shown in Figure 1.41. Overall, autumn months have the highest maximum daily rainfall, with September and October having the highest average values (evident from the mean and median values), and having the highest extremes. Variability is similar for all months. The summer months (July) have the lowest maximum daily rainfall amounts and the least variability.

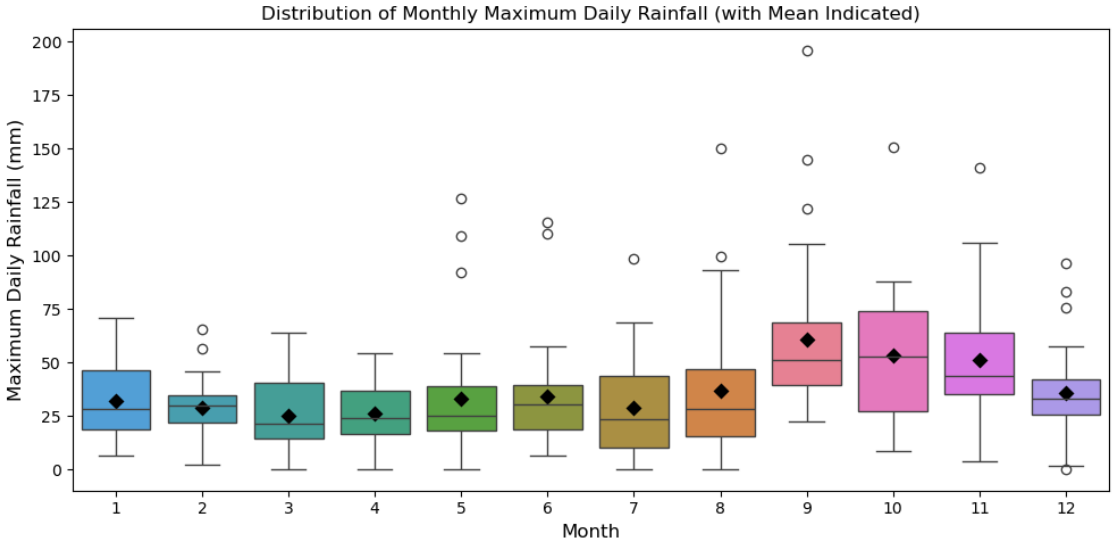

Figure 1.41. Inter-annual distribution of monthly maximum daily rainfall at Novi Vinodolski station (1991-2023).

1.3. Climate projections for rainfall

Climate change impacts on precipitation in this region were recently investigated by Pichelli et al. (2021). This study provides high-resolution climate projections (kilometer-scale resolution) for precipitation over the Alpine region, including the north Adriatic region. It is particularly relevant for two pilot areas (Municipality of Vinodolska općina and City of Novi Vinodolski), where small-scale topographic and coastal features strongly influence precipitation extremes.

This study introduces an advanced approach to climate modeling, using a multi-model ensemble of high-resolution regional climate simulations at kilometer-scale, known as “convection-permitting” models. These simulations focus on key historical and future climate periods (end-of-century scenarios) and are built by first refining global climate model (GCM) outputs from the CMIP5 dataset to an intermediate resolution of 12–15 km, then further downscaling them to a kilometer-scale grid. The research aims to explore precipitation patterns and their future changes across the Alpine region as part of the Coordinated Regional Climate Downscaling Experiment (CORDEX) Flagship Pilot Study and the European Climate Prediction system project, which investigates convective processes in fine detail.

The study analyzes 12 simulations conducted by leading European research teams, comparing them with high-resolution observational data and using the 12 km resolution models as benchmarks. Results show that kilometer-scale models provide a more accurate representation of precipitation characteristics, including daily averages, frequency, intensity, and extreme events like heavy rainfall. These models also better capture the timing and peak of summer convective storms, improving the simulation of the daily cycle of precipitation.

Importantly, the finer resolution of these models not only enhances the clarity of projected precipitation changes but also shifts the expected patterns in some cases, including changes in the intensity and frequency of heavy rainfall. For instance, the convection-permitting models suggest larger increases in the frequency of severe precipitation and a potential shift in the duration of convective storms. These findings highlight the potential of kilometer-scale simulations to provide more reliable and detailed assessments of how climate change may impact precipitation locally, offering a powerful tool for planning and adaptation strategies in regions sensitive to extreme weather.

Figure 1.42 shows the results of this study, the ensemble mean percent change in precipitation indices for the period 2090–2099 compared to the historical period (1996–2005). The figure includes results from two ensembles, the CPRCM Ensemble (3 km resolution) and driving RCM Ensemble (12 km resolution). The figures show most of Croatia. The indices analyzed are intensity change, frequency change and heavy precipitation change (99,9-percentile).

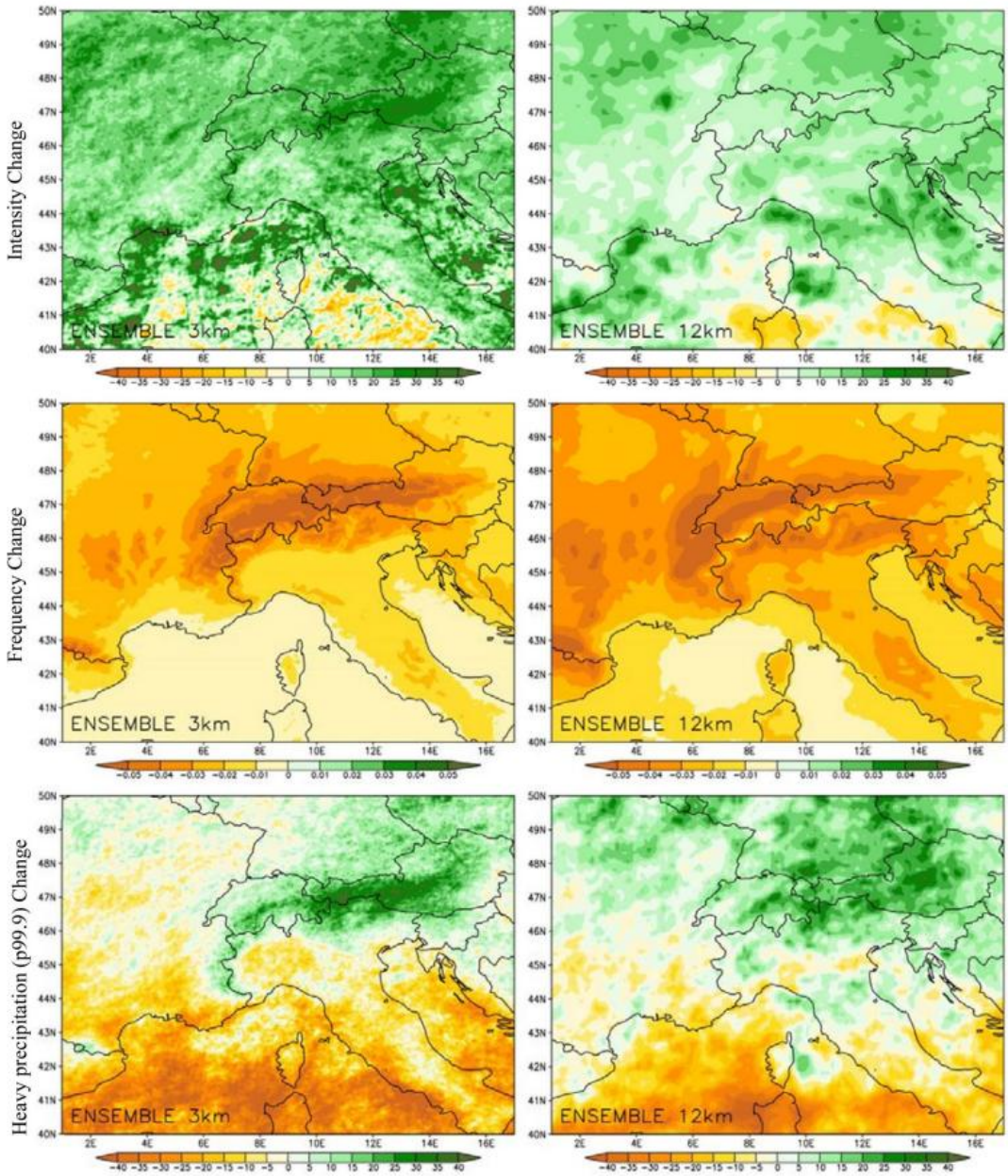

Figure 1.42. Ensemble mean percent change of the indices analysed over 2090-2099 for the summer hourly precipitation (historical simulation is the reference, 1996-2005). From top to bottom: intensity, frequency and heavy precipitation (p99.9) change. The results are obtained from the CPRCM ensemble (left) and the driving RCM ensemble (right) (Pichelli et al, 2021).

Intensity Change:

- 12 km Ensemble: The pilot area shows slight increases in precipitation intensity, indicating slightly more intense rainfall events compared to the historical period.

The 12 km resolution results also suggest modest increases in intensity, though the spatial patterns are smoother, reflecting the lower resolution.

- 3 km Ensemble: The 3 km resolution results also suggest modest increases in intensity, though the spatial patterns are more variable, reflecting the higher resolution.

Frequency Change:

- 12 km Ensemble: The pilot area experiences a slight decrease in the frequency of precipitation events. This indicates that rainfall events may become less frequent during the analyzed period.
- 3 km Ensemble: The 3 km resolution also shows a slight decrease in frequency, though the changes are somewhat weaker.

Heavy Precipitation (p99.9) Change:

- 12 km Ensemble: The pilot area exhibits an increase in extreme precipitation events (p99.9). This suggests that the heaviest rainfall events will become more intense, potentially contributing to increased flood risks.
- 3 km Ensemble: The 3 km resolution ensemble also shows different projections, ranging from no change to a weak decrease of heavy precipitation in the pilot area, and a weak increase in the continental part.

Overall, the results from this study indicate that **rainfall intensity in the two pilot areas will likely increase**, which could exacerbate short-duration rainfall events in the region. **The frequency of precipitation events is projected to stay the same or even slightly decrease**, particularly in summer. This could lead to less frequent rainfall occurrences. **The intensity and occurrence of extreme rainfall events (p99.9) are expected to stay the same or slightly increase**. This could elevate the risks of flash flooding, especially in urbanized coastal areas with limited drainage capacity.

2. FLOOD HAZARD ASSESSMENT DUE TO HEAVY RAINFALL

2.1. Introduction to flood hazard assessment

The assessment of flood hazards presented in this document has been conducted following the Croatian **Water Act** (Zakon o vodama) (NN 66/2019, 84/2021, 47/2023) which regulates, among other things, protection against harmful effects of water. This Act also transposes Directive 2007/60/EC of the European Parliament and of the Council of October 23, 2007, on the assessment and management of flood risks (hereinafter referred to as **the EU Floods Directive**) into the legal system of the Republic of Croatia. The main purpose of the EU Floods Directive is to establish a framework for assessing and managing flood risks to reduce the adverse effects of floods on human health, environment, cultural heritage, and economic activity.

The Water Act stipulates that Croatian Waters must prepare flood hazard maps and flood risk maps for each river basin. The content of the maps and the scenarios for which they are prepared are prescribed by **the River Basin Management Plan (RBMP)** and **the Flood Risk Management Plan (FRMP).** It is important to note that at the time of writing this document, the RBMP valid until 2027 (NN 84/2023) is in force.

The EU Floods Directive contains more detailed information on the process of preparing flood hazard and flood risk maps. The flood hazard maps must be generated according to the following scenarios:

a) floods with a low probability, or extreme event scenarios,
b) floods with a medium probability and
c) floods with a high probability.

For each scenario, the flood hazard maps must show the following elements:

a) the flood extent,
b) water depths or water level,
c) the flow velocity or the relevant water flow.

The flood risk maps should show the potential adverse consequences associated with flood scenarios and expressed in terms of the following:

a) the indicative number of inhabitants potentially affected,
b) type of economic activity of the area potentially affected,
c) installations that might cause accidental pollution in case of flooding and potentially affected protected areas,
d) other information that the Member State considers useful and information on other significant sources of pollution.

Flood is a term that is defined in the Water Act (NN 66/2019, 84/2021, 47/2023).

„**A flood** is a temporary inundation of land that is usually not covered by water, caused by the overflow of rivers, torrents, temporary watercourses, lakes, and ice accumulation, as well as

coastal flooding due to seawater and excessive groundwater levels. This definition does not include flooding caused by public drainage systems.

The flood risk management plan (FRMP) (NN 84/2023) recognizes several basic types of flooding based on the source of flooding:

- river flooding caused by heavy rainfall and/or rapid snowmelt (fluvial flooding),
- flash floods in smaller watercourses due to short-duration, high-intensity rainfall,
- flooding in karst areas due to heavy rainfall and/or rapid snowmelt, combined with the insufficient drainage capacity of natural sinkholes,
- flooding of the inland waters in low-lying areas,
- ice jam flooding,
- flooding due to storm surges and seiches,
- accidental flooding due to failure of dams or levees, landslides, inadequate construction, and similar events.

In a current planning cycle, FRMP addresses:

- river (fluvial) flooding, including flooding caused by the ice jam on major rivers and flooding due to failure of the flood defense system,
- flooding due to underground water which is characteristic of the karst areas,
- flooding due to high sea levels,
- flooding due to failure of water infrastructure – canals and reservoirs.

Flooding due to heavy rainfall (pluvial flooding), while an important source of flooding in Croatia, is only partially covered due to legal and technical considerations. Meanwhile, flooding caused by sewer systems is not considered in this FRMP planning cycle.

To assess the risk of pluvial flooding, it is important to define them and distinguish them from other types of flooding. It is important to note that different types of flooding can often co-occur, usually due to the same cause or source of flooding (e.g. heavy rainfall), but they differ in their spatial extent and flooding mechanisms. First, it is necessary to clarify how pluvial floods differ from fluvial floods and to explain the relationships between terms such as pluvial floods, flash floods, urban floods, and sewer floods.

In general, **fluvial or river flooding** occurs when the water level of a river, lake, or stream rises and overflows the levees or riverbanks onto the neighboring land. The water level rise of the river can be due to excessive rain or snowmelt near or far from the flood site (Figure 2.1).

On the other hand, **pluvial flooding** arises due to intense rainfall-runoff but is independent of water bodies (Figure 2.2). The term pluvial flooding generally refers to two different forms of flooding: a) urban flooding and b) flash flooding. Urban floods occur in urban areas and are often caused by the combination of stormwater drainage systems exceeding their capacity and a high level of land urbanization. Flash floods are formed in mountainous or steep terrain and are characterized by their sudden occurrence and high water velocity. As highlighted in the RAINMAN project (2020), a key

aspect of pluvial floods in urban areas is not only the lack of an adequate drainage system but also the insufficient retention and infiltration capacity of the land, which is mostly a consequence of intense urbanization. Sewer flooding is a subcategory of urban flooding that is directly related to undersized or poorly maintained stormwater drainage systems.

Through the RAINMAN project (2020), significant progress has been made in the clarity and precision of defining pluvial flooding. It was also emphasized that it is crucial to distinguish pluvial floods from fluvial floods and flash floods. In general, it can be considered that (RAINMAN, 2020):

- **Fluvial flooding** describes the surface waters that **originate from** the water bodies.
- **Pluvial flooding** describes the surface waters **flowing towards** the water bodies.

According to these guidelines, flash floods can only be considered an integral part of pluvial floods if they occur in areas where the clearly defined torrent channels are lacking or if the dominant flooding mechanism is a surface water runoff towards watercourses. Otherwise, floods that occur when water overflows from a torrential channel onto the surrounding land should be treated as a separate type of flood — flash floods.

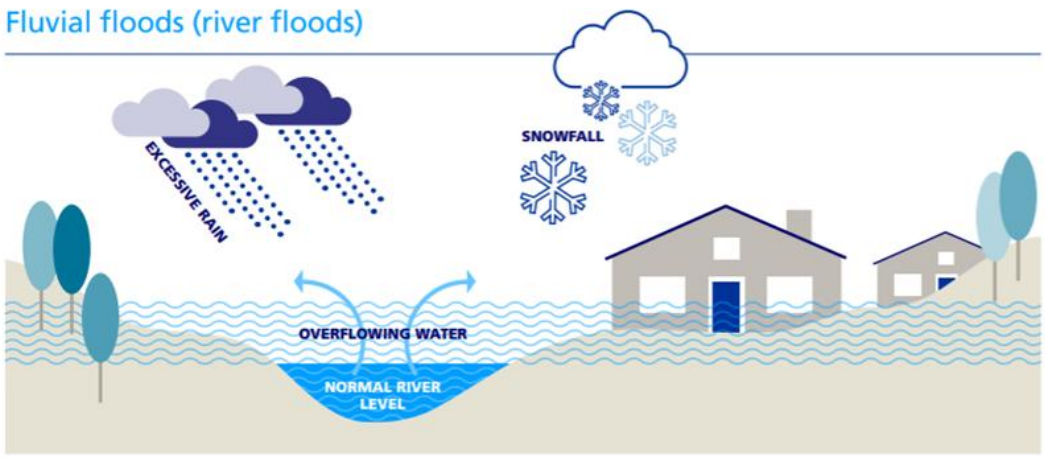

Figure 2.1. Fluvial (river) flooding scheme (www.zurich.com).

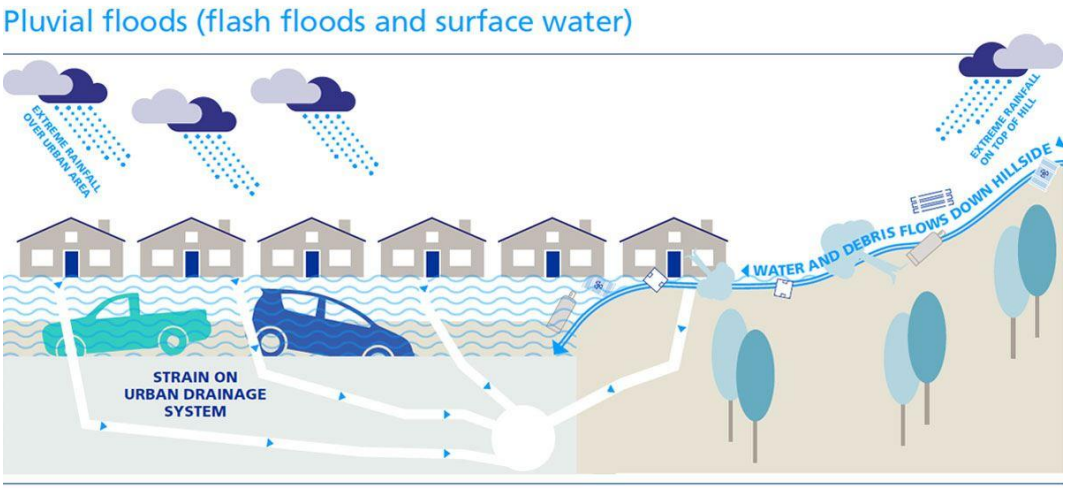

Figure 2.2. Pluvial and flash flooding scheme (www.zurich.com).

2.1.1. Definitions

The term **risk** has multiple possible meanings and is used in different ways within the scientific and professional community. Therefore, it is necessary to define all the elements and indicators used to assess the flood risk. The Water Act (NN 66/2019, 84/2021, 47/2023), which is aligned with the EU Floods Directive, provides a formal definition of the flood risk.

„**Flood risk** is a combination of the probability of a flood event and of the potential adverse consequences to human life, health, and property, the environment, cultural heritage and economic activity associated with a flood event."

The flood risk can be mathematically expressed as:

$$RISK = p_h \times C$$

where p_h is the probability of the hazardous process and C is the potential adverse consequence (EXCIMAP, 2007.).

The risk usually encompasses two aspects: **hazard and vulnerability** (Merz *et al*., 2007.).

Flood hazard is defined as the exceedance probability of potentially damaging flood situations in a given area and within a specified period of time Flood hazard statements do not convey information about the consequences of such floods on society, the built environment, or the natural environment (Merz *et al*., 2007.). A somewhat broader definition of hazard is provided by the UN (2004):

„**Hazard** is a dangerous phenomenon, substance, human activity or condition that may cause loss of life, injury or other health impacts, property damage, loss of livelihoods and services, social and economic disruption, or environmental damage." UNISDR (2009.).

Flood hazard is usually expressed through **flood extent** and **water depth,** as the water depth has the most significant impact on the adverse consequences of flooding. In the case of flash floods and urban flooding, **water velocity** is often used as an indicator, as it affects the damage to buildings and infrastructure. In addition, the **flow rate** (calculated as the product of water depth and velocity) is taken into account to assess the impact on the stability of people, animals, and movable objects.

For river flooding and coastal flooding, additional indicators such as the **duration of the flood** and the **velocity of propagation** are used. The velocity of propagation can be expressed as the time until the flood wave arrives or as the rate of water level rise, which is crucial for early warning systems and evacuation planning. In some cases, it is also important to assess the **concentration** and size of transported materials such as sediments or pollutants, which can cause significant damage not only to the built environment but also to entire ecosystems.

All of the previously mentioned indicators are quantitative, however, sometimes it can be more useful to express the flood hazard qualitatively – as a **flood severity** which reflects a combination of different indicators (e.g. low, medium, and high hazard levels).

It should be noted that, as part of flood hazard analysis, the extent of flooding and/or water depth for selected historical floods is often presented. In such cases, the exceedance probability does not necessarily have to be defined. However, these results are still referred to as flood hazard maps, although a different term (flood danger) is used in the Anglo-American context.

Besides the flood hazard, the risk assessment also includes the identification of the elements at risk, which include all subjects and objects in the built and natural environment that can potentially be flooded – **the risk receptors**. For example, that can include population, vehicles, buildings, infrastructure, economic activities, ecosystems, and others.

The definition of risk directly implies that **the assessment of flood risk** involves the analysis of **potential adverse consequences**, which depend not only on the characteristics and probabilities of flood events (as defined by the hazards) but also on the **vulnerability of receptors** exposed to flooding. There are various definitions of **vulnerability** in the literature. Merz (2007), for example, defines vulnerability as a combination of two elements: **exposure** and **susceptibility**. The assessment of exposure answers the question: "Who or what can be affected by a flood?", while susceptibility assessment answers the question: "How and to what extent will the exposed receptors be affected or damaged?" (Merz, 2007).

Therefore, the following concise definition of potential adverse consequences can be provided:

$$C = S \times V \times E$$

where C is the potential adverse consequence, *S* is a susceptibility, *V* is the value of the element at risk and *E* is the exposure (EXCIMAP, 2007.).

Susceptibility S describes the adverse effect on the risk receptors and is usually defined with depth-damage curves (percentage of damage in relation to the water depth). It can have values in a range from 0 to 1. **The value of element V** can be expressed not only in economic terms, but also by the number of inhabitants or specific population groups, economic activity, the length of infrastructure, the number of buildings, the location of installations containing pollutants or hazardous substances, and similar factors. **The exposure E** is defined as the probability of a receptor being exposed to flooding (related to the flood hazard) and can also take a value between 0 and 1. In practice, exposure is more often expressed directly as a combination of the value of the element and its exposure level.

It is important to note that vulnerability is a complex and dynamic characteristic of a receptor that describes its susceptibility to the adverse consequences of flooding. The susceptibility of a receptor emerges from its own characteristics, i.e. a set of socio-cultural, physical, economic, and environmental factors. High vulnerability of a receptor is often the result of poor spatial management, such as uncontrolled urbanization, lack of infrastructure and environmental maintenance and associated degradation, or loss of adequate support due to demographic change (Cardona et al., 2012).

„**Vulnerability** is a set of the characteristics and circumstances of a community, system or asset that make it susceptible to the damaging effects of a hazard.“ (UNISDR, 2009).

2.1.2. Conceptual model for assessment of flood from heavy rainfall

The conceptual SPRC model (Source-Pathway-Receptor-Consequence) is often used in the risk assessment process to better understand individual risk elements and the relationships between all relevant indicators (Samuels & Gouldby, 2009). This concept defines the relationship between hazard, vulnerability, and risk as a linear functional chain of the hazard source, the pathway between the occurrence of the hazard and the receptor, the receptor characteristics, and the resulting adverse consequences (Figure 2.3).

In the context of pluvial flooding, the primary hazard source is short-term intense rainfall and the process of generating surface runoff. The pathway from the hazard source to the receptor is described by the surface runoff of the rainwater. Receptors are subjects and objects that are exposed to the flood hazard and potentially susceptible to adverse consequences. The term consequence refers to all negative and undesirable processes such as damage to buildings (economic consequences), injuries and trauma to the population (social consequences), and the pollution of water resources or soils (environmental consequences).

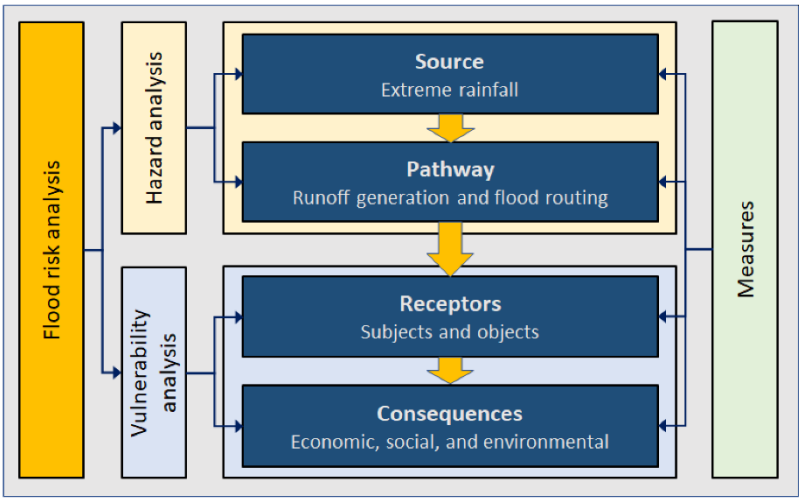

Figure 2.3. SPRC concept scheme (Krvavica et al., 2023).

Risk mitigation measures can alter each element of the SPRC concept. For example, the construction of retention basins can positively influence stormwater runoff, while advanced land use/cover management can reduce the hazard source — the amount of generated runoff. When conducting a risk analysis, it is important to consider the entire system integrally and carefully evaluate the impact of available measures on each system component.

2.1.3. Levels of complexity and flood mapping

The levels of complexity determines the choice of methodological approach, the data requirements and the technical, financial, and other effort needed to assess the pluvial flooding risk. Within the EU project RAINMAN (Sauer *et al.,* 2018.), three levels of complexity were described, together with proposed methods for hazard and vulnerability analysis, as well as appropriate levels for risk analysis and mapping (Table 2.1).

Table 2.1. Levels of complexity in relation to goals and the scale of an assessment, to data availability as well as to capacities of the administrative actors involved (Sauer et al., 2018).

Complexity level	Description	Example for risk assessment
Level 1	**Basic level analysis:** • Indicative information basis • Relatively low effort and experience • Appropriate for contexts with very limited data availability and financial resources **Criteria:** • Hazard: experience and observations • Vulnerability: experience and observations	Estimation of priority areas for risk management based on empiric knowledge about flood extents and observed damages in the area. No explicit risk information due to missing data on probabilities or damage potentials.
Level 2	**Medium level analysis:** • More elaborate than basic analysis but often still general information, based on simplified data requirements • Medium effort • Appropriate for contexts with better data availability, good availability of professional experience as well as financial resources **Criteria:** • Hazard: GIS analysis (static modelling) • Vulnerability: Damage assessment without using water levels/water velocities	Risk estimation applying flow path analysis and damage estimations based on general/rough damage estimation per area.
Level 3	**High level analysis:** • Detailed results • Use of modern and advanced methodological possibilities • Appropriate for contexts with good data availability, very good availability of professional experience as well as financial resources **Criteria:** • Hazard: Non-statonary models and simulations • Vulnerability: Damage functions based on water-levels and water velocities	Risk analysis applying hydraulic models and synthetic damage modelling based on building type specific water depth-damage functions, allowing detailed assessment and specific conclusions for prioritisation and management.

Detailed examples of the analysis of each of the aforementioned complexity levels according to the SPRC approach is provided below (Sauer et al., 2018.). If methodologically appropriate, different

levels of detail can be combined in the risk analysis depending on the available data, resources, and the characteristics of the area.

1. Hazard analysis (source and pathway):

- Level 1: Survey and documentation of observed events (watermarks, sedimentation, and erosion, damages).
- Level 2: Topographic flow paths and depression analysis (elevation, slope, landforms with relevance for runoff and flooding).
- Level 3: Hydrodynamic modelling (including precipitation analysis as a primary driver of the models).

2. Vulnerability analysis (receptor and consequence):

- Level 1: Survey and documentation of observed damages, firefighters' and civil protection interventions.
- Level 2: GIS-based vulnerability assessment with the identification of the number of potentially exposed receptors (e.g. people, buildings, road length…) or areas (e.g. built-up, commercial, agricultural, …)
- Level 3: Quantitative vulnerability assessment of monetary damage potentials and processes (e.g. development and application of receptor-specific depth-damage functions).

3. Risk analysis (combination of hazards and risks via exposure).

4. Map generation for hazard and risk (translation of analysis results into static visualizations or dynamic geographic information system).

According to the presented methodological framework, Merz et al. (2007) suggest that the following maps should be generated during the flood risk assessment:

- **Flood hazard map** that, for different probabilities, shows the flood extent, the spatial distribution of the water depth, water velocity, water flow, and other relevant indicators.
- **Flood vulnerability map** that, for different probabilities, shows the exposure of population, built and natural environment, and other relevant elements.
- **Flood risk map** that, for different probabilities, shows the spatial distribution of expected damages either for specific elements or per unit area.

First of all, it is important to know that flood maps form the basis for the development of a flood risk management plan. Understanding the spatial distribution and extent of flood hazard and risk across the study area is a prerequisite for producing a high-quality flood risk management plan. In addition, various stakeholders will use flood maps — not only for flood risk management but also for land use planning, spatial planning management, natural disaster response planning, raising awareness, and even in the private sector, such as the insurance industry.

Given their purpose, each potential user has specific requirements for the content and scale of flood maps. Tables 2.2 – 2.5 provide an overview of the levels, scales, users, and content from the perspective of the different uses of flood maps, based on the Handbook on good practices for flood mapping in Europe (EXCIMAP, 2007) and the Report on Map Preparation (Vincze et al., 2014).

Table 2.2. Levels, scales, purposes, readership, and content of the flood maps from the perspective of flood risk management.

Level / scale	Purpose	Readership / complexity	Content of flood maps	
			Essential elements	Desirable elements
National / 1:100.000 – 1:1.000.000	Broad-scale planning and prioritisation of flood risk management measures National strategies	Decision makers / easy-to-understand, simplified maps	Flood extent Flood risks Sites of environmental vulnerability Pollution risks Assets at risk	Indicative vulnerability
Regional / 1:25.000 – 1:100.000	Broad-scale planning and prioritisation of flood risk management measures Regional strategies Flood risk management within the river basin Public participation	Decision makers Technical services General public / easy-to-understand, simplified maps	Flood extent Flood risks Sites of environmental vulnerability Pollution risks Assets at risk	Indicative vulnerability
Local / 1:2.000 – 1:25.000	Planning and evaluation of local and specific flood management measures Public participation	Decision makers Technical services General public Experts / More complex maps	Flood extent Water depth Water velocity	Vulnerability Damages Environmental impacts

Table 2.3. Levels, scales, purposes, readership and content of the flood maps from the perspective of spatial planning.

Level / scale	Purpose	Readership / complexity	Content of flood maps	
			Essential elements	Desirable elements
National and Regional / 1:100.000 – 1:500.000	Spatial planning (national and county spatial plans) Allocation of land for development Planning of national infrastructure	Decision makers Land-use and spatial planners / Simplified maps	Flood extent Flood risks Sites of environmental vulnerability Pollution risks Assets at risk	Additional indicators relevant for assessing the hazard
Local / 1:5.000 – 1:25.000 (cadastre level)	Spatial planning (specific city or village planning) Watershed management Meeting specific needs of planners as a basis or guidance for decisions.	Local authorities City, village planners, and rural planners / Simplified maps	Flood extent	Additional parameters of hazard (water depth, water velocity, duration) and/or hazard classes

Table 2.4. Levels, scales, purposes, readership, and content of the flood maps from the perspective of emergency planning and management.

Level / scale	Purpose	Readership / complexity	Content of flood maps	
			Essential elements	Desirable elements
National and Regional / 1:100.000 – 1:500.000	Broad-scale planning for major emergencies that may require national or regional intervention	Spatial planners Civil defence planners Civil defence planners Politicians and high-level decision-makers	Flood extent Flood risks Affected population Affected infrastructure	Other relevant data for assessing the hazards. Vulnerability and risks
Local / 1:5.000 – 1:25.000	Planning of localized emergency response	Civil defence planners Politicians and high-level decision-makers Health authorities and emergency services	Flood extent Water depth Vulnerability of the population Risks (infrastructure, pollution, historical heritage, etc.)	Real-time information is useful where/when available

Table 2.5. Levels, scales, purposes, readership, and content of the flood maps from the perspective of public awareness.

Level / scale	Purpose	Readership / complexity	Content of flood maps	
			Essential elements	Essential elements
Local / 1:5.000 – 1:25.000	Public information about flooding	Public Professional advisors / Easy-to-read maps	Flood extent Water depth	Historic flood events, Water velocity. Water flow, erosion, debris, and similar appropriate elements.

2.2. Methodology for assessment of flood hazards

The assessment of the flood hazard due to heavy rainfall (pluvial flooding) in the present study is conducted following the Water Act (NN 66/2019, 84/2021, 47/2023), the EU Floods Directive (EC 2007/60/EZ) and the Handbook on good practices for flood mapping in Europe (EXCIMAP, 2007). The concept and elements of the flood hazard assessment are shown in Figure 2.4.

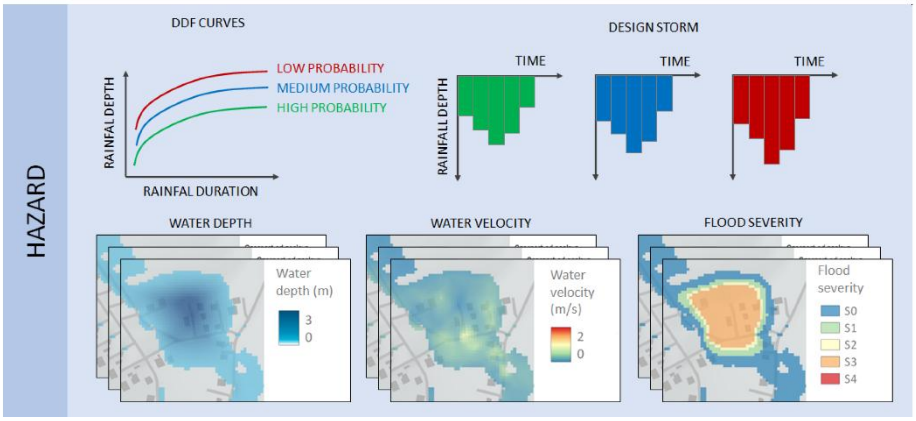

Figure 2.4. Elements and indicators of pluvial flood hazard, vulnerability and risk assessment.

The following section provides an overview of the methodology for assessing the pluvial flood hazard. Flood hazards are evaluated through the hydrologic-hydraulic simulations of surface rainfall-runoff. The main input for the simulations is rainfall defined by a design storm for different probabilities. The results of the flood hazard analysis are water depth and water velocity maps, as well as flood severity for each probability considered.

This analysis is performed in relation to the complexity levels at a high complexity level with specific individual characteristics listed in Table 2.6.

Table 2.6. Complexity levels of flood risk assessment

SPRC Element	Method	Complexity level		
		Level 1	Level 2	Level 3
Source	**Historic flood events** temporal resolution 5 min. **Design rainfall** duration 1, 3, 6, 12, i 24 h for the scenarios with high, medium and low probability (AEP 20, 4, i 1 %). **Infiltration described with the SCS method** and spatially variable CN curve numbers.			×
Pathway	**Hydrologic-hydraulic non-stationary simulations** for the surface rainfall-runoff. **2D numerical model** (HEC-RAS 6.6) Indicators: **Depth, velocity, flow.**			×

2.2.1. Flood hazard analysis

For the purpose of flood hazard assessment, meteorological and spatial data sets were created, which are described in more detail below. Data on short-term extreme rainfall, including DDF and IDF curves as well as the design storm, were obtained for the nearest rain gauge station Rijeka from the Hydrological Study of the Adriatic (IE, 2023), prepared within the VEPAR project. The final results of the rainfall analysis are design storms combined with DDF curves, which define synthetic rainfall of varying durations for three probabilities (return periods of 5, 25, and 100 years meaning 20%, 4%, and 1% annual exceedance probability, respectively). The result of the design storm shape (pluviograms) for the Rijeka station is shown in Figure 2.5.

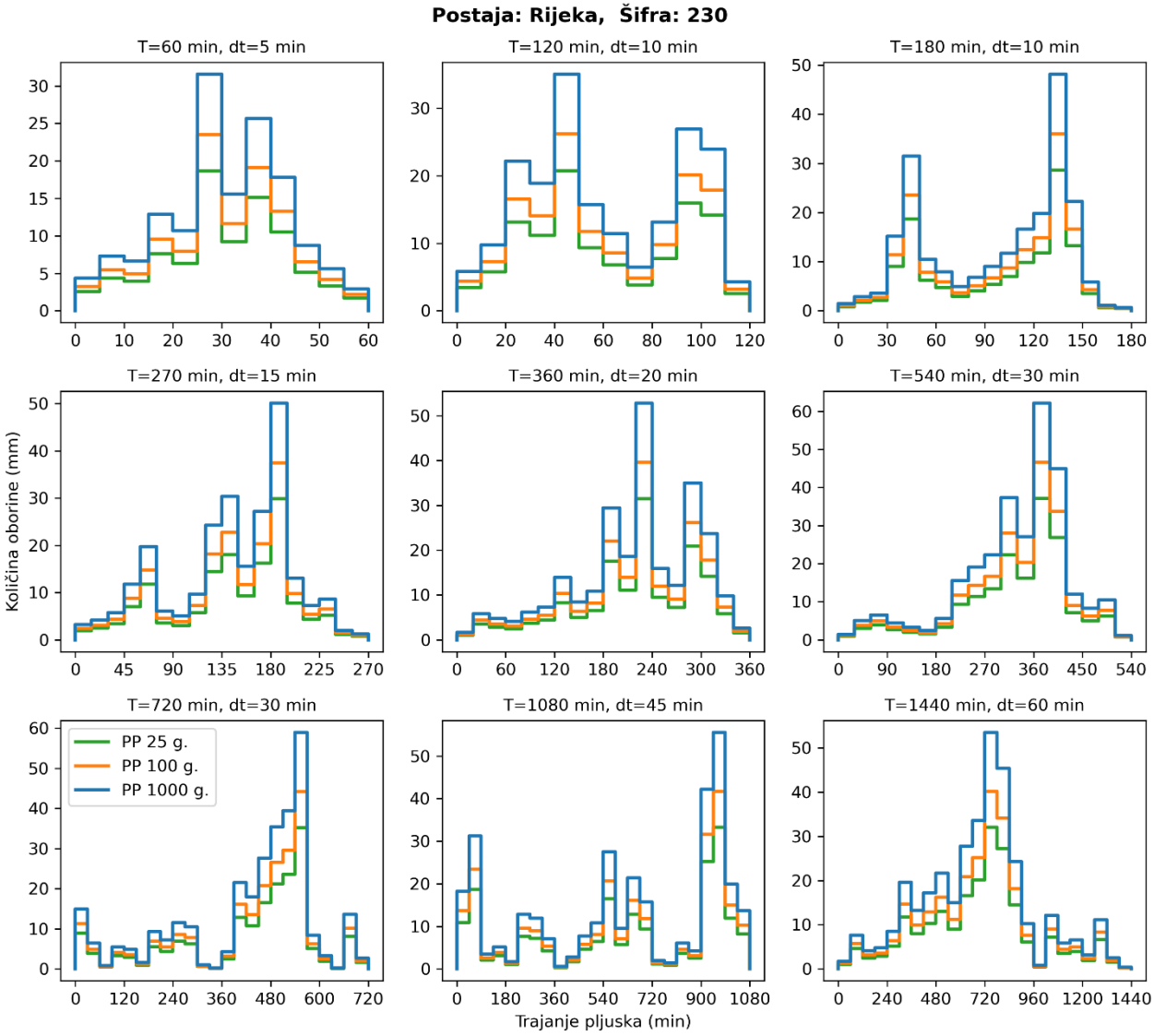

Figure 2.5. Example of a synthetic rainfall event – pluviograms of the design rainfall for the Rijeka station (IE, 2023).

In order to carry out a hydrologic-hydraulic analysis of rainfall runoff - flood hazard assessment, the basic spatial datasets have been obtained and processed. Table 2.7 provides an overview of all obtained and generated spatial data with descriptions and sources.

Table 2.7 Overview of all obtained and generated spatial data required for the pluvial flood hazard assessment.

Data	Type	Source
Digital terrain model (DTM)	Raster, 1 m resolution	Digital terrain model was generated based on the LiDAR data obtained from the State Geodetic Administration.
Land-cover	Raster, 10 m resolution	CLCplus Backbone 2021., Copernicus Land Monitoring Service
Imperviousness density	Raster, 10 m resolution	Imperviousness Density 2018., Copernicus Land Monitoring Service.
Surface roughness	Raster, 1 m resolution	Generated based on the land-cover map using appropriate Manning's roughness coefficient data from the literature.
Soil infiltration (CN curve numbers)	Raster, 1 m resolution	Generated based on the land-cover map and the hydrological soil group using appropriate CN data from the literature.

The digital terrain model and land-cover map were obtained in their final form (Figure 3.6), while the overview of the methodology for generating the surface roughness and the soil infiltration maps is given below.

For the surface roughness and the soil infiltration assessment, the CLCplus Backbone 2021 land-cover map was used. It is a 10 m resolution raster that provides a pan-Europen spatially consistent and seamless, detailed land cover inventory showing the dominant land cover for each pixel among the 11 basic land cover classes (CLCplus Backbone 2021 (raster 10 m), Europe, 3-yearly, *European Union's Copernicus Land Monitoring Service*).

Since there are no unified and widely accepted values for surface roughness based on land cover classes, values were adapted according to the National Resources Conservation Service's (2004) Hydrology National Engineering Handbook. The most widely used Manning's roughness coefficient was applied (Chow, 2010). The infiltration capacity of the soil was described by the CN curve number according to the NRCS methodology (USDA, 2017; Hong and Adler, 2008), and appropriate values were assigned to each land cover class. Table 2.8 presents the adopted values of Manning's roughness coefficient and CN curve numbers for the four hydrological soil groups.

Table 2.8. Manning's roughness coefficient and CN curve number for the four hydrological soil groups for each land cover class from CLCplus backbone 2021.

Class	Code	n	CN A	CN B	CN C	CN D
Sealed	1	0.013	98	98	98	98
Woody needle leaved trees	2	0.14	36	60	73	79
Woody Broadleaved deciduous trees	3	0.14	36	60	73	79
Woody Broadleaved evergreen trees	4	0.14	36	60	73	79
Low-growing woody plants	5	0.09	45	65	75	80
Permanent herbaceous	6	0.035	45	65	75	80
Periodically herbaceous	7	0.035	49	69	79	84
Lichens and mosses	8	0.035	98	98	98	98
Non and sparsely vegetated	9	0.035	70	81	88	92
Water	10	0.033	100	100	100	100
Snow and ice	11	0.033	98	98	98	98
Coastal seawater buffer	253	0.033	100	100	100	100
Outside area	254	0.06	70	81	88	92

Figure 2.6 shows an example of the spatial data used for the analysis of the section of the City of Novi Vinodolski:

- digital orthophoto (2021./22.),
- digital terrain model (LIDAR 1 m resolution),
- land cover model (CLCplus backbone 2021.).

The flood hazard analysis was conducted for three scenarios: low, medium, and high probability of flooding. For these scenarios, the probabilities refer to the return period or the annual exceedance probability (AEP) and are listed in Table 2.9. A high probability flood corresponds to an annual exceedance probability (AEP) of 20%, a medium probability flood corresponds to an AEP of 4%, while a low probability flood corresponds to an AEP of 1%. The hazard analysis was carried out under the assumption that the probability of occurrence of extreme rainfall and pluvial flooding are equal (for example, rainfall with an annual exceedance probability of 4% results in a flood with an annual exceedance probability of 4%)

Table 2.9. Scenarios for assessing the pluvial flood hazard and risk.

Scenario	Return Period (RP)	Annual Exceedance Probability (AEP)
High probability flooding	5	20%
Medium probability flooding	25	4%
Low probability flooding	100	1%

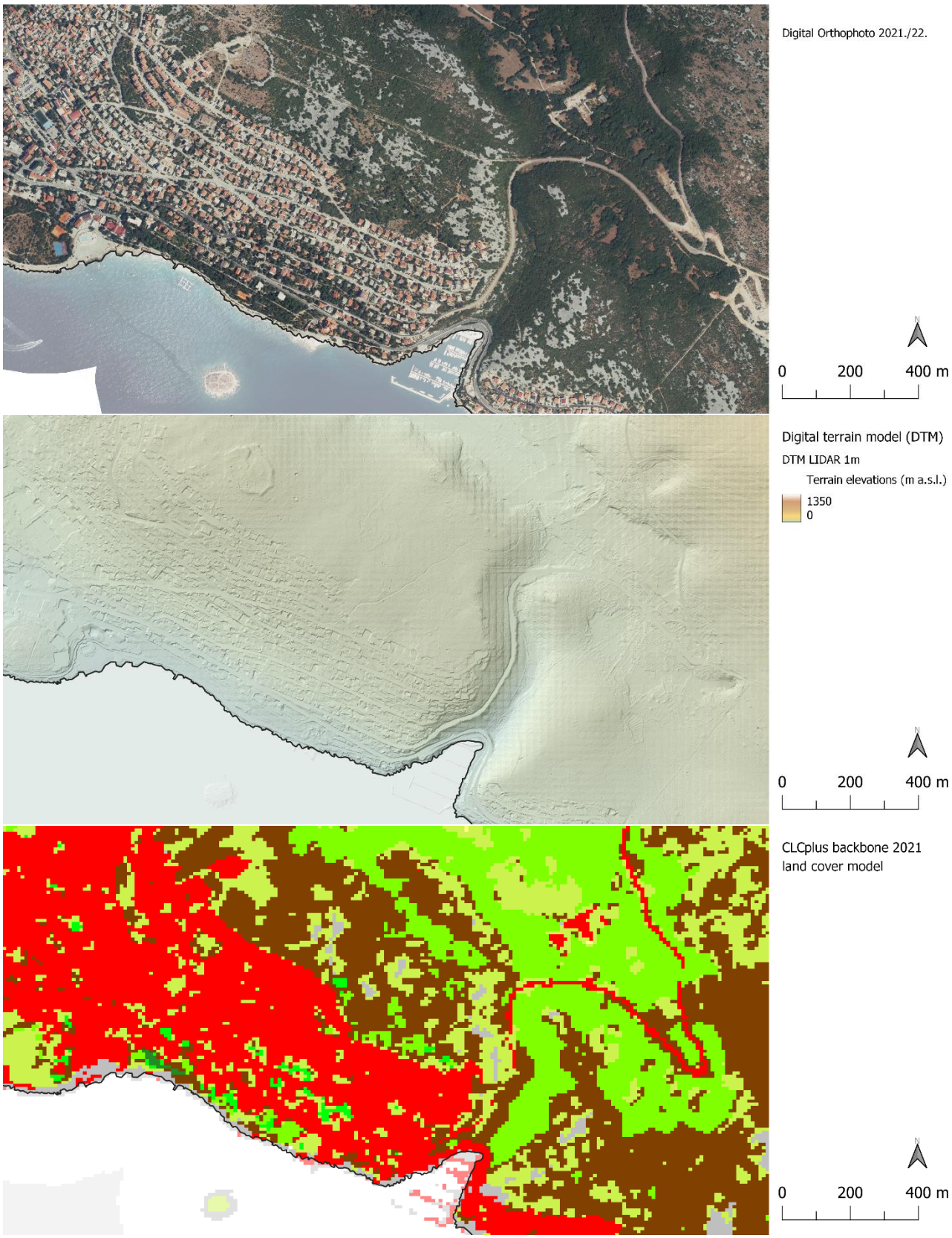

Figure 2.6. . Spatial data used for the assessment of flood hazard (a detail of coast of the City of Novi Vinodolski): a) digital orthophoto (2021./22.), b) high-resolution digital terrain model (LIDAR 1 m), c) CLCplus backbone 2021 land cover model (2021.).

Flood hazard analysis is based on the hydrologic-hydraulic simulations of rainfall-runoff processes. The flood simulations were performed using the Hydrologic Engineering Center – River Analysis System (HEC-RAS 6.6) (Brunner, 2021.), a widely used software for hydraulic calculations that enables 1D or 2D steady and unsteady analysis of surface water flows. The model uses the approach known as rain-on-grid (RoG), where the hydrologic and hydrodynamic flood processes are modeled entirely with the 2D hydrodynamic model, rather than two different model systems (Krvavica et al., 2023). Furthermore, the model allows the definition of additional hydrological elements for the calculations, such as soil infiltration, which can be defined with a constant coefficient, the SCS method, or with the Green and Ampt equation.

The establishment of a mathematical model of rainfall-runoff consists of the following steps:

a) Defining the digital terrain model,
b) Defining the spatial parameters of the infiltration process,
c) Defining the imperviousness density,
d) Defining the spatial distribution of surface roughness,
e) Defining the spatial domain of the model and generating the computational grid,
f) Defining the boundary conditions,
g) Defining the numerical computation parameters,
h) Defining the scenarios.

The digital terrain model is generated within the HEC-RAS software and is based on a 1 m resolution DTM derived from LiDAR data.

Figure 2.7 shows an example of the computational grid, the spatial distribution of Manning's roughness coefficient values assigned using the CLCplus backbone 2021 land cover, and the spatial distribution of CN values that define the rainfall infiltration process into the soil. The CN map and the roughness map were directly implemented in the mathematical model based on the spatial datasets shown in the previous chapter.

It should also be noted that at this level of analysis (for the entire catchment), the positive effect of the stormwater drainage system was neglected, as recommended in previous studies (RAINMAN, 2020).

The spatial domain of the model is defined by the boundaries of three municipalities and the boundaries of sub-basins in this area but modified in some places to soften the edges. Within the model domain, a computational grid is defined as a structured square grid with a resolution of 100 m, but with the following modifications:

- Populated areas are imported as refinement regions with a resolution of 10 m,
- Waterways are imported as breaklines with 10 m resolution cells along them to better capture the flow,
- Coastal areas and areas of interest (other than populated areas) are imported as refinement regions with a resolution of 20 m,
- Larger areas of interest are imported as refinement regions with a resolution of 50 m.

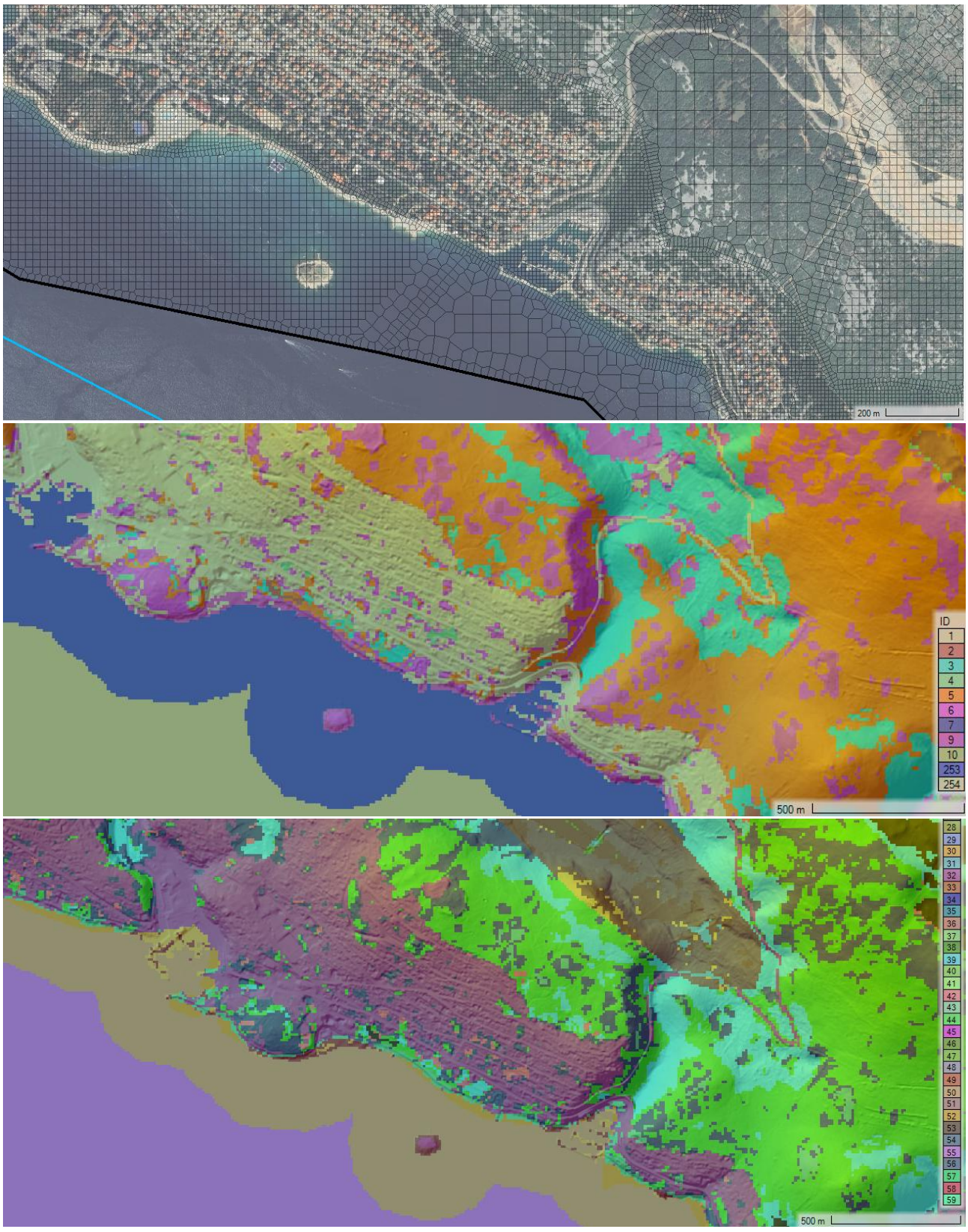

Figure 2.7. Details of data used in the HEC-RAS model: a) computational grid b) Manning's roughness coefficient (10^{-3} $m^{-1/3}s$) c) CN curve number.

Two boundary conditions are defined within the model:

- Spatially uniform precipitation over the entire 2D domain defined by the design storm,
- Uniform stage hydrograph for the Adriatic Sea (southwestern boundary).

For the numerical analysis of the surface water flow, an unsteady 2D flow analysis with a set of equations described by the diffusion wave method and a variable time step was used. In an implicit computation, the parameter θ = 1.0 was used and the PARDISO algorithm was used to solve the matrices (Brunner, 2021). The time step is calculated dynamically based on the CFL number, which ranges from 0.8 to 4.0.

The analysis included three scenarios with different probabilities (Table 3.9), and for each scenario, five simulations were conducted for rainfall durations of 1, 3, 6, 12, and 24 hours, resulting in a total of 15 computational simulations. The simulation results provide a time series of surface runoff dynamics presented in the form of maximum recorded water depths and velocities (Figure 3.8). In addition to water depth (h) and velocity (v), secondary parameters combining depth and velocity (hv and hv^2) were also determined. The final result is given as an envelope of the maximum values of all these parameters for each scenario.

The pluvial flood hazard is expressed based on the three indicators for three scenarios (probabilities):

- Water depth
- Water velocity
- Hazard severity.

Figure 2.8 shows an example of all three indicators mentioned above for one scenario. Water depth in the flooded area has the most significant impact on flood damage and is considered the primary indicator of flood hazard. Water velocity also influences the extent of damage to buildings. However, this indicator is particularly important for assessing the hazard to the population, including human stability and vehicle stability. In order to assess human (in)stability, an additional indicator — the specific water flow (the product of water depth and velocity) — is calculated in this study, but not presented as a separate map. In order to better assess the hazard to the population, vehicles, and buildings, a hazard severity assessment is also conducted.

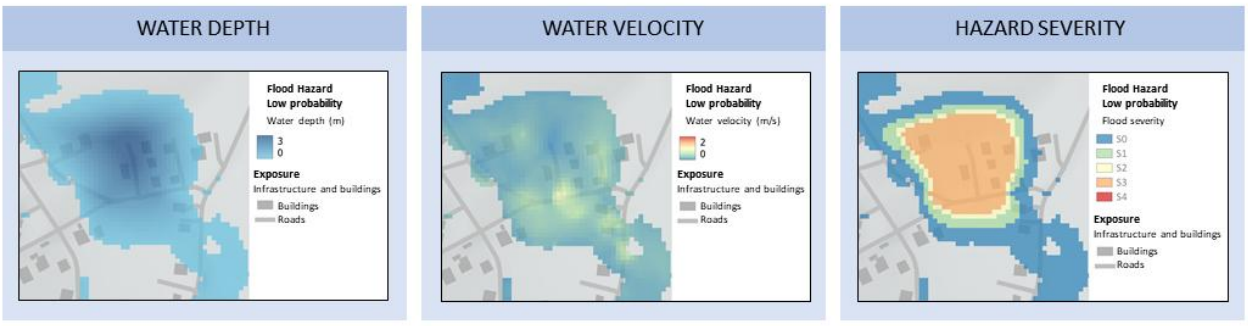

Figure 2.8. Example of selected hazard indicators for pluvial flooding: Water depth, water velocity, and hazard severity.

The hazard severity assessment in this study is conducted using the SUFRI method, developed as part of the European project *Sustainable Strategies of Urban Flood Risk Management* (Escuder-Bueno et al., 2011). In this project, strategies for sustainable flood risk management were defined, including vulnerability analysis, an advanced flood early warning system, and communication strategies to optimize risk management. A key focus of the SUFRI project was the analysis of flood vulnerability and the risk to the population. The proposed methodology for assessing the hazard severity includes indicators such as water depth (y), water velocity (v), dragging parameter (vy), and sliding parameter (v^2y). The criteria for hazard severity assessment are shown in Figure 2.9 and Table 2.10.

Table 2.10. Flood severity levels for estimating consequences of pluvial flooding (Escuder-Bueno et al., 2011).

Flood severity levels		Depth y (m)	Velocity v (m/s)	Dragging parameter vy (m^2/s)	Sliding parameter v^2y (m^3/s^2)
S0	**Negligible severity.** No victims are expected.	< 0.45	< 1.50	< 0.50	< 1.23
S1	**Low severity.** Pedestrians may suffer loss of stability. People in danger.	< 0.80	< 1.60	< 1.00	< 1.23
S2	**Moderate severity.** Significant loss of stability. Cars can lose road holding. Floating.	< 1.00	< 1.88	< 1.00	< 1.23
S3	**High severity.** High risk for the population. Low risk for buildings.	≥ 1.00	≥ 1.88	≥ 1.00	≥ 1.23
S4	**Extreme severity.** Structural damages on buildings.	≥ 1.00	≥ 1.88	≥ 3.00	≥ 1.23

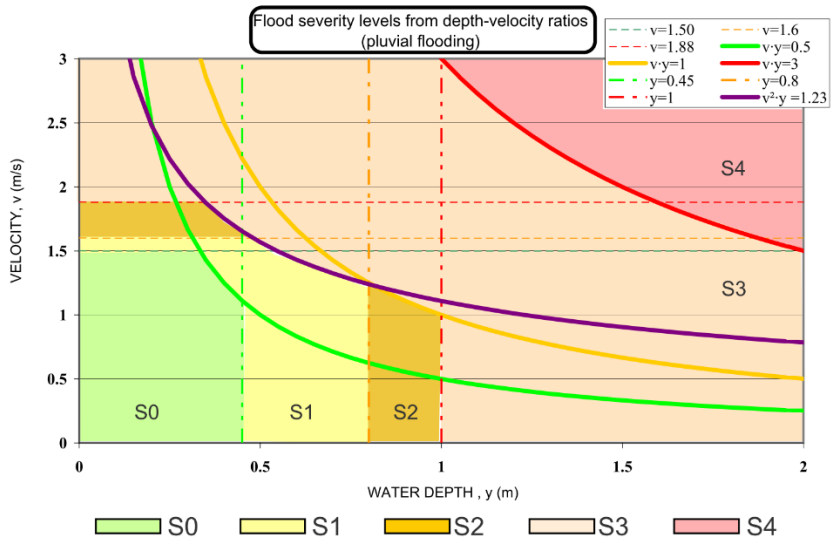

Figure 2.9. Flood severity levels for estimating consequences in pluvial flooding (Escuder-Bueno et al., 2011).

2.3. Results of the pluvial flood hazard assessment

2.3.1. Hydrologic–hydraulic model for rainfall-runoff processes

Based on the conducted hydrological analyses of the catchment area, the domain for hydrological-hydraulic flood analyses using a 2D mathematical model was defined. Figure 2.10 shows the model domain for the entire area of the Municipality of Vinodolska općina and the City of Novi Vinodolski. The flood mathematical model was developed using the HEC-RAS software in accordance with the methodology presented in Chapter 2.2.

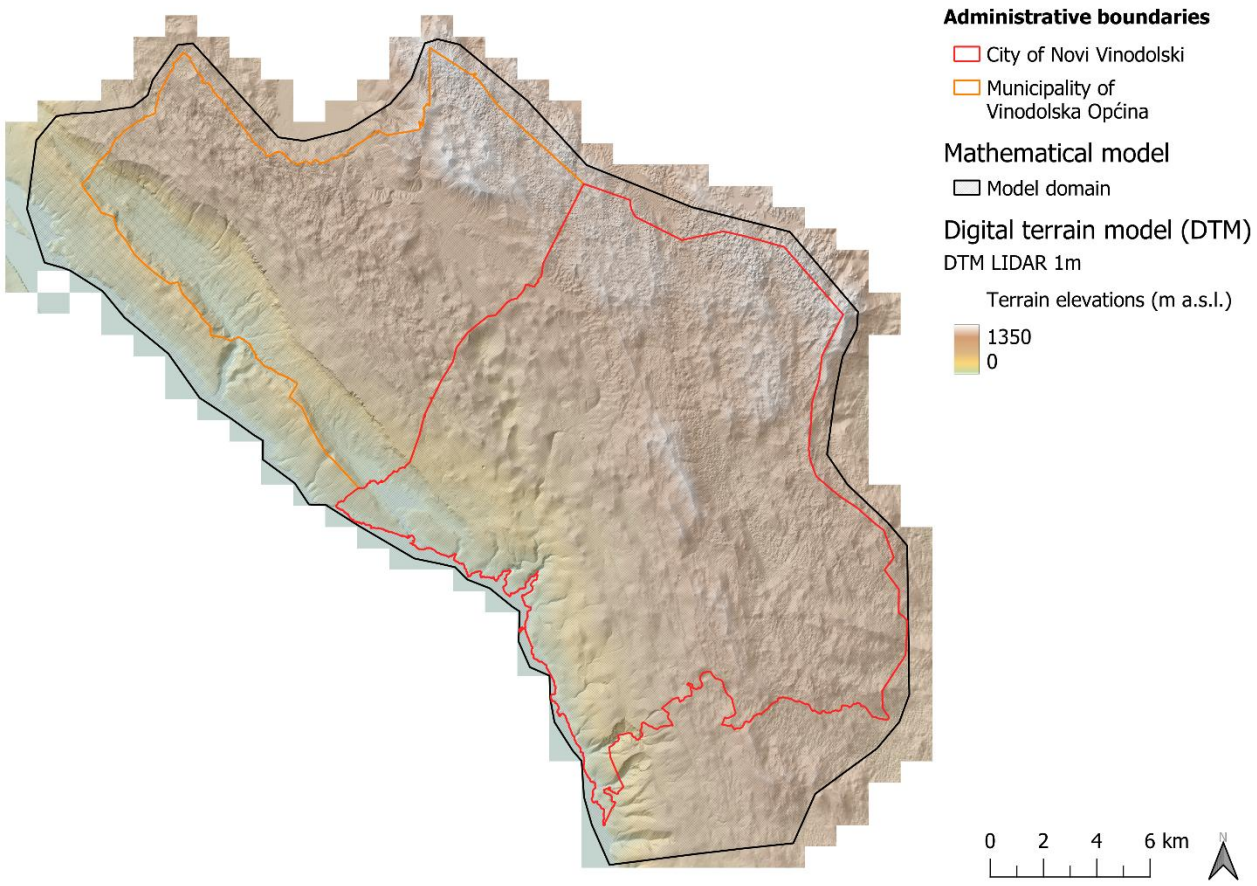

Figure 2.10. Domain of the surface runoff mathematical model for stormwater, overlaid on a high-resolution DTM for the Municipality of Vinodolska općina and the City of Novi Vinodolski.

2.3.2. Pluvial flood hazard assessment for the Municipality of Vinodolska općina

The flood hazard assessment for the Municipality of Vinodolska općina was carried out for three scenarios—low, medium, and high probability—which correspond to annual exceedance probabilities of 1%, 5%, and 20%, respectively. The pluvial flood hazard maps show the spatial distribution of water depths and velocities, as well as severity levels for each of the specified probabilities.

Figures 2.11 to 2.13 present examples of hazard maps showing water depths for low, medium, and high probability events in the area, with detailed results shown in Figures 2.14 to 2.16.

Figures 2.17 to 2.19 present examples of hazard maps showing water velocities for low, medium, and high probability events in the area, with detailed results in Figures 2.20 to 2.22.

Figures 2.23 to 2.25 present examples of hazard maps showing severity levels for low, medium, and high probability events in the area, with detailed results in Figures 2.26 to 2.28.

From these maps, the main flood generation processes in the catchment can be characterized, and critical locations identified. The flood generation process primarily depends on terrain characteristics (terrain morphology, as well as geological and pedological features). In most parts of the catchment, which is located in a karst area, no continuous surface runoff of rainfall is observed, and therefore no flooding occurs except in isolated depressions, where water quickly infiltrates into the subsurface. The only exceptions with more pronounced flooding are the Dubračina River catchment in the Vinodol Valley (western and southwestern part of the catchment), the upstream section of Velo polje (southern part of the catchment toward the City of Novi Vinodolski), area around Bribir (central to eastern part of the catchment), and to a lesser extent, in Lič polje (northeastern part of the catchment). Highest velocities are observed in river and drainage channels.

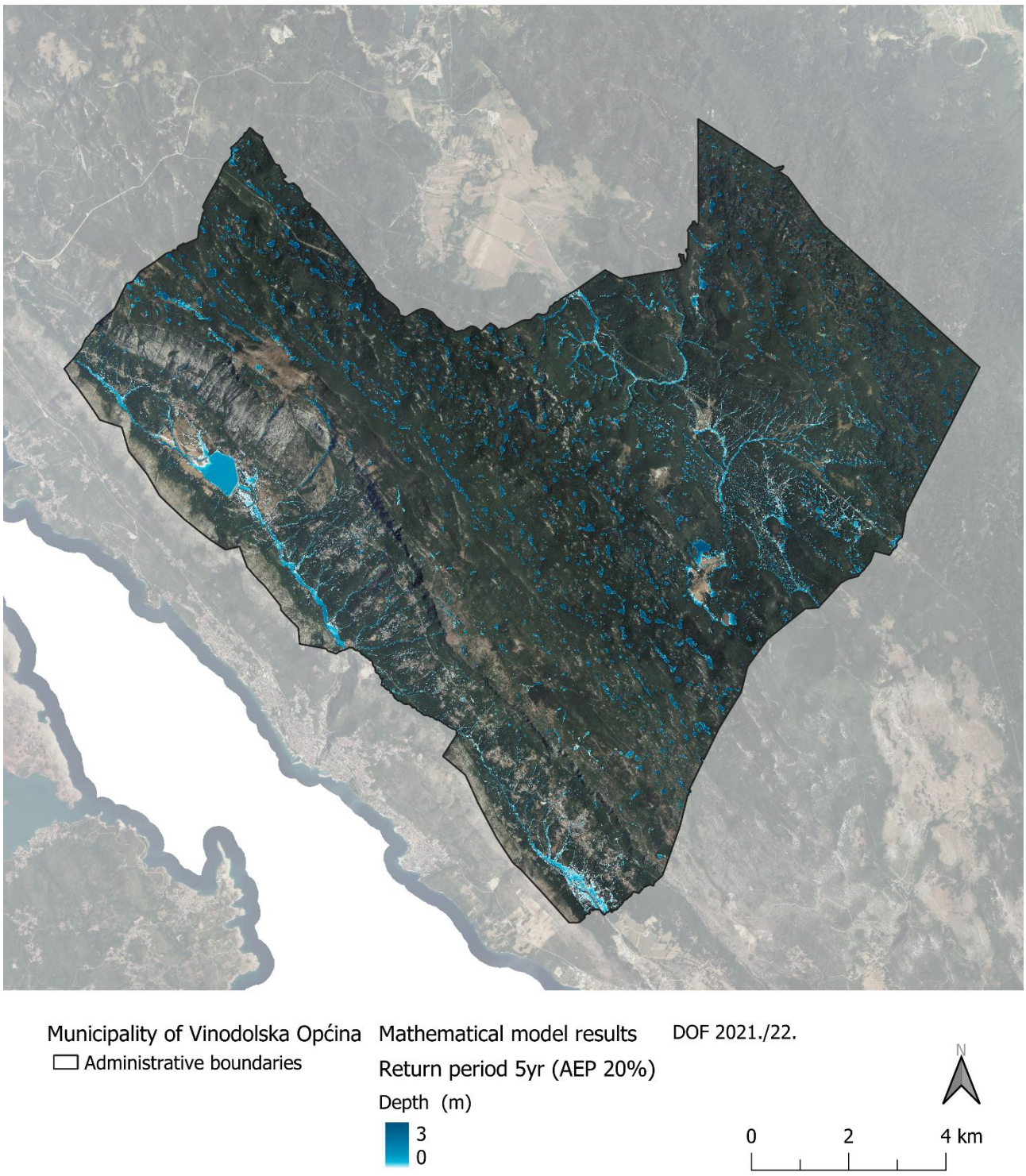

Figure 2.11. Flood hazard map for a return period of 5 years (AEP 20%) for the Municipality of Vinodolska općina - water depth.

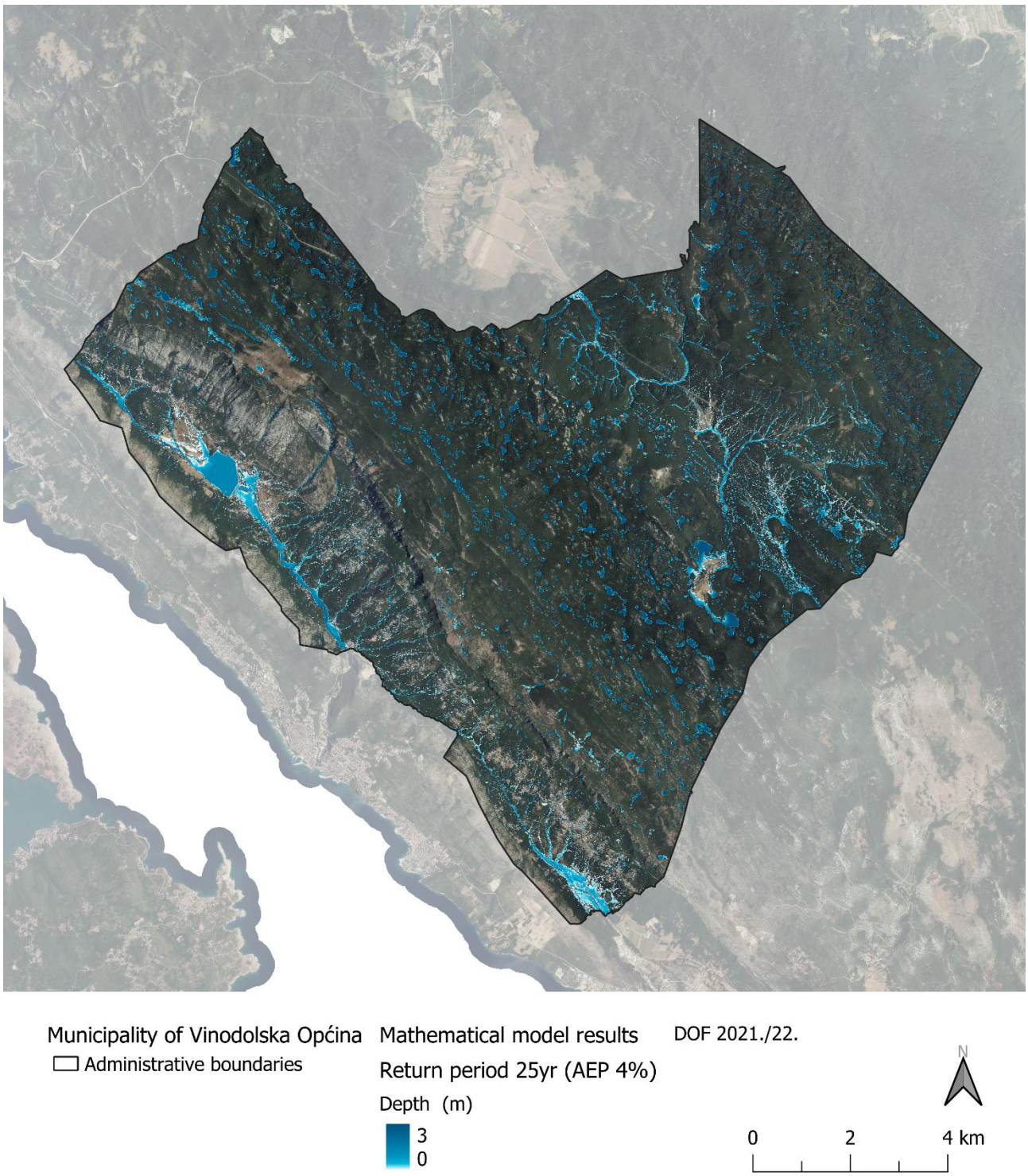

Figure 2.12. Flood hazard map for a return period of 25 years (AEP 4%) for the Municipality of Vinodolska općina - water depth.

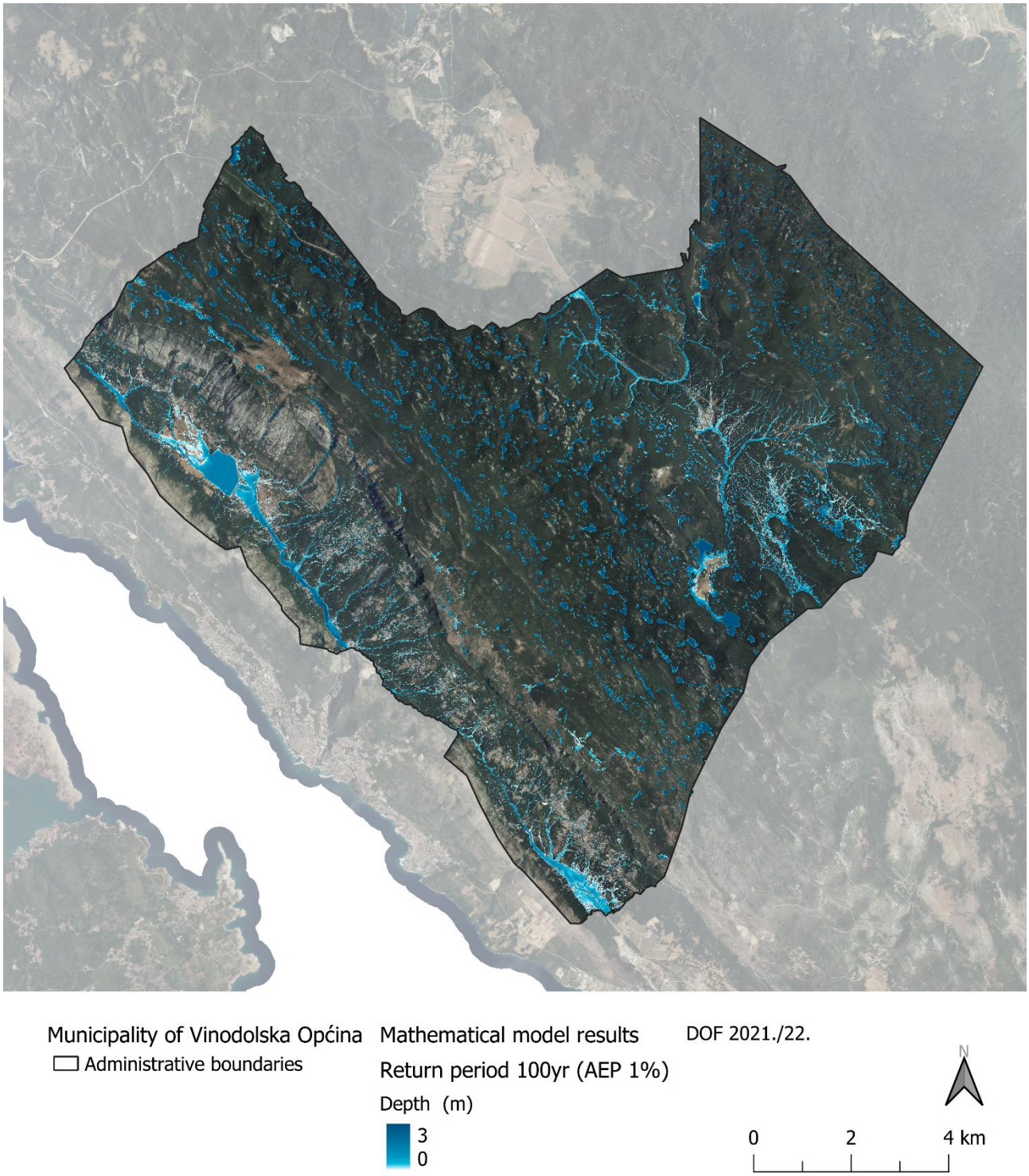

Figure 2.13. Flood hazard map for a return period of 100 years (AEP 1%) for the Municipality of Vinodolska općina - water depth.

Figure 2.14. Detail from the flood hazard map for a return period of 5 years (AEP 20%) for the selected microlocation in the Municipality of Vinodolska općina - water depth.

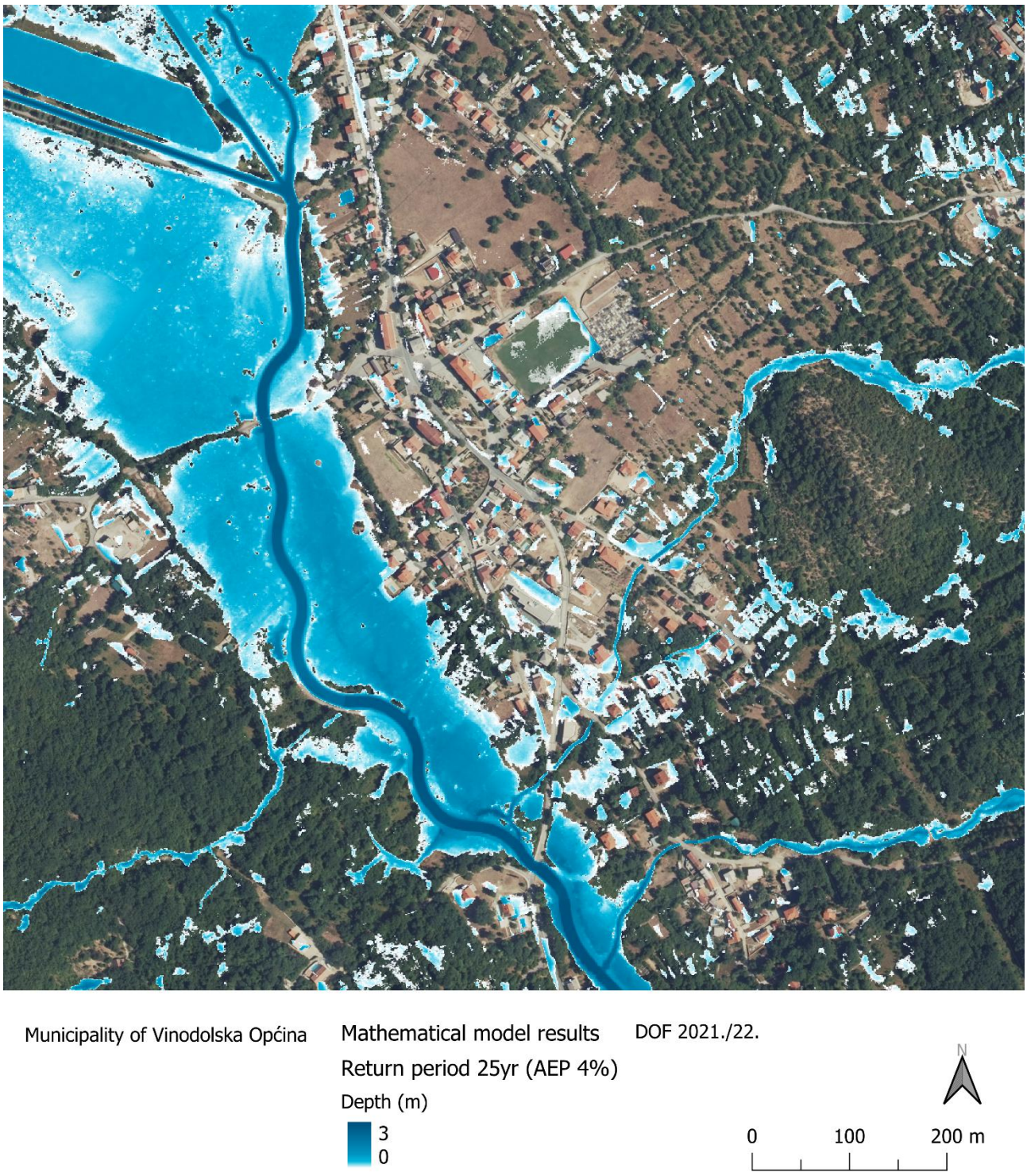

Figure 2.15. Detail from the flood hazard map for a return period of 25 years (AEP 4%) for the selected microlocation in the Municipality of Vinodolska općina - water depth.

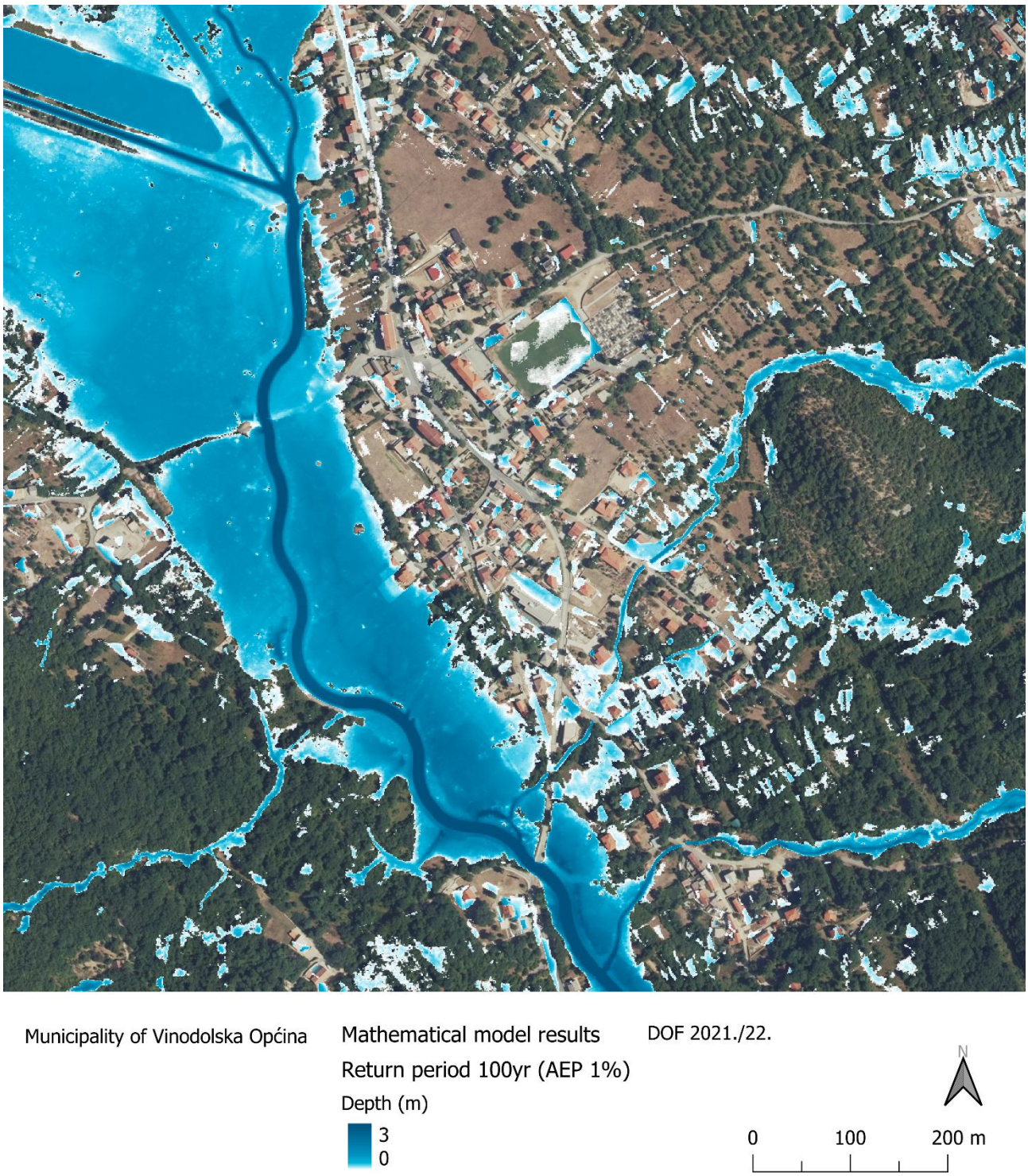

Figure 2.16. Detail from the flood hazard map for a return period of 100 years (AEP 1%) for the selected microlocation in the Municipality of Vinodolska općina - water depth.

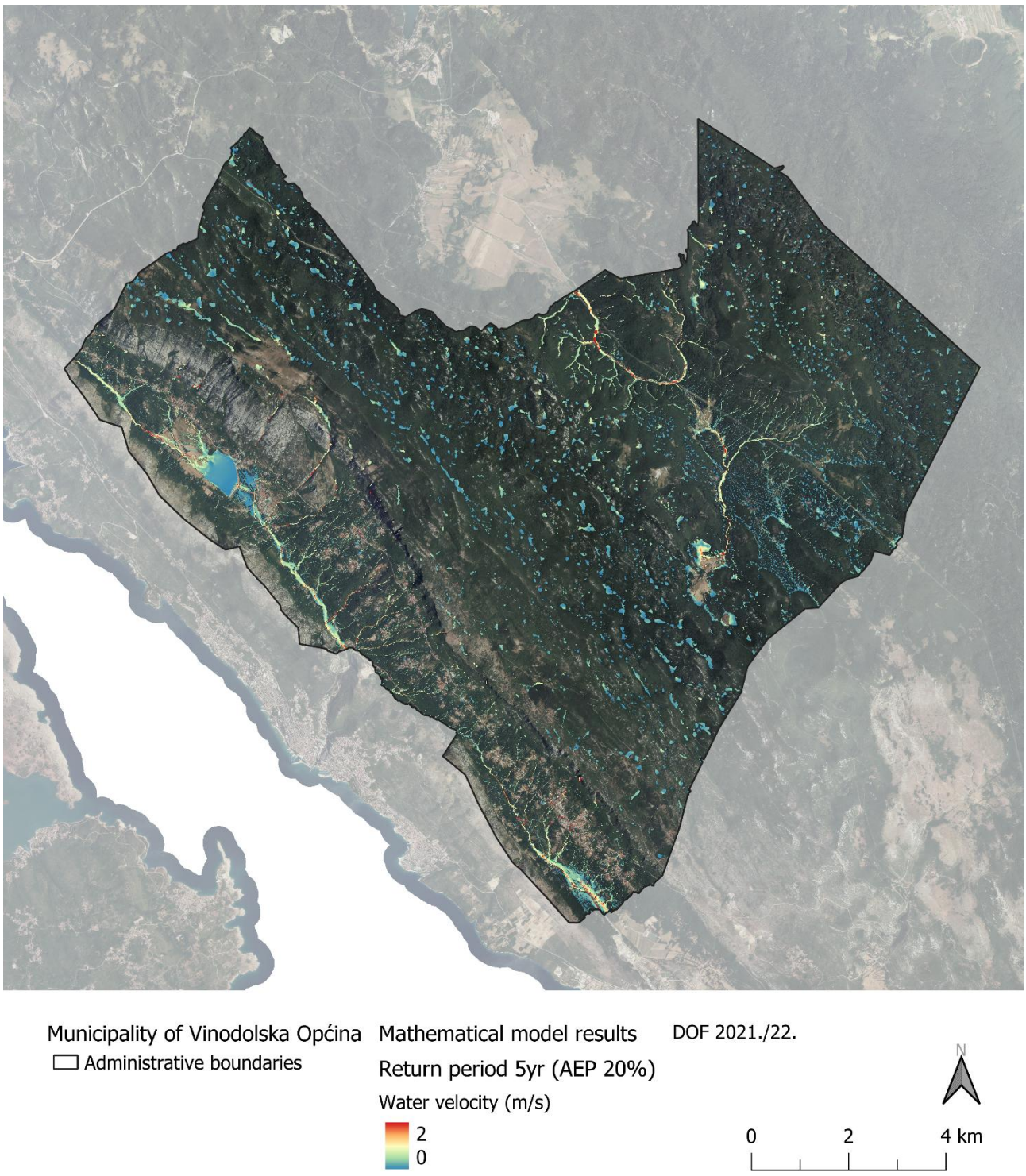

Figure 2.17. Flood hazard map for a return period of 5 years (AEP 20%) for the Municipality of Vinodolska općina - water velocity.

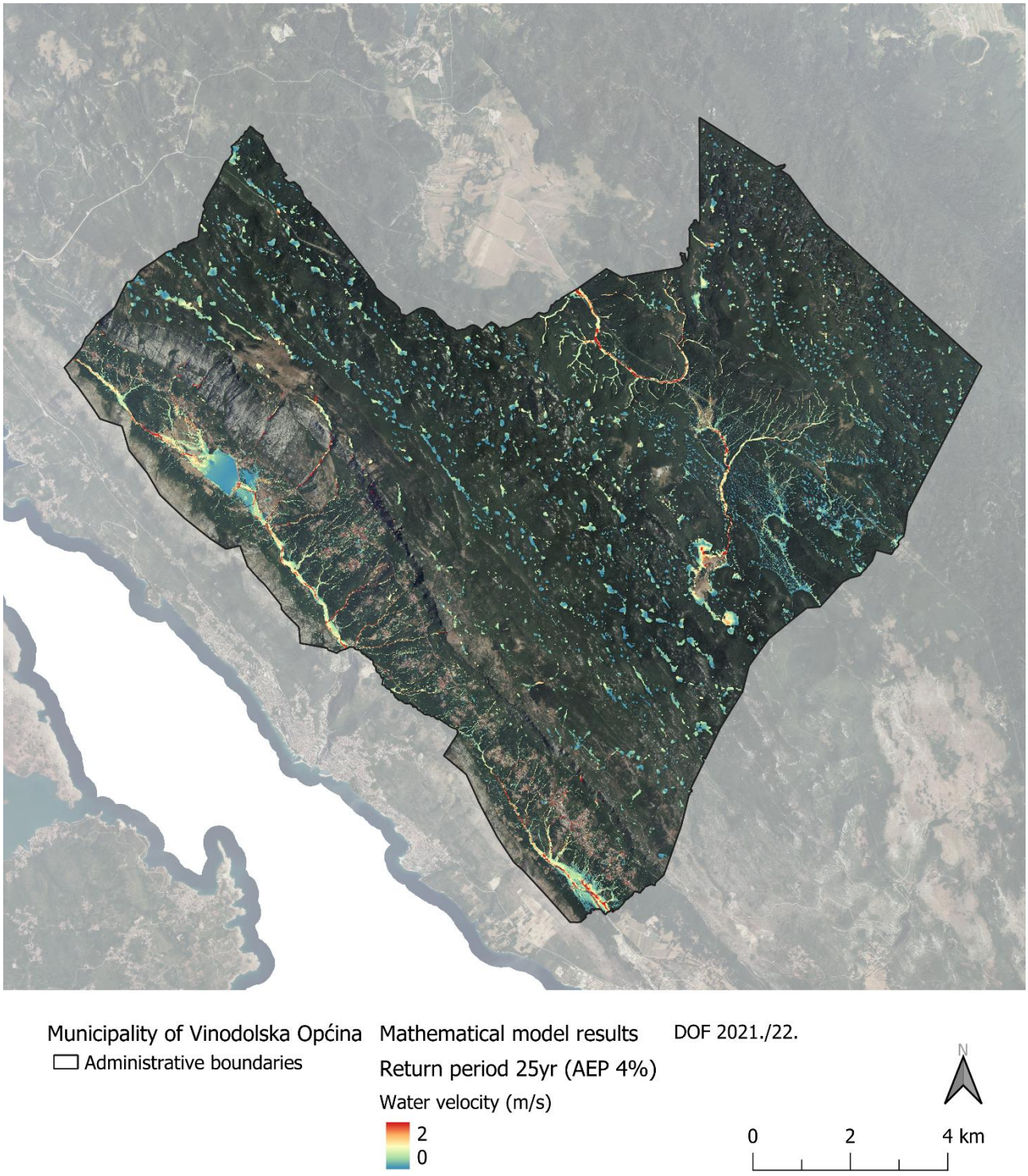

Figure 2.18. Flood hazard map for a return period of 25 years (AEP 4%) for the Municipality of Vinodolska općina - water velocity.

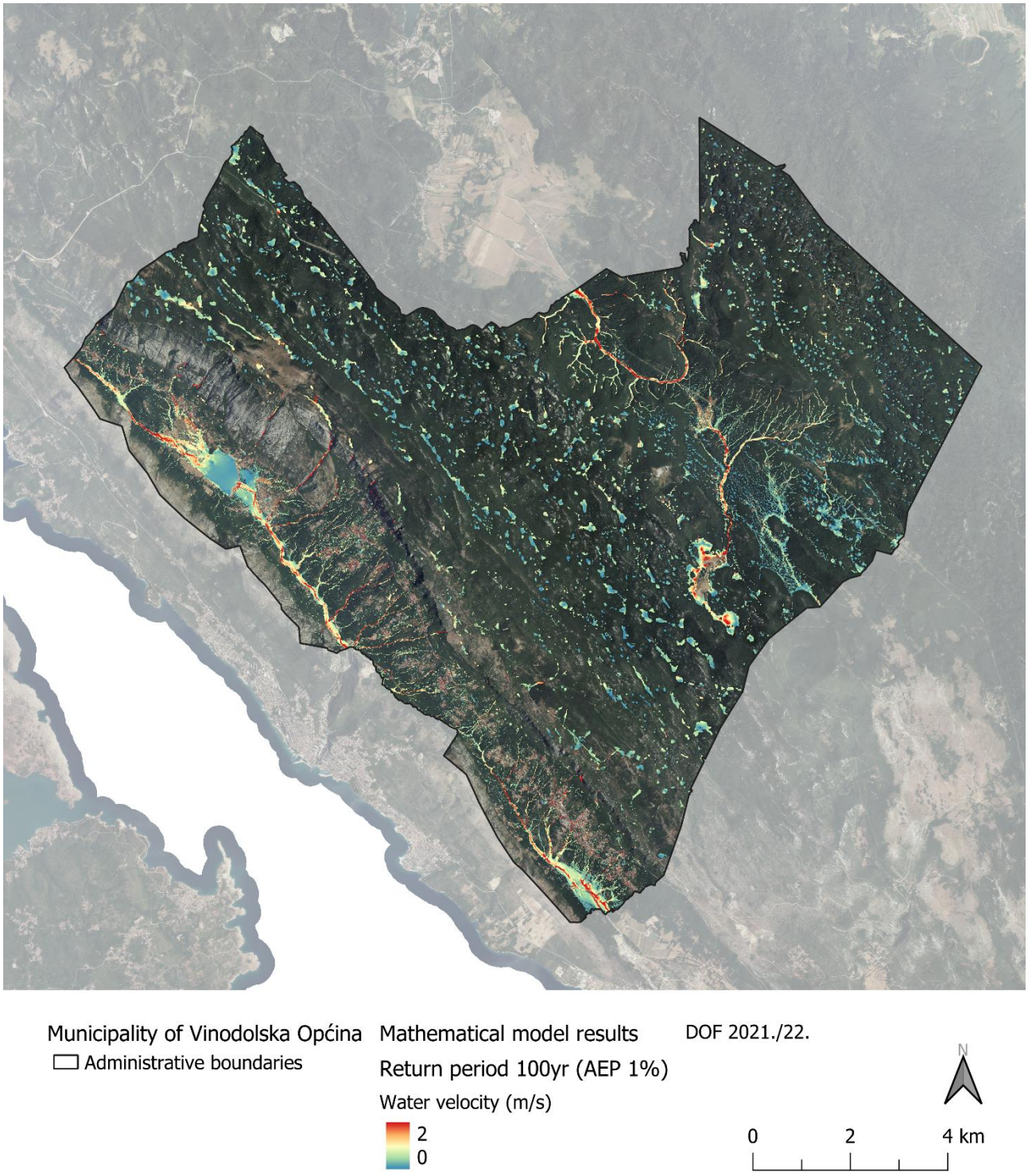

Figure 2.19. Flood hazard map for a return period of 100 years (AEP 1%) for the Municipality of Vinodolska općina - water velocity.

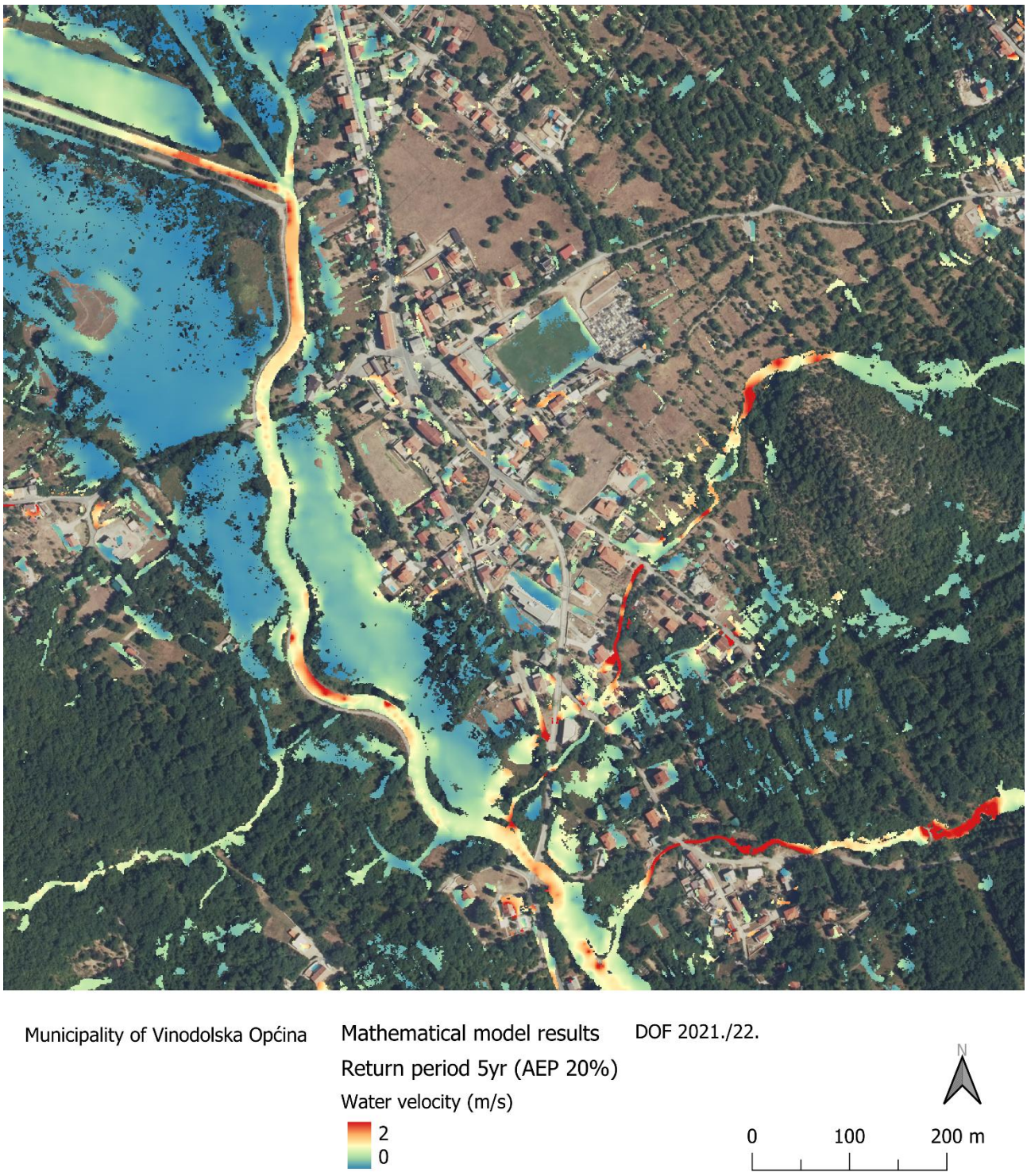

Figure 2.20. Detail from the flood hazard map for a return period of 5 years (AEP 20%) for the selected microlocation in the Municipality of Vinodolska općina - water velocity.

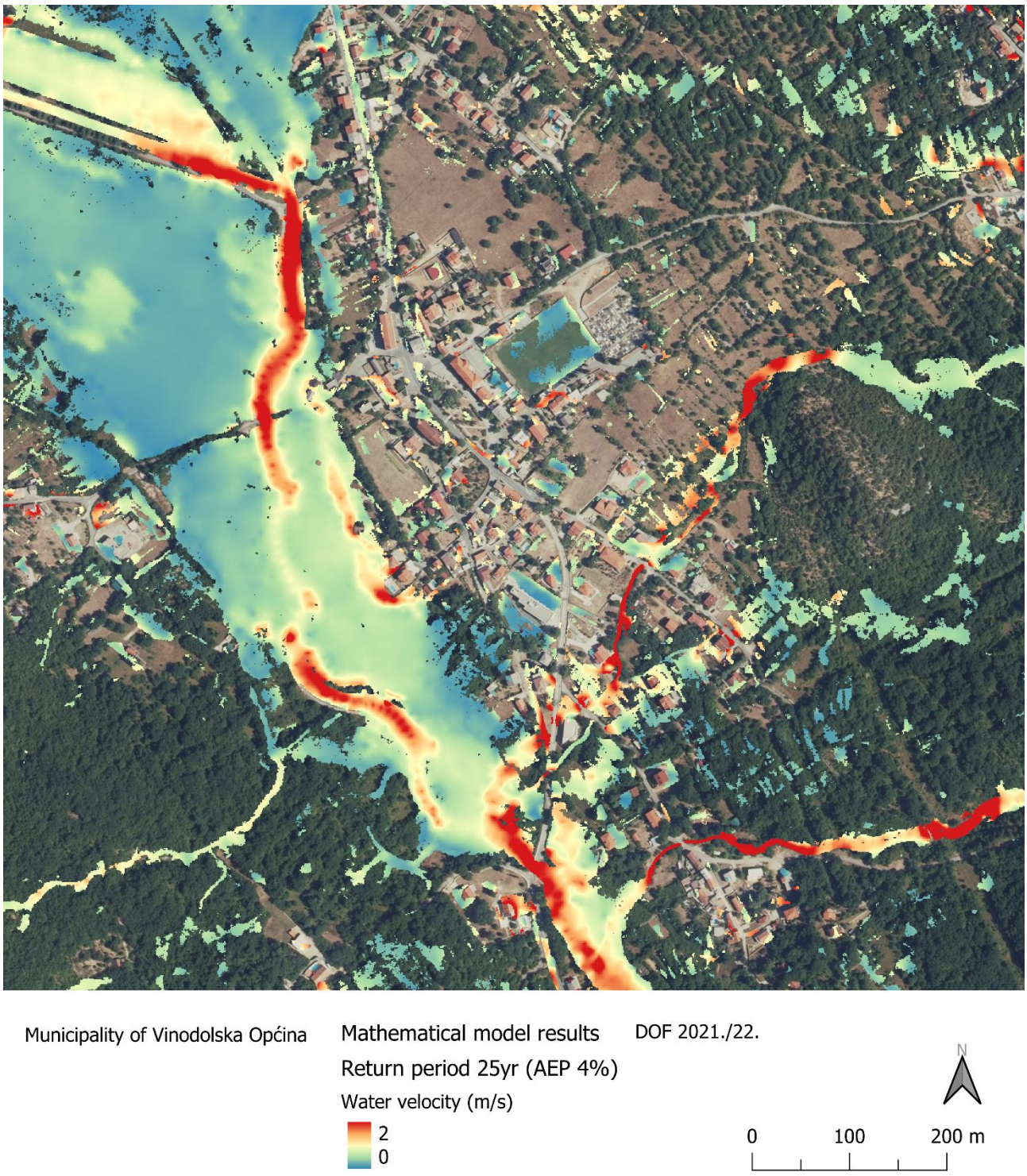

Figure 2.21. Detail from the flood hazard map for a return period of 25 years (AEP 4%) for the selected microlocation in the Municipality of Vinodolska općina - water velocity.

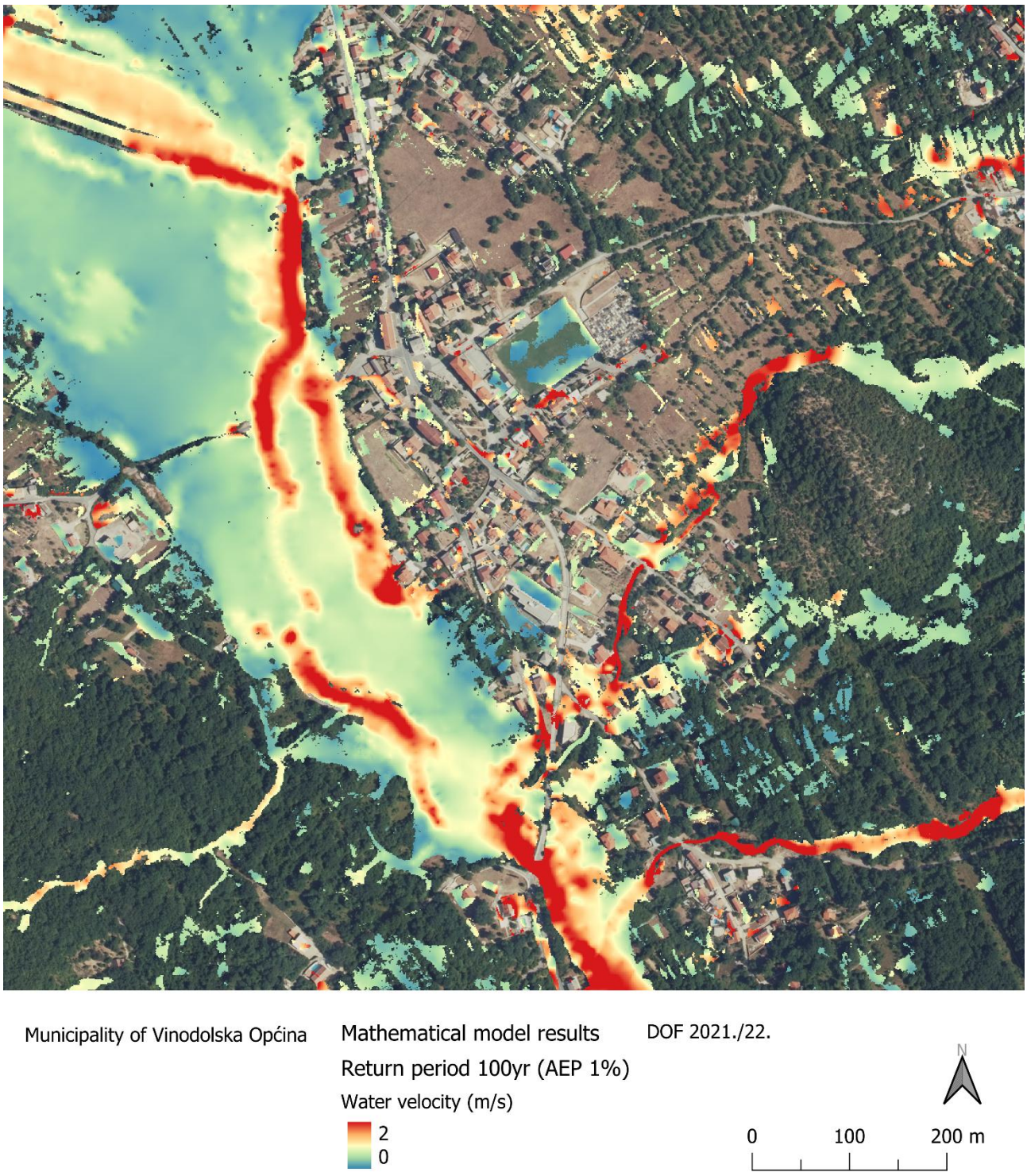

Figure 2.22. Detail from the flood hazard map for a return period of 100 years (AEP 1%) for the selected microlocation in the Municipality of Vinodolska općina - water velocity.

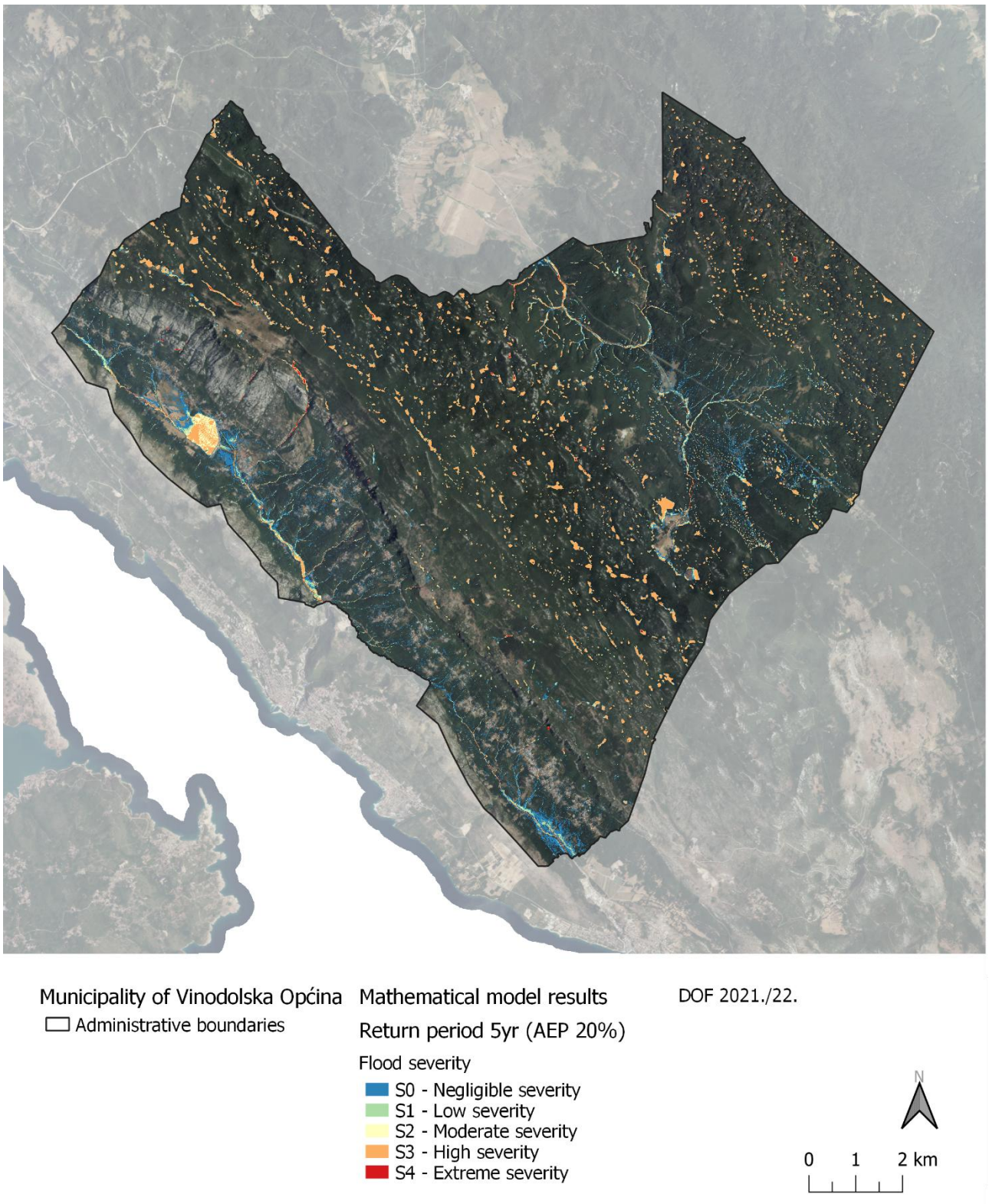

Figure 2.23. Flood hazard map for a return period of 5 years (AEP 20%) for the Municipality of Vinodolska općina - flood severity.

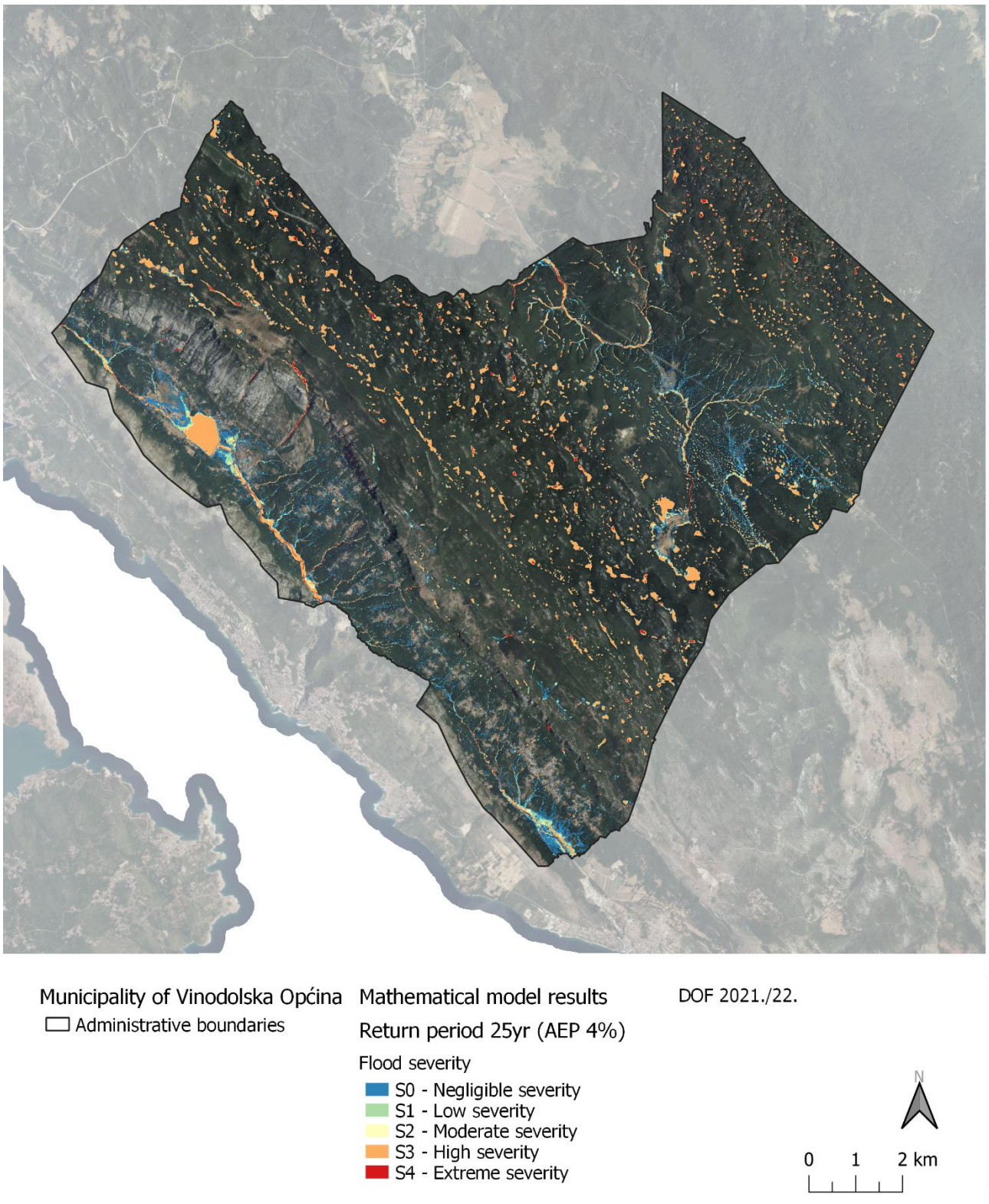

Figure 2.24. Flood hazard map for a return period of 25 years (AEP 4%) for the Municipality of Vinodolska općina - flood severity.

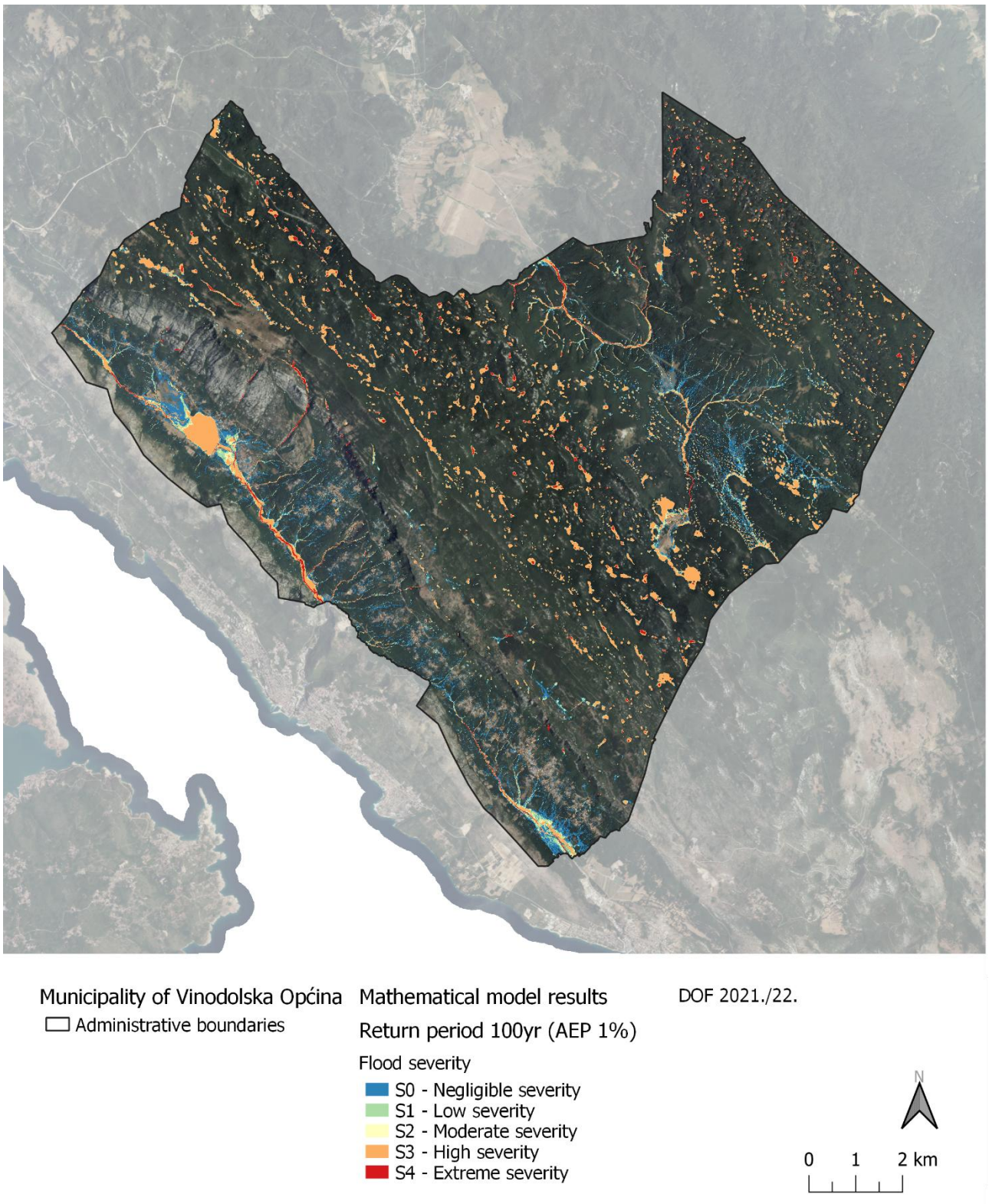

Figure 2.25. Flood hazard map for a return period of 100 years (AEP 1%) for the Municipality of Vinodolska općina - flood severity.

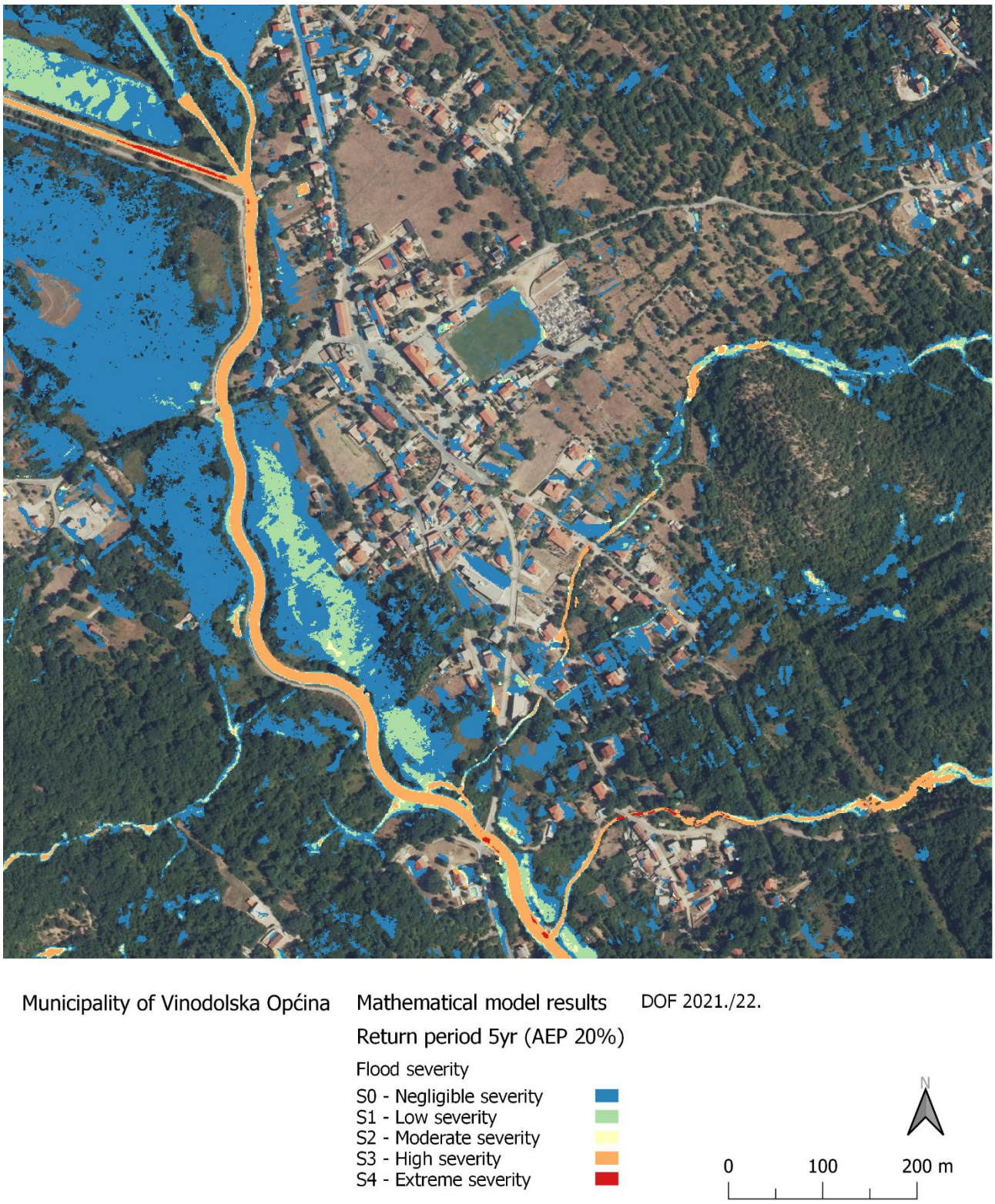

Figure 2.26. Detail from the flood hazard map for a return period of 5 years (AEP 20%) for the selected microlocation in the Municipality of Vinodolska općina - flood severity.

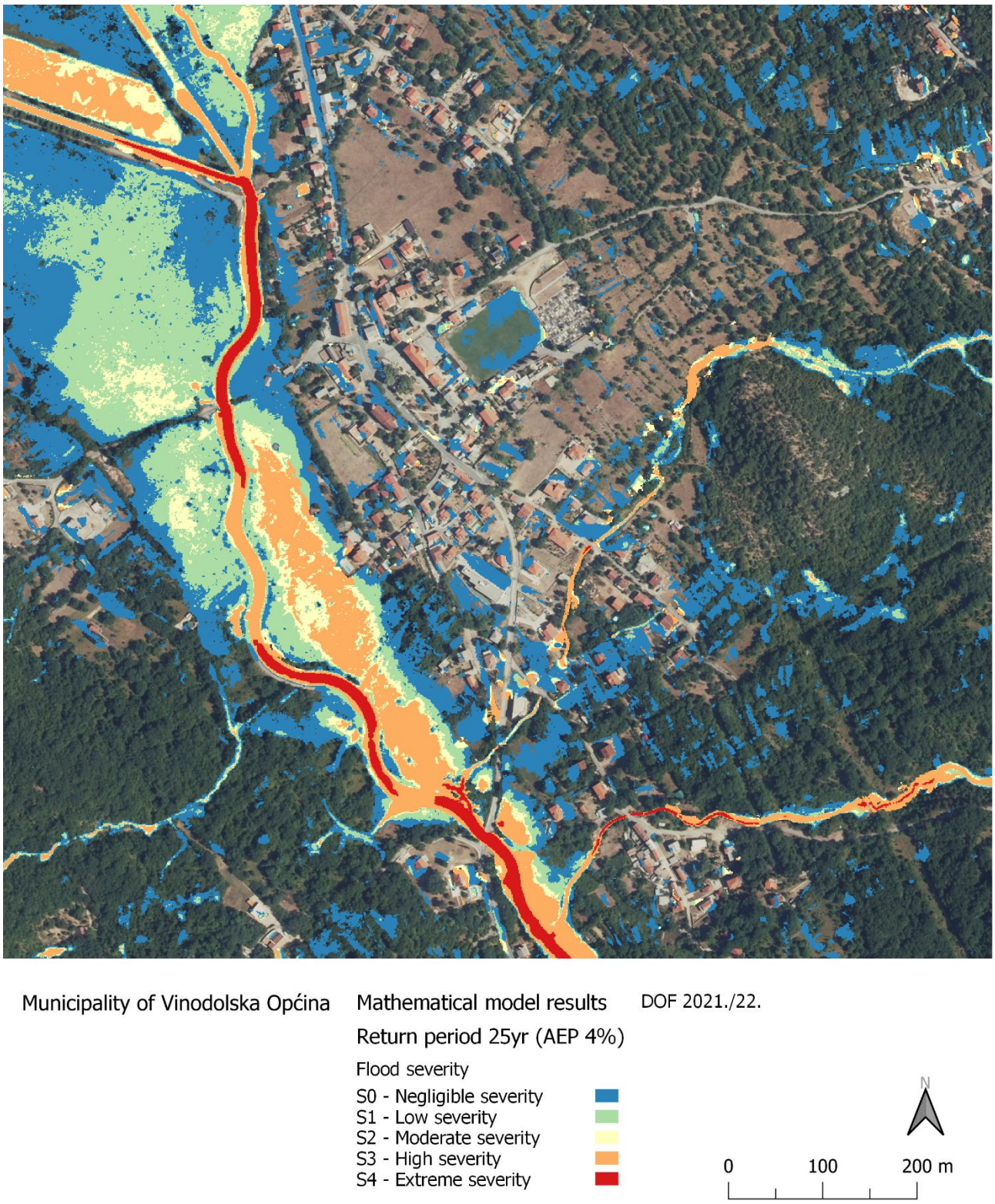

Figure 2.27. Detail from the flood hazard map for a return period of 25 years (AEP 4%) for the selected microlocation in the Municipality of Vinodolska općina - flood severity.

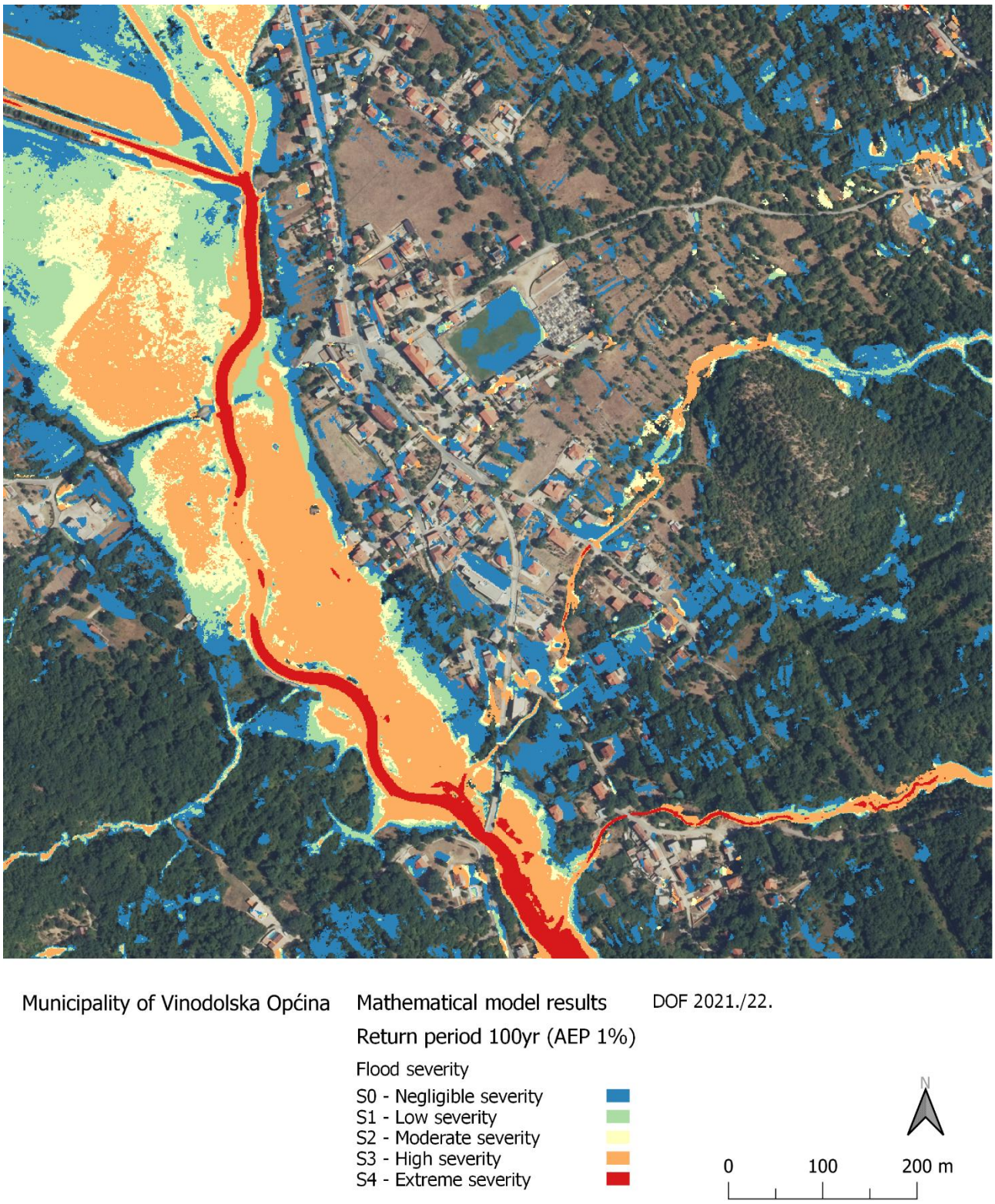

Figure 2.28. Detail from the flood hazard map for a return period of 100 years (AEP 1%) for the selected microlocation in the Municipality of Vinodolska općina - flood severity.

2.3.3. Pluvial flood hazard assessment for the City of Novi Vinodolski

The flood hazard assessment for the City of Novi Vinodolski Općina was carried out for three scenarios—low, medium, and high probability—which correspond to annual exceedance probabilities of 1%, 5%, and 20%, respectively. The pluvial flood hazard maps show the spatial distribution of water depths and velocities, as well as severity levels for each of the specified probabilities.

Figures 2.29 to 2.31 present examples of hazard maps showing water depths for low, medium, and high probability events in the area, with detailed results shown in Figures 2.32 to 2.34.

Figures 2.35 to 2.37 present examples of hazard maps showing water velocities for low, medium, and high probability events in the area, with detailed results in Figures 2.38 to 2.40.

Figures 2.41 to 2.43 present examples of hazard maps showing severity levels for low, medium, and high probability events in the area, with detailed results in Figures 2.44 to 2.46.

From these maps, the main flood generation processes in the catchment can be characterized, and critical locations identified. The flood generation process primarily depends on terrain characteristics (terrain morphology, as well as geological and pedological features). In most parts of the catchment, which is located in a karst area, no continuous surface runoff of rainfall is observed, and therefore no flooding occurs except in isolated depressions, where water quickly infiltrates into the subsurface. The only exceptions with more pronounced flooding are the Ričina River catchment in the Velo polje and easter part of the urbanized area (western part of the catchment), and the urbanised center of Novi Vinodolski (caused by high impermeability), with also several smaller torrential streams near the coastline.

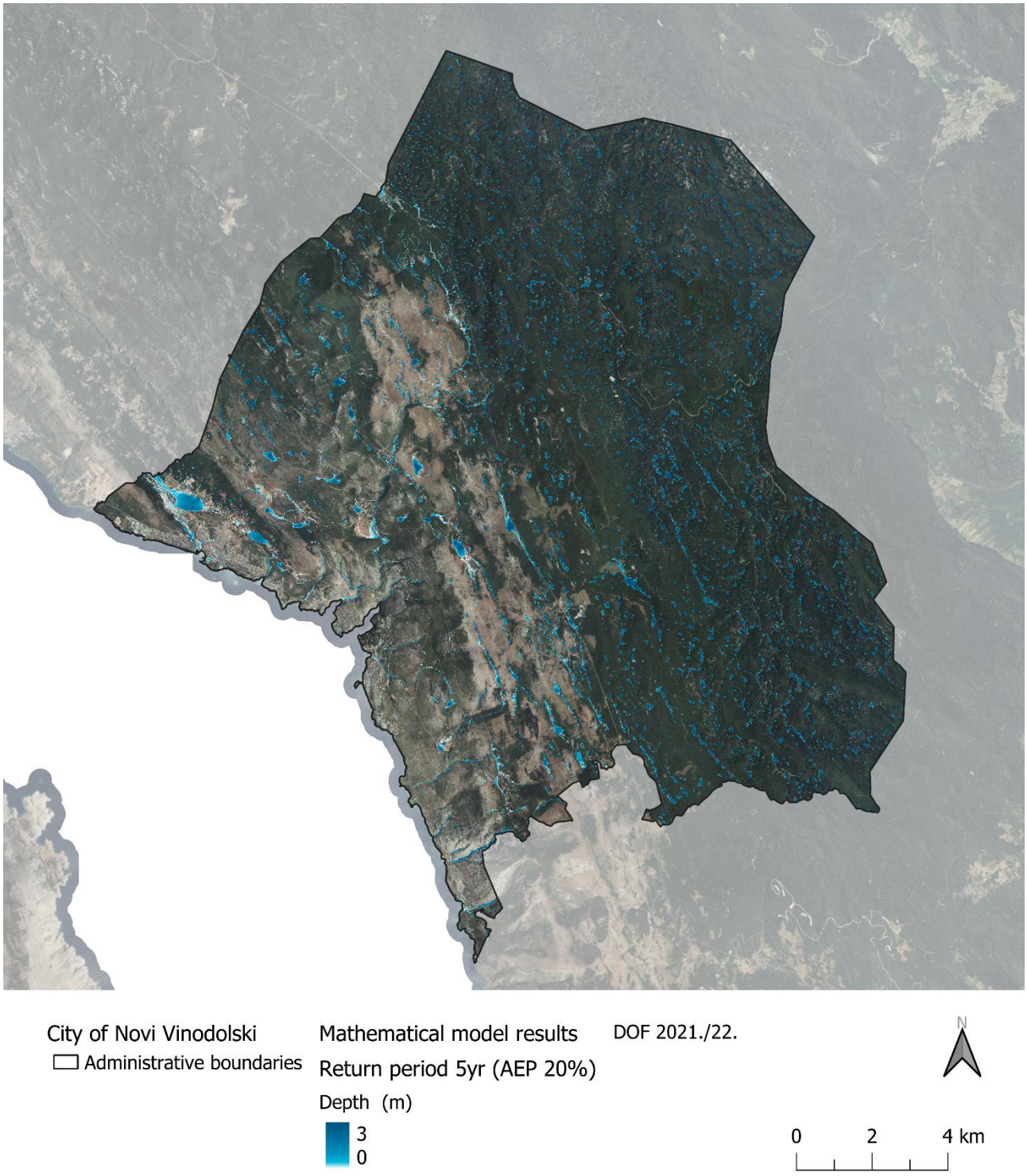

Figure 2.29. Flood hazard map for a return period of 5 years (AEP 20%) for the City of Novi Vinodolski - water depth.

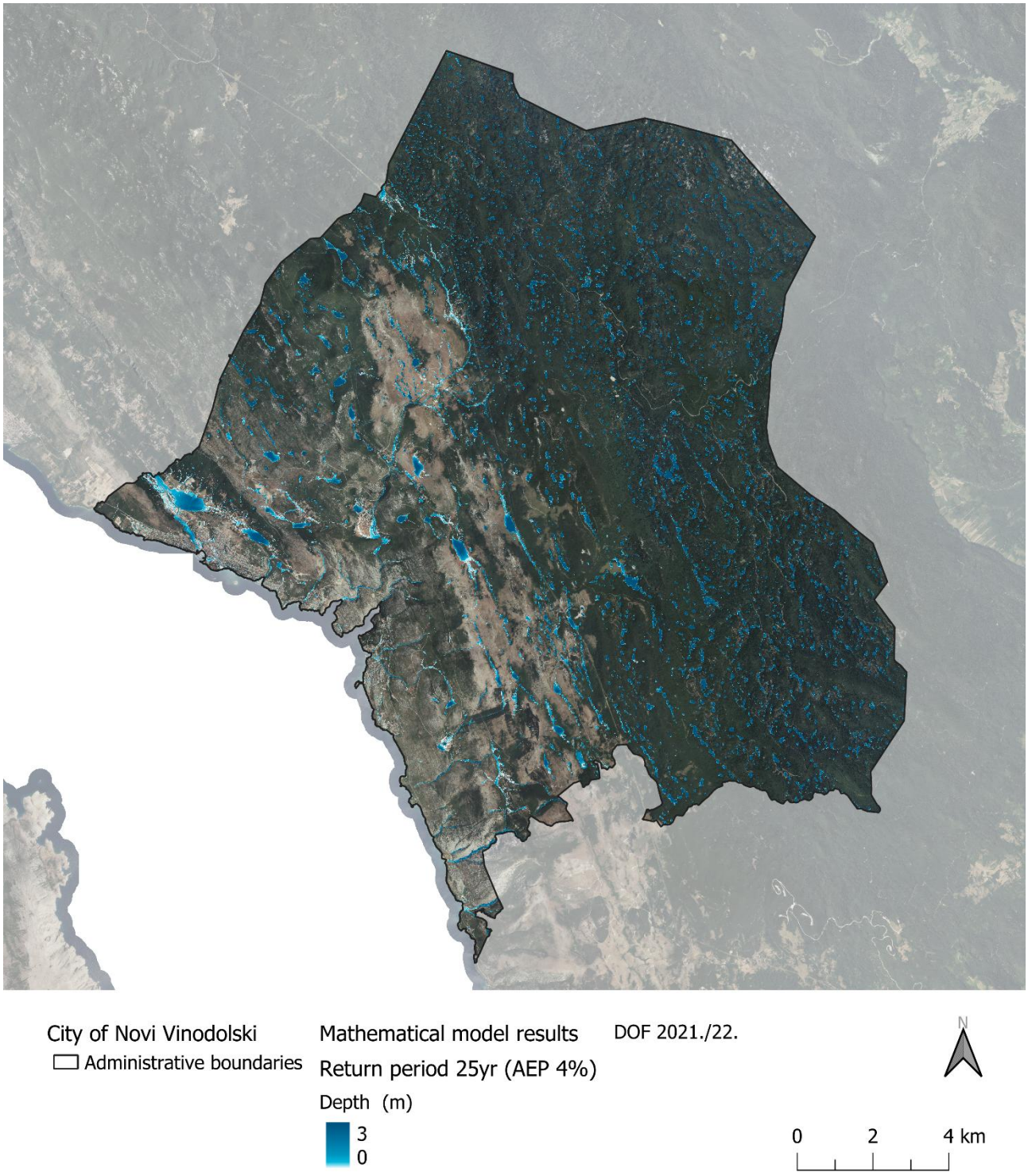

Figure 2.30. Flood hazard map for a return period of 25 years (AEP 4%) for the City of Novi Vinodolski - water depth.

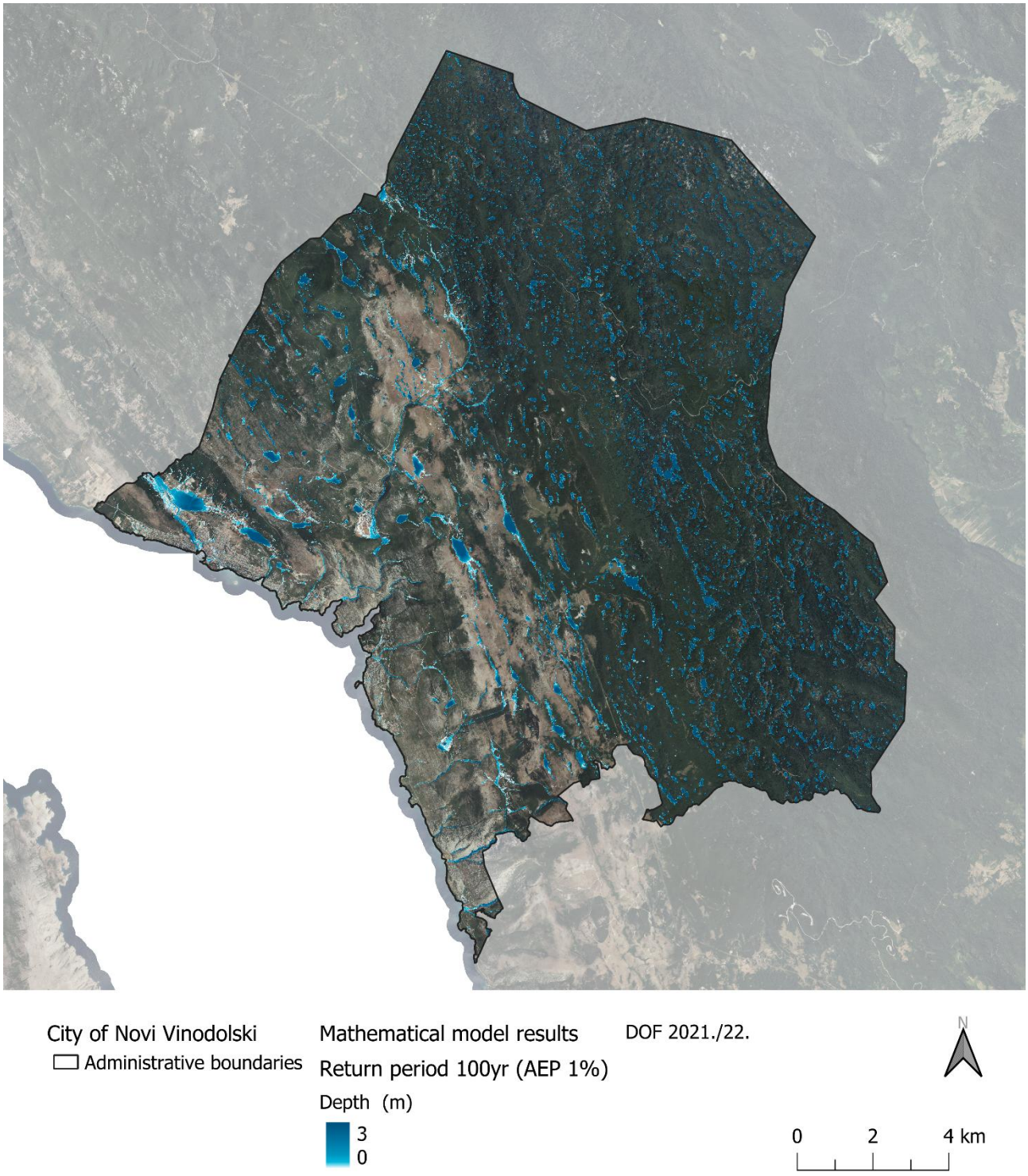

Figure 2.31. Flood hazard map for a return period of 100 years (AEP 1%) for the City of Novi Vinodolski - water depth.

Figure 2.32. Detail from the flood hazard map for a return period of 5 years (AEP 20%) for the selected microlocation in the City of Novi Vinodolski - water depth.

Figure 2.33. Detail from the flood hazard map for a return period of 25 years (AEP 4%) for the selected microlocation in the City of Novi Vinodolski - water depth.

Figure 2.34. Detail from the flood hazard map for a return period of 100 years (AEP 1%) for the selected microlocation in the City of Novi Vinodolski - water depth.

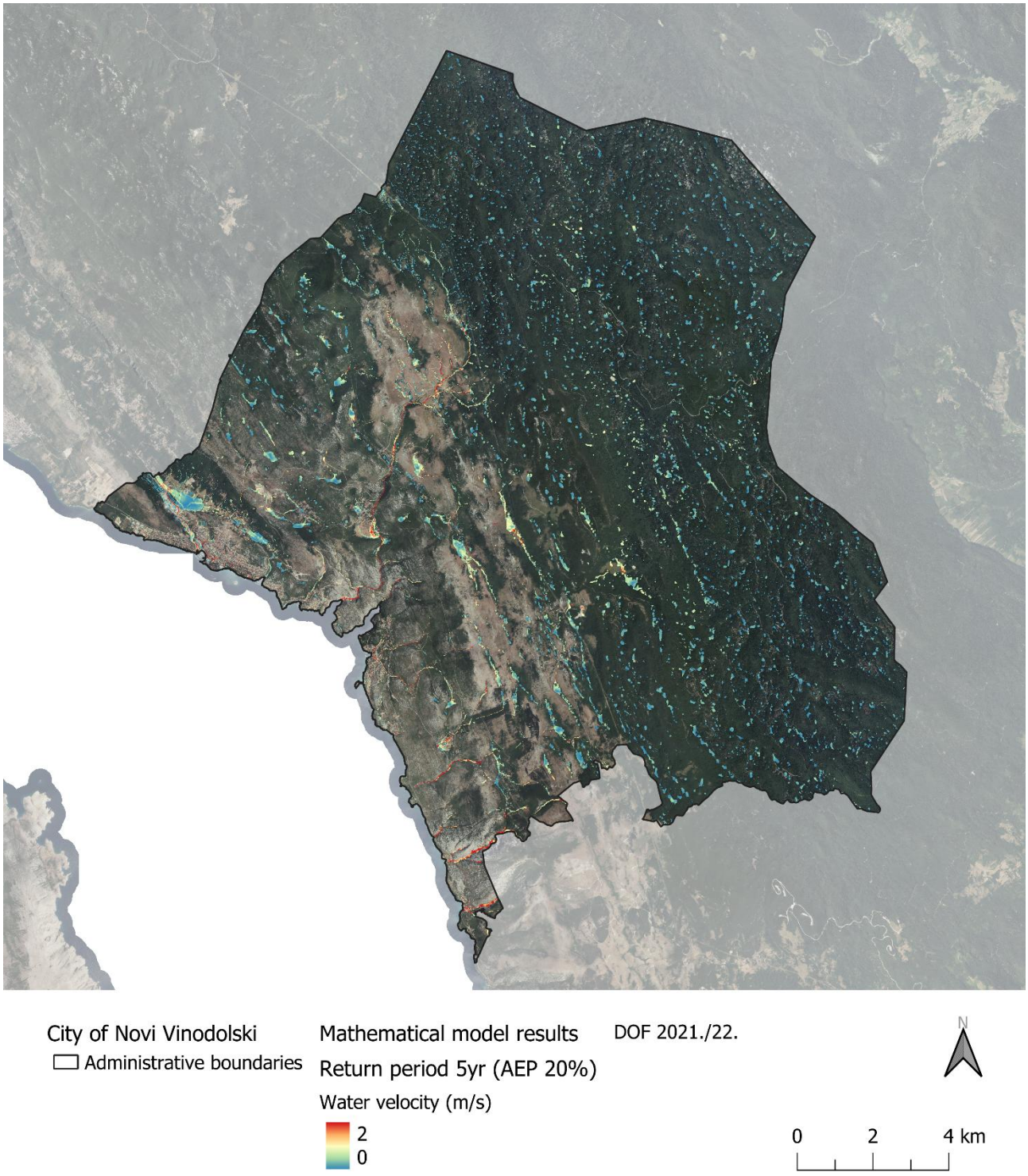

Figure 2.35. Flood hazard map for a return period of 5 years (AEP 20%) for the City of Novi Vinodolski - water velocity.

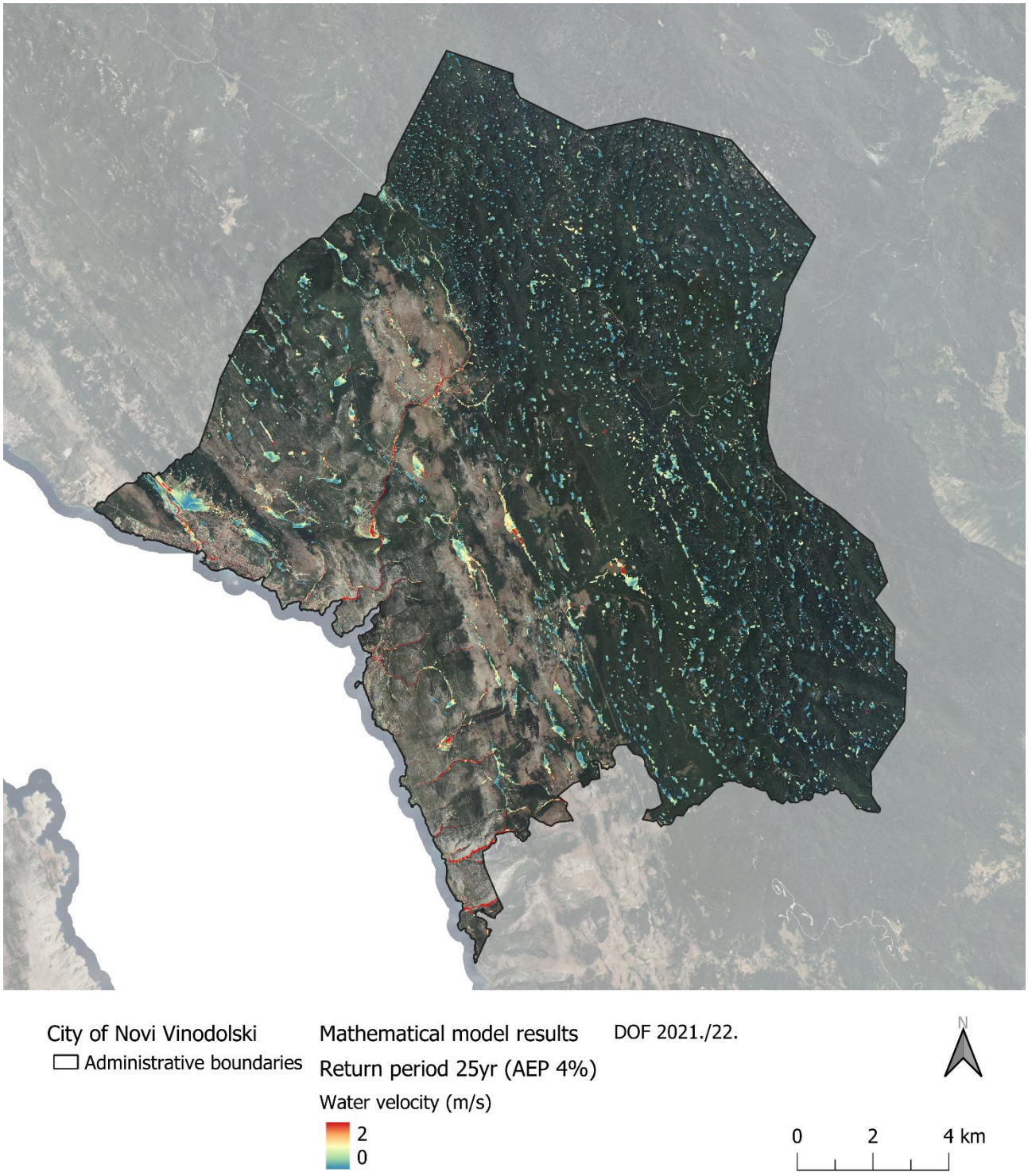

Figure 2.36. Flood hazard map for a return period of 25 years (AEP 4%) for the City of Novi Vinodolski - water velocity.

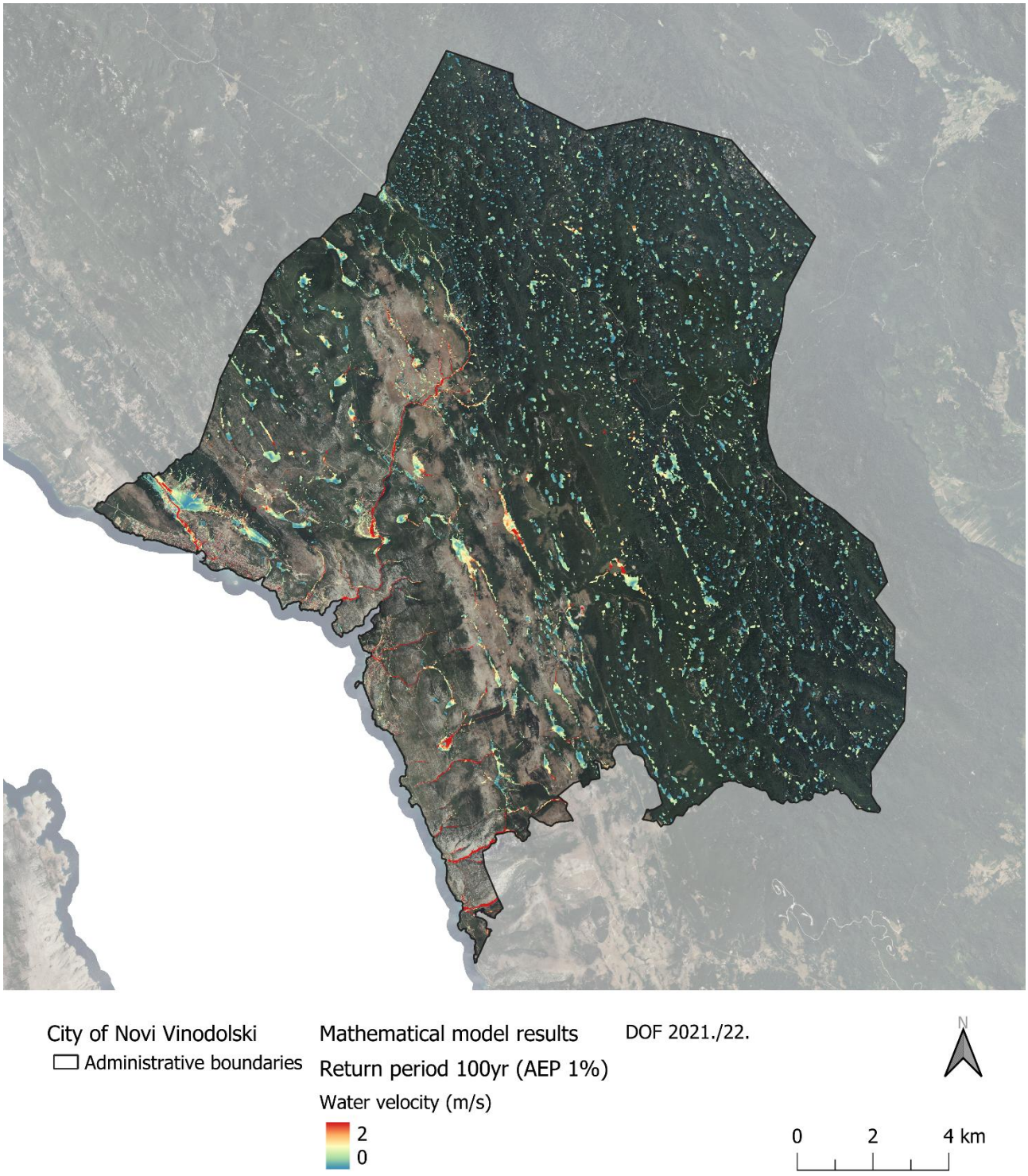

Figure 2.37. Flood hazard map for a return period of 100 years (AEP 1%) for the City of Novi Vinodolski - water velocity.

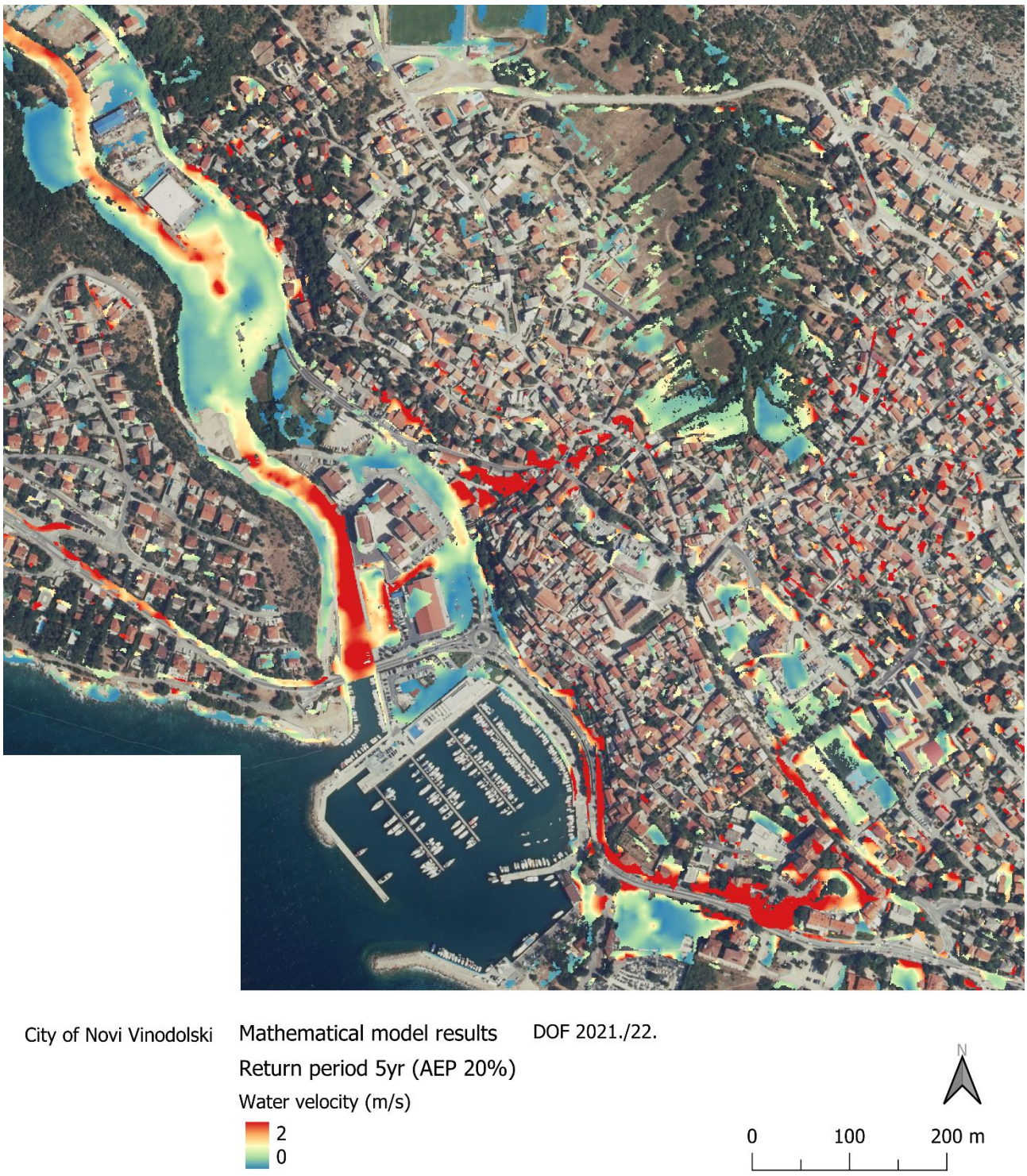

Figure 2.38. Detail from the flood hazard map for a return period of 5 years (AEP 20%) for the selected microlocation in the City of Novi Vinodolski - water velocity.

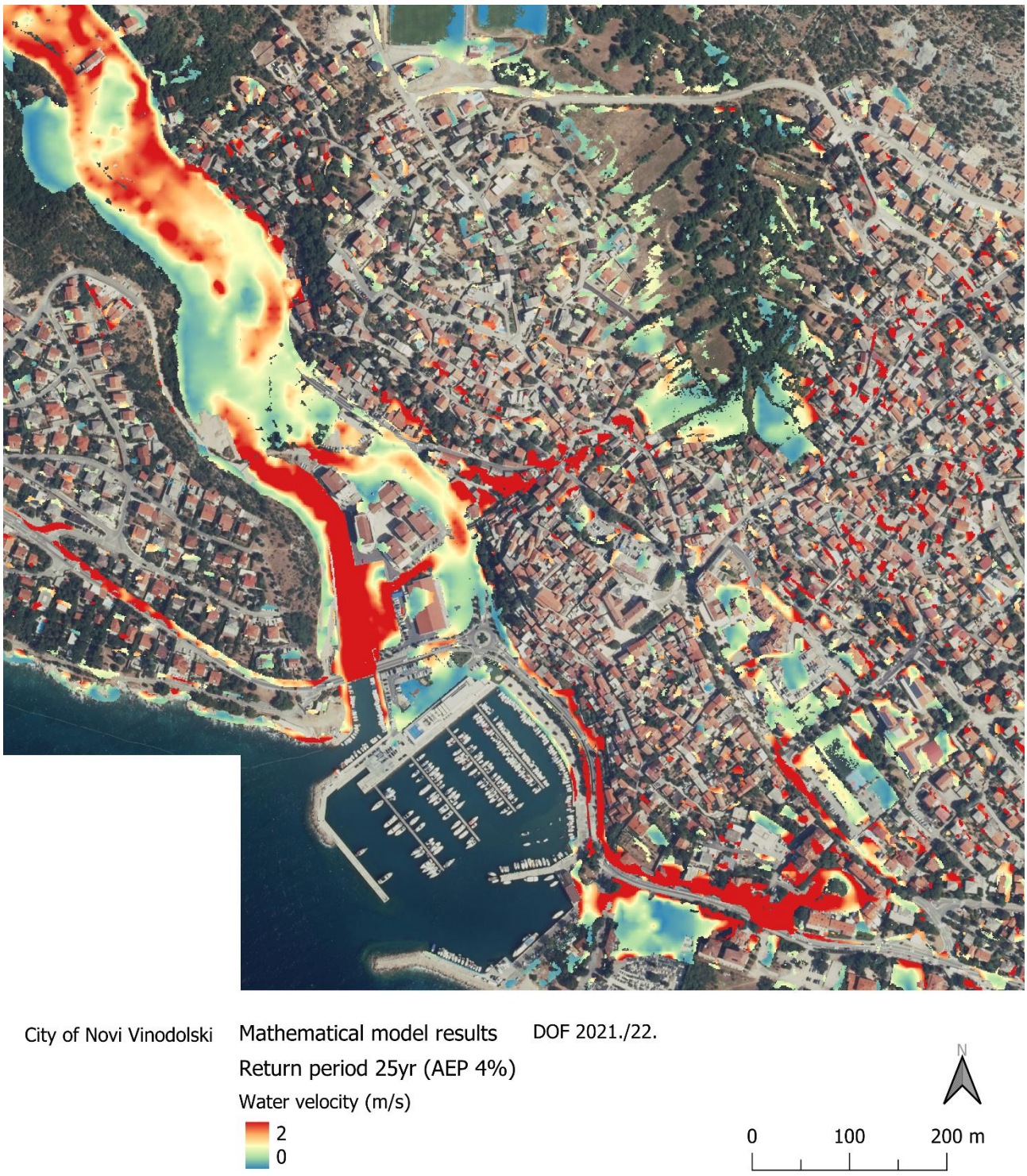

Figure 2.39. Detail from the flood hazard map for a return period of 25 years (AEP 4%) for the selected microlocation in the City of Novi Vinodolski - water velocity.

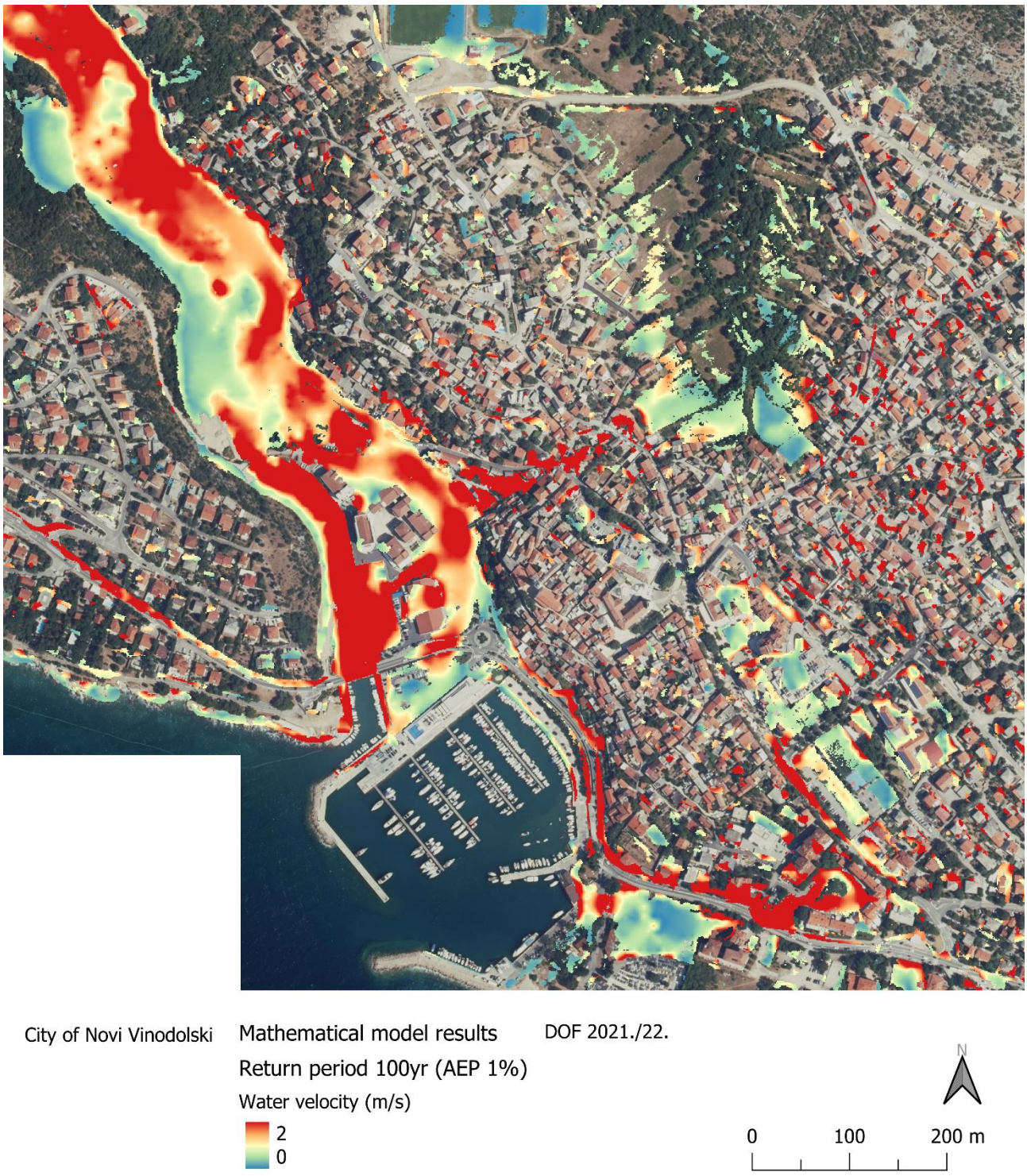

Figure 2.40. Detail from the flood hazard map for a return period of 100 years (AEP 1%) for the selected microlocation in the City of Novi Vinodolski - water velocity.

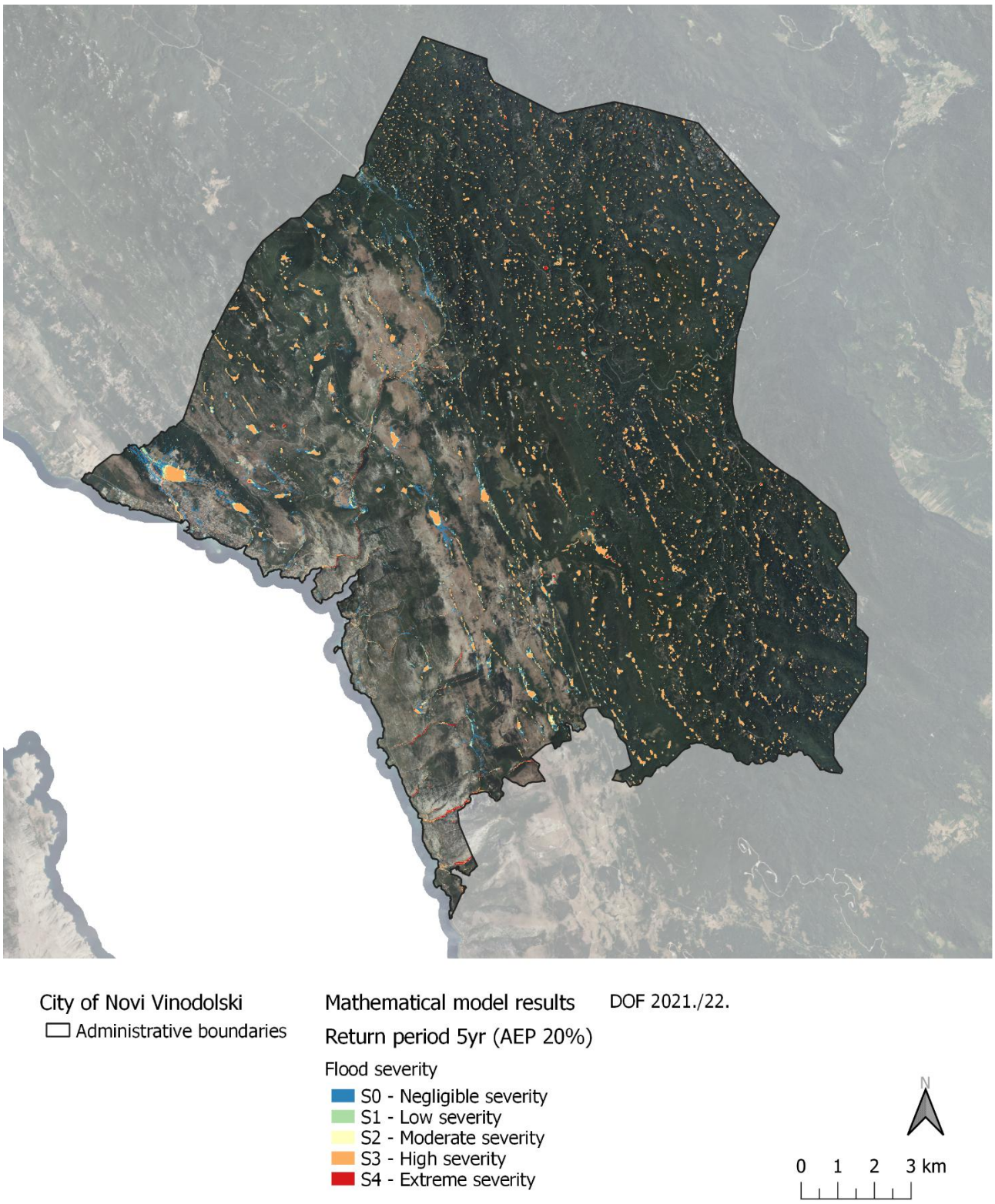

Figure 2.41. Flood hazard map for a return period of 5 years (AEP 20%) for the City of Novi Vinodolski - flood severity.

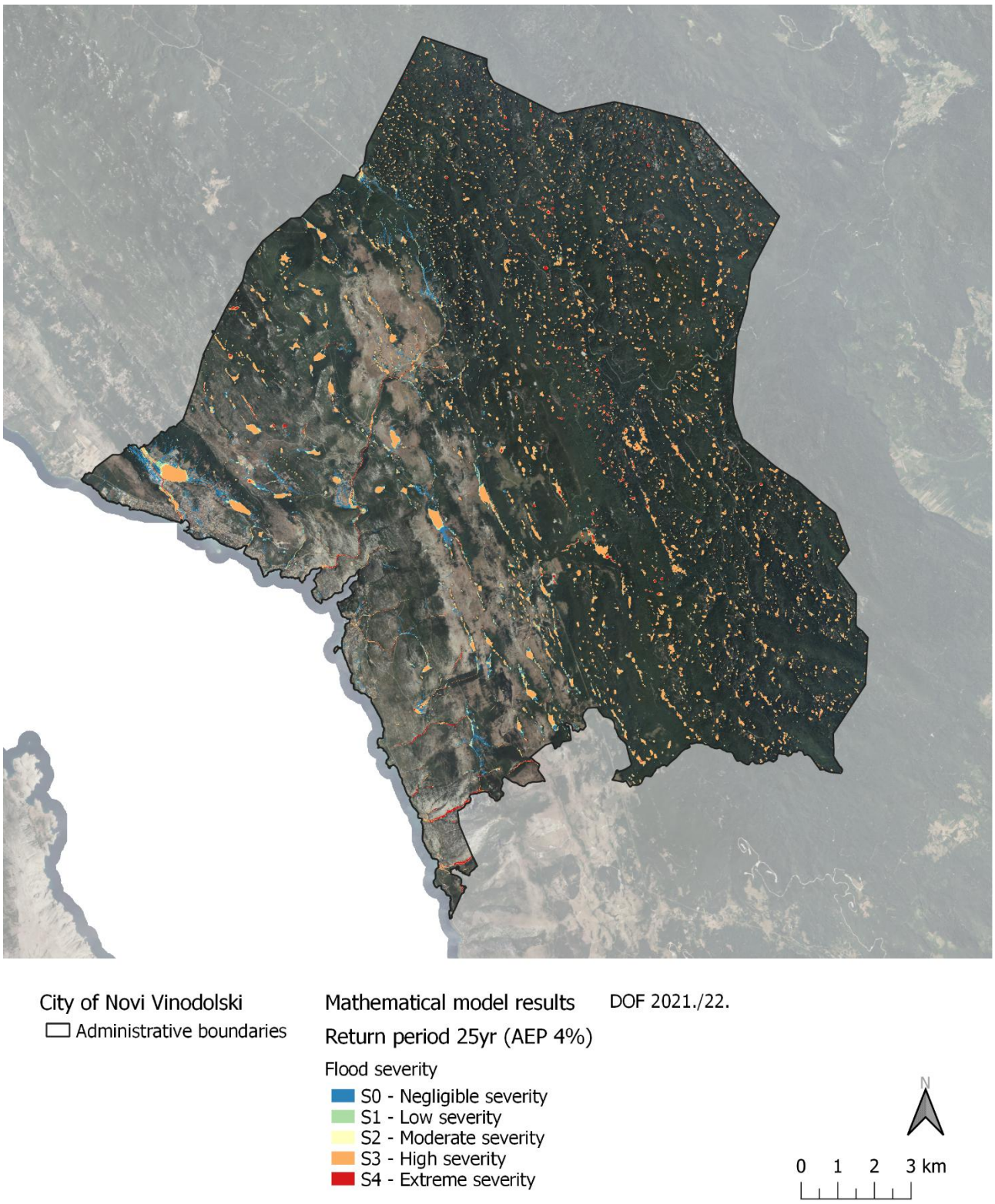

Figure 2.42. Flood hazard map for a return period of 25 years (AEP 4%) for the City of Novi Vinodolski - flood severity.

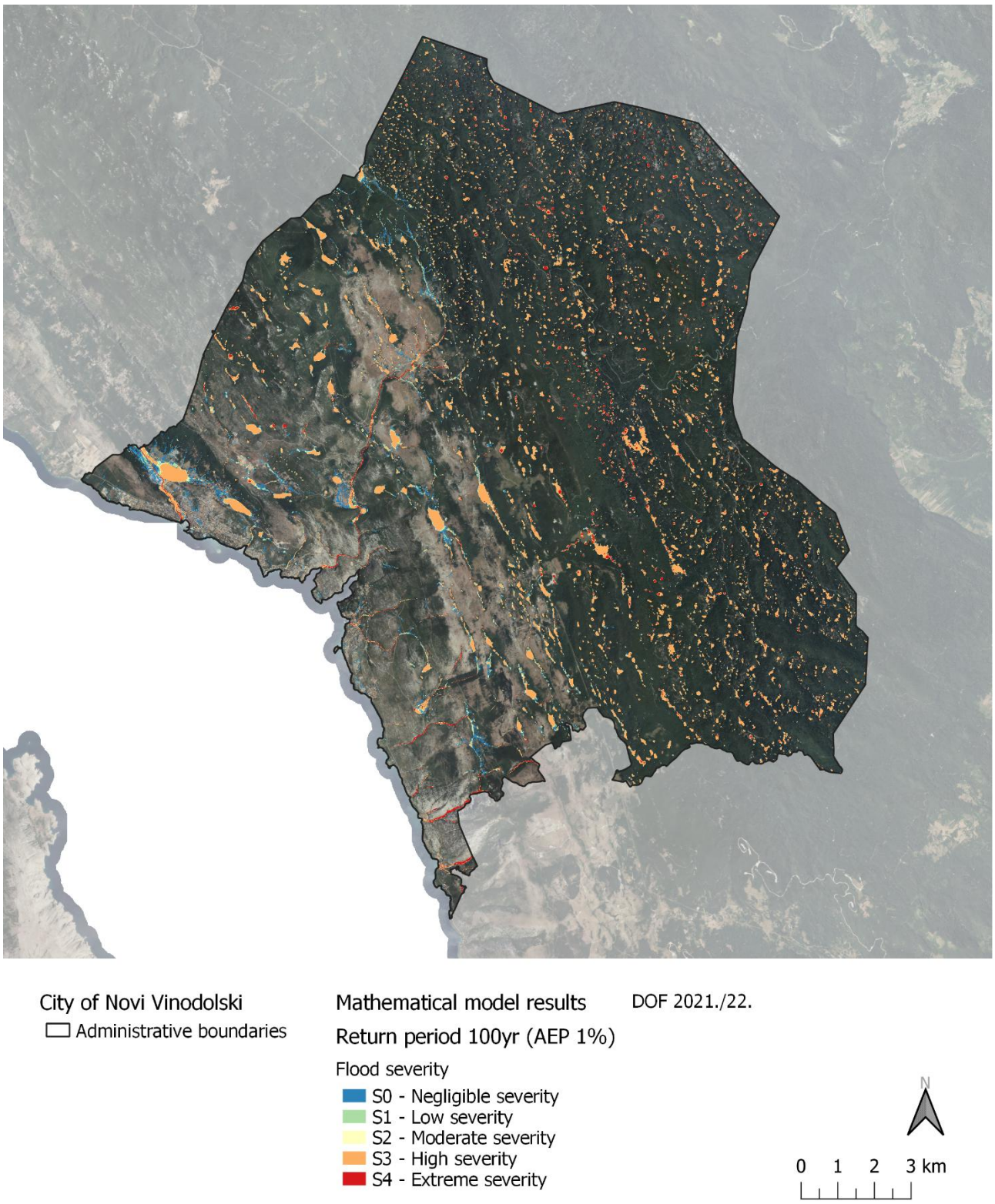

Figure 2.43. Flood hazard map for a return period of 100 years (AEP 1%) for the City of Novi Vinodolski - flood severity.

Figure 2.44. Detail from the flood hazard map for a return period of 5 years (AEP 20%) for the selected microlocation in the City of Novi Vinodolski - flood severity.

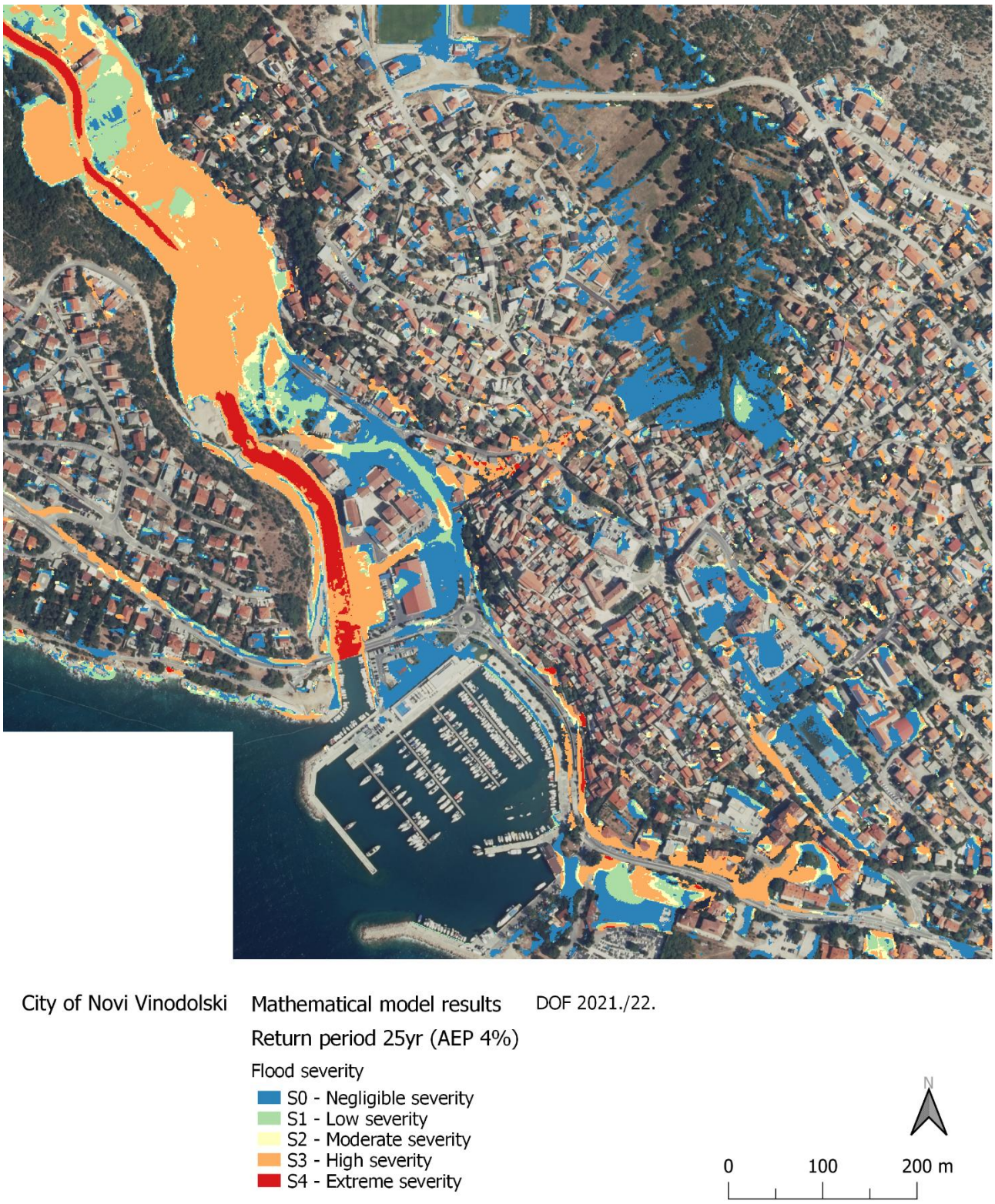

Figure 2.45. Detail from the flood hazard map for a return period of 25 years (AEP 4%) for the selected microlocation in the City of Novi Vinodolski - flood severity.

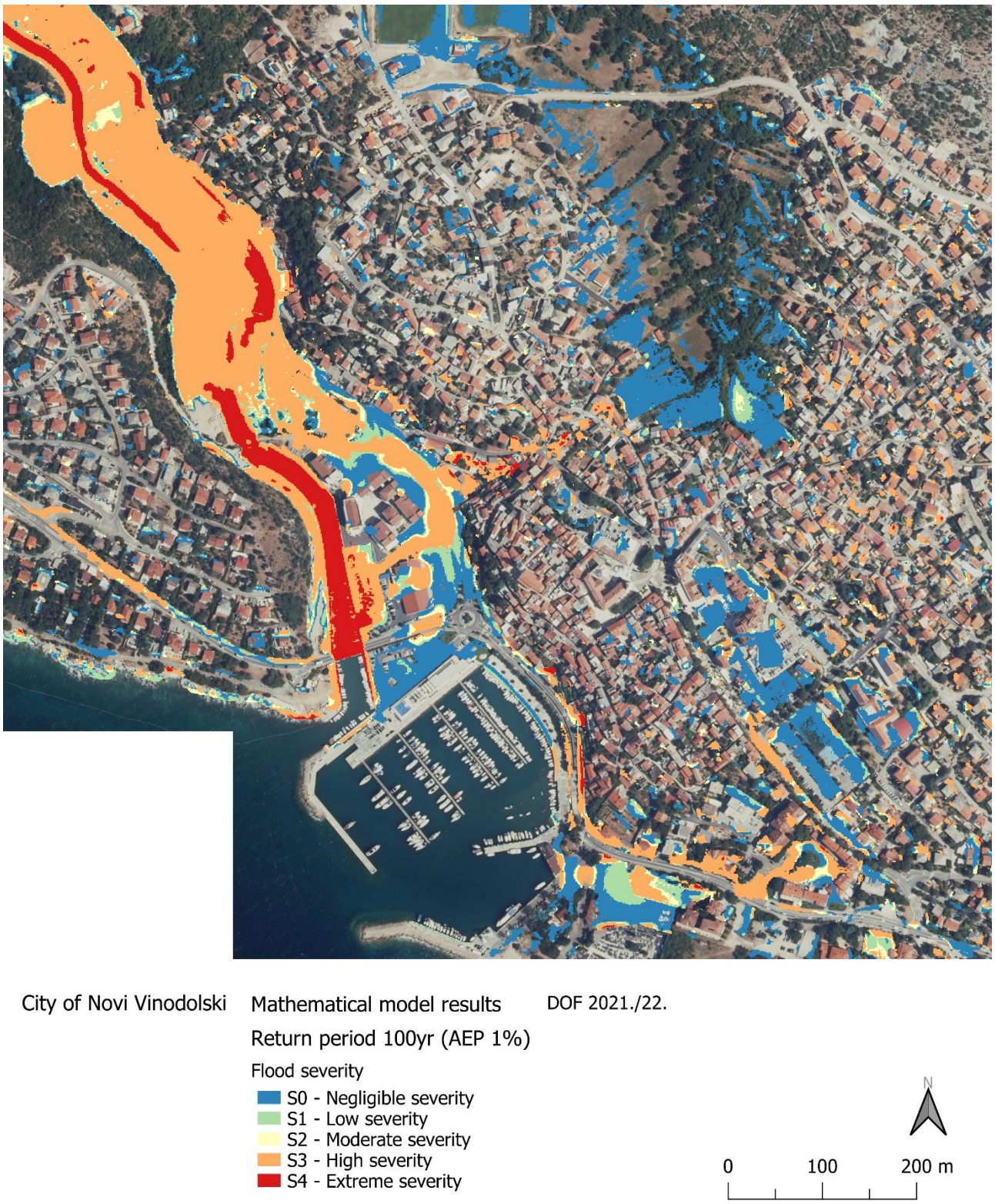

Figure 2.46. Detail from the flood hazard map for a return period of 100 years (AEP 1%) for the selected microlocation in the City of Novi Vinodolski - flood severity.

3. CONCLUSIONS

This report presents rainfall analysis and flood hazard assessment for two pilot areas: the **Municipality of Vinodolska općina** and the **City of Novi Vinodolski**.

3.1. Rainfall regime

Rainfall regimes were first analyzed using data from the **Crikvenica climatological station** (for Vinodolska općina) and the **Novi Vinodolski station** (for the City of Novi Vinodolski). Several rainfall indicators were investigated to better understand climate variability and flood potential, including **total rainfall**, **number of rainy days**, **number of heavy rainfall days**, and **maximum daily rainfall**.

General Findings (both stations):

- **Autumn** is the rainiest season, especially **October and November**, with the highest total rainfall, number of rainy days, and frequency of heavy rainfall events.
- **Summer** (especially **July and August**) is the driest season, characterized by the lowest rainfall amounts, fewest rainy days, and lowest variability.
- All indicators show **notable interannual variability**, influenced by natural climate variability and occasional extreme events.

Crikvenica Station (1990–2023):

- **Annual rainfall** averages **1270 mm**. An increasing trend is observed but is **not statistically significant**.
- A **significant increasing trend** is found for **winter rainfall** (+5 mm/year).
- **Rainy days** account for **26.9% of the year**, with a slight, non-significant increasing trend.
- **Winter rainy days** show a **statistically significant increase** (+3.7 days/decade).
- **Heavy rainfall days** (~5.5% annually) show **no significant trend**, though **winter shows a small but significant increase** (+1.3 days/decade).
- **Maximum daily rainfall** is highly variable (up to **191.2 mm**), with **no significant long-term trend**, though **positive anomalies** are noted in some years.
- **Seasonal maxima** are highest in **autumn**, and lowest in **spring and summer**.

Novi Vinodolski Station (1991–2023):

- **Annual rainfall** averages **1250 mm**, with **no statistically significant trend**.
- **Winter rainfall** shows a **significant increasing trend** (+5 mm/year).
- **Rainy days** represent **25.9% of the year**, with **no overall significant trend**, though **winter rainy days** increase significantly (+4 days/decade).

- **Heavy rainfall days** (~5.6% annually) show **no significant trend**, although **autumn months** dominate in both frequency and variability.
- **Maximum daily rainfall** is variable (up to **195.9 mm**) with **no significant long-term trend**; **autumn months** again show the most extreme values.

The **nearest rain gauge station** capable of capturing 5-minute rainfall intensities for both pilot sites is located in **Rijeka**. Data from a recent hydrological study, including **DDF and IDF curves** and **design storm patterns**, were used for intensity-based rainfall analysis.

Climate Projections

Recent **high-resolution climate projections** (Pichelli et al., 2021) based on **kilometer-scale convection-permitting models** suggest the following for the study region:

- **Rainfall intensity** is expected to **increase**, potentially exacerbating short-duration rainfall events.
- **Rainfall frequency** may remain stable or **slightly decrease**, particularly in **summer**, leading to **longer dry periods**.
- The **intensity and occurrence of extreme rainfall events (p99.9)** are projected to remain the same or **slightly increase**, raising the **risk of flash floods**, especially in **urbanized coastal zones** with **limited drainage capacity**.

3.2. Flood hazard assessment

In line with the **Floods Directive** and methodology established in a previous project on pluvial flood risk management, flood hazard assessments were conducted for **three probability scenarios** (low, medium, and high), corresponding to return periods of **5, 20, and 100 years** (i.e., annual exceedance probabilities of **20%, 5%, and 1%**). A **2D hydrological-hydraulic surface runoff model** was used, based on **high-resolution terrain data** and **design storms** of 1, 3, 6, 12, and 24 hours.

Vinodolska općina:

- Flood generation depends largely on **terrain morphology** and **geological/pedological characteristics**.
- Due to its **karst landscape**, most of the area shows **little or no continuous surface runoff**, except in **depressions** where water infiltrates rapidly.
- Notable exceptions with **pronounced flooding** include:
  - The Dubračina River catchment (western and southwestern part)
  - The upper Velo polje (southern part)
  - The Bribir area (central to eastern part)
  - Lič polje (northeastern part, less pronounced)
- Highest **flow velocities** occur in **river and drainage channels**.

City of Novi Vinodolski:

- Similar terrain-driven behavior is observed due to **karst conditions**.
- Most of the area has **limited surface runoff**, with flooding occurring primarily in:
  - The **Ričina River catchment** (Velo polje and eastern urban area)
  - The **urban center of Novi Vinodolski** (due to high imperviousness)
  - Several **small torrential streams** near the coast

The results are available in full spatial detail within the GIS database, while this report provides selected outputs in the appendix as maps formatted for A3 paper size.

These results and findings provide a robust basis for **spatial planning**, **flood risk management**, and **climate adaptation strategies**, but should be interpreted in light of the **investigation scale (1:25,000)**.

The results presented at a scale of 1:25,000 mean that 1 centimeter on the map represents 250 meters in reality, allowing for the identification of local features, such as water level accumulation zones and main drainage channels. This level of detail is suitable for spatial planning at the level of the Municipality or City, but not precise enough for parcel-level or detailed urban infrastructure design.

REFERENCES

Ball J, Babister M, Nathan R, Weeks W, Weinmann E, Retallick M, Testoni I, (2019): Australian Rainfall and Runoff: A Guide to Flood Estimation, Commonwealth of Australia (Geoscience Australia).

Brunner, G.W. (2021): HEC-RAS 6.0 2D User's Manual.

Cardona, O. D., Van Aalst, M. K., Birkmann, J., Fordham, M., Mc Gregor, G., Rosa, P., ... & Thomalla, F. (2012). Determinants of risk: exposure and vulnerability. In Managing the risks of extreme events and disasters to advance climate change adaptation: special report of the intergovernmental panel on climate change (pp. 65-108). Cambridge University Press.

Cindrić, K., Nirnac, I., Gajić-Čapka, M., Rubinić, J. (2014): Vremenske promjene kratkotrajnih jakih oborina u razdoblju 1955.-2010. za Split i Varaždin, Hrvatske vode 22/89, 239-250.

Chow, V. (2010). Applied hydrology. Tata McGraw-Hill Education.

Coles, S. (2001): An Introduction to Statistical Modeling of Extreme Values. Springer, 208 pp.

Copernicus Land Monitoring Service. (2021). CLCplus Backbone 2021 (raster 10 m). European Environment Agency. https://doi.org/10.2909/71fc9d1b-479f-4da1-aa66-662a2fff2cf7

Escuder-Bueno, I., Castillo-Rodriguez, J. T., Perales-Momparler, S., and Morales-Torres, A. (2011): SUFRI methodology for pluvial and river flooding risk assessment in urban areas to inform decision making, SUFRI project, WP3, final report.

EXCIMAP (2007): Handbook on good practices for flood mapping in Europe, European exchange circle on flood mapping.

GFRI i DHMZ (2019): Flood Risk Management Due to Heavy Rainfall – RAINMAN, Study, Građevinski fakultet u Rijeci (GFRI) i Državni hidrometeorološki zavod (DHMZ).

GFRI, VPB i DHMZ (2022): Studija procjene opasnosti i rizika od poplava uslijed jakih oborina i djelovanja mora. Knjiga 1: Analiza oborina na pilot područjima. Građevinski fakultet u Rijeci (GFRI), Vodoprivredno-projektni biro d.d. (VPB) i Državni hidrometeorološki zavod (DHMZ).

Helsel, D. R., Hirsch, R. M. (2002): Statistical Methods in Water Resources Techniques of Water Resources Investigations, U.S. Geological Survey.

Hong, Y. and Adler, R.F. (2008) Estimation of Global SCS Curve Numbers Using Satellite Remote Sensing and Geospatial Data. Journal International Journal of Remote Sensing, 29, 471-477. https://doi.org/10.1080/01431160701264292

Institut za elektroprivredu d.d. (IE), Hidroing d.o.o. Osijek, Vodoprivredno-projektni biro d.d., Proning DHI d.o.o. (2023): Unaprjeđenje hidroloških podloga – Hidrološka studija Jadran (Knjiga 3). Zagreb. (in Croatian).

Kendall, M. G. (1975). Rank Correlation Methods (4th ed.). London: Charles Griffin.

Klein Tank, A. M. G., Zwiers, F. W., Zhang, X. (2009): Guidelines on analysis of extremes in a changing climate in support of informed decisions for adaptation. World Meteorological Organisation, WMO-TD No. 1500, WCDMP-No. 72, 52 pp.

Krvavica, N., Jaredić, K., Rubinić, J. (2018): Metodologija definiranja mjerodavne oborine za dimenzioniranje infiltracijskih sustava. Građevinar, 70(8), 657-669.

Krvavica, N., i Rubinić, J. (2020). Evaluation of design storms and critical rainfall durations for flood prediction in partially urbanized catchments. Water, 12(7), 2044.

Krvavica, N., Šiljeg, A., Horvat, B., & Panđa, L. (2023). Pluvial Flash Flood Hazard and Risk Mapping in Croatia: Case Study in the Gospić Catchment. Sustainability, 15(2), Article 2. https://doi.org/10.3390/su15021197

McKee, T. B., Doesken, N. J., & Kleist, J. (1993). The relationship of drought frequency and duration to time scales. In Proceedings of the 8th Conference on Applied Climatology (pp. 179–184). American Meteorological Society.

Merz, B., Thieken, A. H., & Gocht, M. (2007). Flood risk mapping at the local scale: concepts and challenges. In Flood risk management in Europe (pp. 231-251). Springer, Dordrecht.

MZOE (2017.): Strategije prilagodbe klimatskim promjenama u Republici Hrvatskoj za razdoblje do 2040. godine s pogledom na 2070. Godinu.

Natural Resources Conservation Service (NRCS (2004). Part 630 Hydrology National Engineering Handbook, Chapter 9: Hydrologic Soil-Cover Complexes. United States Department of Agriculture.

Pandžić, K. i suradnici, 2008: Naputak za opažanja i mjerenja na glavnim meteorološkim postajama, DHMZ, Zagreb, 342 str.

Pilgrim, D.H. (1987): Australian rainfall and runoff, a guide to flood estimation. The Institution of Engineers, ACT, Australia, 1987.

RAINMAN (2020): Policy brief - Integrating pluvial flood risk management into flood risk management plans according to the EU Floods Directive and beyond.

Samuels, P., Gouldby, B. (2009). Language of risk: project definitions. T32-04-01.

Sauer, A., Olfert, A., Korte, L, Neubert, M, Ortlepp, R (2019): Joint definitions and analytical framework, RAINMAN. Leibniz Institute of Ecological Urban and Regional Development.

Sen, P. K. (1968): Estimates of the regression coefficient based on Kendall's tau. J. Am. Stat. Assoc. 63, 1379 –1389.

Šegota, T. i Filipčić, A. (2003). Köppenova podjela klima i hrvatsko nazivlje. Geoadria, 8 (1), 17-37. https://doi.org/10.15291/geoadria.93

Vincze, G., Moulin, C., Schlacher, C., Wubbels, T. (2014): Glavni elementi pripreme karata opasnosti od poplava i karata rizika od poplava. Izvješće o Komponenti 3.

UNISDR (2009): Terminology on Disaster Risk Reduction, UN, Geneva, Switzerland.

USACE (2021): Creating Land Cover, Maning's N Values, and % Impervious Layers. US Army Corps of Engineers.

USDA (2017): Part 630 Hydrology: National Engineering Handbook, Chapter 9: Hydrological Soil-Cover Complexes.

Zaninović, K., Gajić-Čapka, M., Perčec Tadić, M. et al, 2008: Klimatski atlas Hrvatske / Climate atlas of Croatia 1961-1990., 1971-2000. Državni hidrometeorološki zavod, Zagreb.

APPENDIX

A. MAPS

1. Flood hazard map (water depth) for a return period of 5 years (AEP 20%) for the Municipality of Vinodolska općina
2. Flood hazard map (water depth) for a return period of 25 years (AEP 4%) for the Municipality of Vinodolska općina
3. Flood hazard map (water depth) for a return period of 100 years (AEP 1%) for the Municipality of Vinodolska općina
4. Flood hazard map (water velocity) for a return period of 5 years (AEP 20%) for the Municipality of Vinodolska općina
5. Flood hazard map (water velocity) for a return period of 25 years (AEP 4%) for the Municipality of Vinodolska općina
6. Flood hazard map (water velocity) for a return period of 100 years (AEP 1%) for the Municipality of Vinodolska općina
7. Flood hazard map (severity) for a return period of 5 years (AEP 20%) for the Municipality of Vinodolska općina
8. Flood hazard map (severity) for a return period of 25 years (AEP 4%) for the Municipality of Vinodolska općina
9. Flood hazard map (severity) for a return period of 100 years (AEP 1%) for the Municipality of Vinodolska općina
10. Flood hazard map (water depth) for a return period of 5 years (AEP 20%) for the City of Novi Vinodolski
11. Flood hazard map (water depth) for a return period of 25 years (AEP 4%) for the City of Novi Vinodolski
12. Flood hazard map (water depth) for a return period of 100 years (AEP 1%) for the City of Novi Vinodolski
13. Flood hazard map (water velocity) for a return period of 5 years (AEP 20%) for the City of Novi Vinodolski
14. Flood hazard map (water velocity) for a return period of 25 years (AEP 4%) for the City of Novi Vinodolski
15. Flood hazard map (water velocity) for a return period of 100 years (AEP 1%) for the City of Novi Vinodolski
16. Flood hazard map (severity) for a return period of 5 years (AEP 20%) for the City of Novi Vinodolski
17. Flood hazard map (severity) for a return period of 25 years (AEP 4%) for the City of Novi Vinodolski
18. Flood hazard map (severity) for a return period of 100 years (AEP 1%) for the City of Novi Vinodolski

B. GIS DATABASE

The GIS database is organized according to the conducted analysis (hazard analysis and exposure analysis) and the location for which the analysis was made (Municipality of Vinodolska Općina and the City of Novi Vinodolski). The database contains the folders and files described in Table B.1.

Table B.1 Overview of GIS database files.

File name	Analysis type	Indicator	Probability	QGIS Group	QGIS Layer name	QGIS Layer type
DTM_LIDAR_1m.tif	-	-	-	DTM	DTM_LIDAR_1m	Raster
City_Novi_Vinodolski.shp	-	-	-	Locations	City_Novi_Vinodolski	Vector
Municipality_Vinodolska_Opcina.shp					Municipality_Vinodolska_Opcina	
\01-Municipality_of_Vinodolska_Opcina\MVO_Depth_5yr_results.tif	Hazard analysis	Water depth	Return period 5yr (AEP 20%)	Hazard analysis results\ Municipality of Vinodolska Opcina\ Water depth (m)	MVO_Depth_5yr_results	Raster
\01-Municipality_of_Vinodolska_Opcina\MVO_Depth_25yr_results.tif			Return period 25yr (AEP 4%)		MVO_Depth_25yr_results	
\01-Municipality_of_Vinodolska_Opcina\MVO_Depth_100yr_results.tif			Return period 100yr (AEP 1%)		MVO_Depth_100yr_results	
\01-Municipality_of_Vinodolska_Opcina\MVO_Velocity_5yr_results.tif	Hazard analysis	Water velocity	Return period 5yr (AEP 20%)	Hazard analysis results\ Municipality of Vinodolska Opcina\ Water velocity (m/s)	MVO_Velocity_5yr_results	Raster
\01-Municipality_of_Vinodolska_Opcina\MVO_Velocity_25yr_results.tif			Return period 25yr (AEP 4%)		MVO_Velocity_25yr_results	
\01-Municipality_of_Vinodolska_Opcina\MVO_Velocity_100yr_results.tif			Return period 100yr (AEP 1%)		MVO_Velocity_100yr_results	
\01-Municipality_of_Vinodolska_Opcina\MVO_Severity_5yr_results.tif	Hazard analysis	Flood Severity	Return period 5yr (AEP 20%)	Hazard analysis results\ Municipality of Vinodolska Opcina\ Flood Severity	MVO_Severity_5yr_results	Raster
\01-Municipality_of_Vinodolska_Opcina\MVO_Severity_25yr_results.tif			Return period 25yr (AEP 4%)		MVO_Severity_25yr_results	
\01-Municipality_of_Vinodolska_Opcina\MVO_Severity_100yr_results.tif			Return period 100yr (AEP 1%)		MVO_Severity_100yr_results	
\02-City_of_Novi_Vinodolski\CNV_Depth_5yr_results.tif	Hazard analysis	Water depth	Return period 5yr (AEP 20%)	Hazard analysis results\ City of Novi Vinodolski\ Water depth (m)	CNV_Depth_5yr_results	Raster
\02-City_of_Novi_Vinodolski\CNV_Depth_25yr_results.tif			Return period 25yr (AEP 4%)		CNV_Depth_25yr_results	
\02-City_of_Novi_Vinodolski\CNV_Depth_100yr_results.tif			Return period 100yr (AEP 1%)		CNV_Depth_100yr_results	
\02-City_of_Novi_Vinodolski\CNV_Velocity_5yr_results.tif	Hazard analysis	Water velocity	Return period 5yr (AEP 20%)	Hazard analysis results\ City of Novi Vinodolski\ Water velocity (m/s)	CNV_Velocity_5yr_results	Raster
\02-City_of_Novi_Vinodolski\CNV_Velocity_25yr_results.tif			Return period 25yr (AEP 4%)		CNV_Velocity_25yr_results	
\02-City_of_Novi_Vinodolski\CNV_Velocity_100yr_results.tif			Return period 100yr (AEP 1%)		CNV_Velocity_100yr_results	
\02-City_of_Novi_Vinodolski\CNV_Severity_5yr_results.tif	Hazard analysis	Flood Severity	Return period 5yr (AEP 20%)	Hazard analysis results\ City of Novi Vinodolski\ Flood Severity	CNV_Severity_5yr_results	Raster
\02-City_of_Novi_Vinodolski\CNV_Severity_25yr_results.tif			Return period 25yr (AEP 4%)		CNV_Severity_25yr_results	
\02-City_of_Novi_Vinodolski\CNV_Severity_100yr_results.tif			Return period 100yr (AEP 1%)		CNV_Severity_100yr_results	
\01-Municipality_of_Vinodolska_Opcina\MVO_flood_extent_5yrRP.shp	Hazard analysis	Flood Extent	Return period 5yr (AEP 20%)	Hazard analysis results\ Municipality of Vinodolska Opcina\ Flood extent (vector)	MVO_flood_extent_5yrRP	Vector
\01-Municipality_of_Vinodolska_Opcina\MVO_flood_extent_25yrRP.shp			Return period 25yr (AEP 4%)		MVO_flood_extent_25yrRP	
\01-Municipality_of_Vinodolska_Opcina\MVO_flood_extent_100yrRP.shp			Return period 100yr (AEP 1%)		MVO_flood_extent_100yrRP	
\02-City_of_Novi_Vinodolski\CNV_flood_extent_5yrRP.shp	Hazard analysis	Flood Extent	Return period 5yr (AEP 20%)	Hazard analysis results\ City of Novi Vinodolski\ Flood extent (vector)	CNV_flood_extent_5yrRP	Vector
\02-City_of_Novi_Vinodolski\CNV_flood_extent_25yrRP.shp			Return period 25yr (AEP 4%)		CNV_flood_extent_25yrRP	
\02-City_of_Novi_Vinodolski\CNV_flood_extent_100yrRP.shp			Return period 100yr (AEP 1%)		CNV_flood_extent_100yrRP	
\01-Municipality_of_Vinodolska_Opcina\Buildings\MVO_Exp_Buildings5y.shp	Exposure analysis	Exposed Buildings	Return period 5yr (AEP 20%)	Exposure analysis results\ Municipality of Vinodolska Opcina\ Buildings	MVO_Exposure_Buildings_5yrRP	Vector
\01-Municipality_of_Vinodolska_Opcina\Buildings\MVO_Exp_Buildings25y.shp			Return period 25yr (AEP 4%)		MVO_Exposure_Buildings_25yrRP	
\01-Municipality_of_Vinodolska_Opcina\Buildings\MVO_Exp_Buildings100y.shp			Return period 100yr (AEP 1%)		MVO_Exposure_Buildings_100yrRP	
\01-Municipality_of_Vinodolska_Opcina\Buildings\MVO_OSM_Buildings.shp			-		MVO_OSM_Buildings	
\01-Municipality_of_Vinodolska_Opcina\Roads\MVO_Exposure_Roads_5yrRP.shp	Exposure analysis	Exposed Roads	Return period 5yr (AEP 20%)	Exposure analysis results\ Municipality of Vinodolska Opcina\ Roads	MVO_Exposure_Roads_5yrRP	Vector
\01-Municipality_of_Vinodolska_Opcina\Roads\MVO_Exposure_Roads_25yrRP.shp			Return period 25yr (AEP 4%)		MVO_Exposure_Roads_25yrRP	
\01-Municipality_of_Vinodolska_Opcina\Roads\MVO_Exposure_Roads_100yr.shp			Return period 100yr (AEP 1%)		MVO_Exposure_Roads_100yrRP	
\01-Municipality_of_Vinodolska_Opcina\Roads\MVO_OSM_Roads.shp			-		MVO_OSM_Roads	
\02-City_of_Novi_Vinodolski\Buildings\CNV_Exposure_Buildings_5yrRP.shp	Exposure analysis	Exposed Buildings	Return period 5yr (AEP 20%)	Exposure analysis results\ City of Novi Vinodolski\ Buildings	CNV_Exposure_Buildings_5yrRP	Vector
\02-City_of_Novi_Vinodolski\Buildings\CNV_Exposure_Buildings_25yrRP.shp			Return period 25yr (AEP 4%)		CNV_Exposure_Buildings_25yrRP	
\02-City_of_Novi_Vinodolski\Buildings\CNV_Exposure_Buildings_100yrRP.shp			Return period 100yr (AEP 1%)		CNV_Exposure_Buildings_100yrRP	
\02-City_of_Novi_Vinodolski\Buildings\CNV_OSM_Buildings.shp			-		CNV_OSM_Buildings	
\01-Municipality_of_Vinodolska_Opcina\Roads\MVO_Exposure_Roads_5yrRP.shp	Exposure analysis	Exposed Roads	Return period 5yr (AEP 20%)	Exposure analysis results\ City of Novi Vinodolski\ Roads	CNV_Exposure_Roads_5yrRP	Vector
\01-Municipality_of_Vinodolska_Opcina\Roads\MVO_Exposure_Roads_25yrRP.shp			Return period 25yr (AEP 4%)		CNV_Exposure_Roads_25yrRP	
\01-Municipality_of_Vinodolska_Opcina\Roads\MVO_Exposure_Roads_100yr.shp			Return period 100yr (AEP 1%)		CNV_Exposure_Roads_100yrRP	
\01-Municipality_of_Vinodolska_Opcina\Roads\MVO_OSM_Roads.shp			-		CNV_OSM_Roads	